Controlling Exoskeletons with EMG signals and a Biomechanical Body Model

vorgelegt von
Diplom-Ingenieur
Christian Fleischer

Von der Fakultät IV - Elektrotechnik und Informatik
Technische Universität Berlin
zur Erlangung des akademischen Grades

Doktor der Ingenieurwissenschaften
- Dr.-Ing. -

genehmigte Dissertation

Promotionsausschuß:

Vorsitzender:	Prof. Dr. Felix Wichmann
Berichter:	Prof. Dr.-Ing. Dr. h.c. Günter Hommel
Berichter:	Prof. Dr.-Ing. Jörg Raisch
Berichter:	Prof. Maria Chiara Carrozza (Scuola Superiore Sant' Anna)

Tag der wissenschaftlichen Aussprache: 18.07.2007

Berlin 2007

D 83

Zusammenfassung

In dieser Arbeit wird ein Steuerungssystem für Exoskelette vorgestellt, das elektrische Signale von Muskeln als zentrales Kommunikationsmittel zwischen dem menschlichen Benutzer und dem Exoskelett verwendet.

Diese Signale werden auf der Hautoberfläche oberhalb ausgewählter Muskeln aufgezeichnet und spiegeln die Aktivierung der Muskeln wider. Sie werden durch ein ausgeklügeltes, aber vereinfachtes biomechanisches Modell des menschlichen Körpers ausgewertet, um die gewünschte Handlung des Benutzers abzuleiten. Eine Unterstützungsbewegung für diese gewünschte Handlung wird berechnet und durch das Exoskelett ausgeführt.

Das biomechanische Modell vereint Ergebnisse von verschiedenen Forschergruppen aus der Biomechanik und Biomedizin und wendet dabei einige für die betrachtete Anwendung sinnvolle Vereinfachungen an. Es beinhaltet dabei Parameter, die bestimmte Eigenschaften des menschlichen Benutzers und dessen Zustand beschreiben. Für diese Parameter wird ein Kalibrationsverfahren vorgestellt, das sich lediglich auf am Exoskelett befindliche Sensoren stützt. Es bietet außerdem noch einen tiefen Einblick in die Funktionsweise des Modells.

Ein Exoskelett zur Unterstützung der Kniebewegung wurde entworfen und aufgebaut, um das neu entwickelte Modell zu validieren und die Interaktion zwischen dem Menschen und dem Exoskelett während alltäglicher Bewegungen mit Kraftunterstützung zu untersuchen. Die Ergebnisse dieser Untersuchungen werden ebenfalls präsentiert.

Abstract

This work presents a control system for exoskeletons that utilizes electrical signals from the muscles as the main means of information transportation between the human operator and the exoskeleton.

Those signals are picked up from the skin on top of selected muscles and reflect the activation of the observed muscle. They are evaluated by a sophisticated but simplified biomechanical model of the human body to derive the desired action of the operator. A support action is computed in accordance to the desired action and is executed by the exoskeleton.

The biomechanical model fuses results from different biomechanical and biomedical research groups and performs a sensible simplification considering the intended application. It contains parameters which reflect properties of the human operator and his or her current body state. A calibration algorithm for those parameters is presented which relies exclusively on sensors mounted on the exoskeleton, and provides deep inside into the mechanisms of the model.

An exoskeleton for the knee joint support was designed and constructed to verify the model and investigate the interaction between the human operator and the machine in experiments with force support during everyday movements. Those results are also presented here.

Acknowledgments

First of all I would like to thank my supervisor Günter Hommel for providing me with the platform to perform this research. His door was always open, and he was always ready to give advice when needed.

Furthermore I want to thank Konstantin Kondak who helped to initiate the project before I started to work on it.

Also my colleagues deserve a special thanks, especially Andreas Wege, who helped me to sort things out when we discussed topics that occupied my mind.

I would also like to thank all the students who worked with me, either during their diploma theses, as a student aide, or as part of a project group. With their support the project was considerably pushed forward, because they relieved me of developing those tons of details that always take so much time, allowing me to concentrate on the actual research.

A special thanks goes to the company Otto Bock for support and interesting input.

And last but not least I want to thank Laura, for her cheerfulness around me during the last year, when I needed it most. And for everything else.

Contents

List of Figures

List of Tables

1 Introduction

> "To move things is all mankind can do; ... for such the sole executant is muscle, whether in whispering a syllable or in felling a forest."
>
> (Charles Sherrington, *The Linacre Lecture, 1924*)

The human body consists of more than six hundred muscles, producing movements which are inseparably connected to its life. That does not necessarily refer to the vital functions of the body, like breathing or the heartbeat. It refers to movement in general, which is very important for all living creatures.

Aside from the immediate needs to eat, or the desire to communicate, be it with words, gestures or the whole body posture, mobility is one of the most important things in life. It does not only mean to travel around by car to a neighboring city or by airplane around the world. Already the common daily activities are very important for the quality of life: Getting up from bed in the morning and walking to the bathroom, the breakfast table, or the refrigerator. Or during work, whether inside an office or while carrying heavy parts in a factory.

Furthermore, lack of mobility often results in lack of participation in social life, which in turn leads to an undesired reduction of communication. It is also important for the body health to move around to activate the circulation system of the body, the muscles, and to breathe fresh air.

In this work a device and control system are presented which support a human operator with extra force in the knee joint. The device is worn around the leg and should increase his or her mobility by supporting the thigh muscles. Such devices are called *exoskeletons*.

According to [VBSS90], *"Exoskeletons in general, are structures of rigid links, mounted on the body of some living vertebrae and following the main directions and having the main joints of the living organism's endoskeleton."*

To put it into the context of this work, the exoskeleton is in permanent contact with the human body, resembling the limbs, with the intelligence and flexibility to perform a task originating from the human operator, while strength and endurance is contributed by the machine. As far as the operator is able to, the cooperation between the two is designed in such a way that the human is in control of the movements.

While the exoskeleton that is presented here - with one actuated degree of freedom in the knee joint - already offers some support, an extended exoskeleton covering more limbs and using the same interface has a variety of potential applications: For healthy people they can give support while carrying heavy loads, for example in a factory

environment, on a construction site, or at home, transferring the major part of the load to the exoskeleton to protect the body. Depending on the size, weight, and handling of such devices, they could even be beneficial in everyday life at home, especially for elderly people, to improve mobility. But not only healthy people can take advantage of the support: Exoskeletons can offer assistance to patients during rehabilitation of the locomotor system by guiding motions on correct trajectories to teach motion patterns, or give force support to be able to perform certain motions at all. This could intensify the training leading to better results and reduce the cost of the whole rehabilitation process.

But exoskeletons do not always have to work in cooperation with the operator: Exoskeletons also offer a unique way of giving force feedback to the human body. By applying some resistance to the movement of the operator they can act as haptic interfaces for virtual reality, telemanipulation, games, and entertainment: The virtual world can be felt and manipulated. For example, stairs can be simulated, the walking on muddy ground, or the effect of obstacles in an unstructured environment.

In a normal rather unstructured environment movements must be adapted permanently to the situation: Steps have to be climbed, inclinations of the floor have to be compensated, and finally, transitions between movements, like getting up from a chair, walking, and climbing a stair, have to be performed fluently.

If proper hardware exists that actuates sufficient joints to support those movements, the problem of recognizing the intended action of the operator arises. Only if this intention is known to the system it can properly react either by supporting the movement or by hindering it to simulate external influences.

Such a system requires a flexible interface, because of the wide range of movements to be performed, which collects all required information so that the intended action of the operator can be successfully derived.

As diverse as the applications are, so are the operators who will control the device: From healthy and fit persons, to weak and disabled patients. Sometimes, a defect in the locomotor system of the human body is also accompanied with a mental defect, complicating things even more.

Ideally, the control system has to be adaptable: The exoskeleton should offer maximum flexibility for healthy people who can take advantage of that. For disabled people the flexibility must be limited, to avoid undesired behavior of the system if it cannot fully be controlled by the patient. Complex control devices may require too much mental effort, or simply cannot be handled. In such cases the control system must take over some additional functions, for example, maintenance of postural stability.

1.1 Initial Considerations

As was motivated in the previous section, the numerous applications lead to a number of different potential users of such exoskeletons, everyone of them with different abilities, and with different requirements towards the control system. But all have in common that an intuitive interface reduces the mental load that is required to handle the system. The operator can focus on fulfilling a task with the exoskeleton rather than focus on mere control of the device.

When considering the choice of input devices for an intuitive human-machine interface, two aspects are important: First, the latency between the appearance of the desire to perform a movement and the actual support has to be short, and second, the flexibility of the interface to recognize a variety of movements needs to be given. Minimizing the latency is important for a powerful support through the exoskeleton. With a high latency, it is impossible for the operator to control the device, because he or she cannot react quickly to the resulting movement. The flexibility is important to allow the exoskeleton to work in real-life environments.

The optimum would be, if the human wearing the orthosis simply tries to perform the movement naturally, without any additional communication to the exoskeleton. This effort has to be recognized by the interface with appropriate sensors to activate the support. To come near this optimum, the interface should be connected as close to the neurological system of the human as possible.

The worst case would be to connect the exoskeleton to an external device, for example, a keypad or a wheel that has to be manipulated: First, the operator would have to transfer his or her desired movement into a movement that will manipulate the input device. Second, the signals have to travel completely through the body, and fulfill the movement that results in manipulation of the input device. Only then can the control system start the support.

By using the mechanical construction of the exoskeleton as the input device, the transferring thought in the brain can be omitted, reducing the mental load. Unfortunately, the interaction forces between the human operator and the exoskeleton cannot be measured accurately to determine the intended action: During contact with the environment it cannot be distinguished between forces acting from outside, and forces originating from the operator's muscles, which indicate the desire of motion.

Moving one step closer to the origin of the motion leads to the contraction of the muscles. Prototype sensors exist to measure the muscle hardness [YINH04, AJL+06] on top of the skin to derive the level of activation and the force output. But those sensors are not readily available, and only preliminary studies on the quality of the signals exist. But prior to the actual contraction of the muscle, thus even closer to the origin of the desire, a signal is emitted by the muscle which can be detected by either needle electrodes, inserted into the muscle, or surface electrodes, fastened on top of the muscle that should be observed. This signal appears during activation of the muscle, approximately 20–80ms [CK79, ZLMF95, VMIS90] before the resulting contraction begins.

Moving further along the neural pathways towards the brain would further reduce the latency of the system, but unfortunately no sensors are available to extract detailed information about the desired movement from the brain or spinal cord, necessary to correctly identify a variety of movements. Recent results from brain interfaces can be found, for example, in [BDK+06, Moo03, LSW+04, WMV00]. But it has to be kept in mind that not all movements are controlled by the brain, especially rhythmic movements, like walking, and cannot be extracted from there.

Motivated by this fact, this work focuses on investigating an human-machine interface based on the above mentioned biological signals of the muscles, the so-called electromyographic signals (EMG signals). Utilizing those signals is a good balance between proximity to the origin of the desire and interpretability of the signals. According to [BD85], electromyography is *"the study of muscle function through the inquiry of the electrical signal the muscles emanate."*

In the course of this work, electromyography always refers to *surface* electromyography, meaning that the sensors are put on the skin on top of the muscles. Beside the easier application of the electrodes, signals from those sensors give a better estimation of the overall activation of the muscle. Invasive electromyography is rather suited to investigate the internal processes within a muscle, which is not required here.

Advantages of using EMG signals in general are:

- EMG signals are directly linked to the desire of movement of the person, whether the movement is executed voluntarily or is initiated through a reflex response (except for people with certain diseases).
- No movement of the limbs is necessary: If the muscles are too weak or the external load too heavy, the *intention* of movement can *still* be detected, although no movement is performed.
- EMG signals are emitted unconsciously by the operator while he or she is performing the desired movement or is trying to do so. No additional mental load is created.
- The EMG signals are emitted early, *before* the muscles contract, because of signal propagation delays and because the muscle fibers need some time to contract.
- The measurement of the signals is not influenced by temporary external influences like contact forces, in contrast to force sensors.

Unfortunately, EMG signals have some properties which make the practical application difficult. Those are described in section 3.3.

For the purpose of this work, only healthy subjects have been regarded, because the EMG signals utilized here are always present. They may appear different, but the information which is transported remains the same: It is directly linked to the desire of movement. For patients this is not necessarily true, depending on the disease or injury.

The signals may be distorted or almost not detectable in extreme cases. Adapting the system to a variety of patients is a different and complex task, especially because more stringent safety measures have to be implemented.

1.2 Problem Formulation

The exoskeleton is in permanent close contact with the human body. Since it does not necessarily cover all limbs but only the ones that need support, the movement generated by the exoskeleton must be in concert with movements of the other limbs. Otherwise stable and safe locomotion is impossible. To achieve this, several problems have to be solved.

Intention Recognition and Support Computation To compute a sensible support for the actuation, the desired action of the operator has to be known to the system. As motivated in the previous section, the interface between the operator and the exoskeleton is based on EMG signals. In addition, some information about the kinematic state of the operator is known. The activation and the state information have to be read and evaluated with a short latency to deduct the desired action of the operator and subsequently a sensible support that can be contributed by the actuator. The latency of the system has to be kept so small, that stable movement with a useful gain is possible. Otherwise the supported leg would always move late, leading to an unbalanced movement. It is hard to quantify the latency more accurate than *short enough*. The validity of the realized latency can only be verified with experiments that show the overall performance of the system.

Predictability of Support The resulting support or joint trajectory has to be predictable by the operator, because he or she has to take the support into account during the movement. If the operator is surprised or frightened by the behavior of the system, he or she cannot take advantage of the support and will become cramped and feel unwell. But naturally, the operator has to learn to incorporate the given support into the movements. This can be compared to two people working together on the same task, for example, carrying a table. It is best if both can predict the behavior of the other one to coordinate the own movement appropriately.

Parameter Calibration A system that is working so close to a human operator possesses parameters that have to be optimized for the individual person. A calibration algorithm has to be developed and implemented that determines all necessary parameters. To avoid limitation of the practical application of such an exoskeleton, it is desirable that the calibration can be performed with a reasonable time and effort, and without a complex external calibration setup. Some of those parameters have to be calibrated whenever the exoskeleton is donned. It would render the idea of a mobile

system useless if the calibration could only be performed in a special place, or with a special laboratory setup.

Validation with Experiments The feasibility of the proposed system can only be verified in experiments with a powered exoskeleton because of the interaction between the human and the machine. The most important movements that should be supported by the system and are used for evaluation of the algorithms, are: getting up from a chair (similar to knee bends or when lifting an object), sitting down, slow walking, and climbing stairs up and down. Arbitrary transitions between those movements should be possible, and the movements should be adaptable by, for example, stride-length, gait velocity, and step height. To actually perform the experiments and to investigate the human-machine interaction, an exoskeleton has to be designed and constructed.

1.3 Contributions of this Thesis

The work presented here is a study on the interface and control system based on biological signals which are recorded from the operator. By proper evaluation of those signals, the intention of performing the movement can be detected, and the movement can be adequately supported.

Although biological signals are a very good interface between human and machine, those signals have rarely been utilized to control exoskeleton systems. As is described in section 2.1, many of the current projects rely on computation of inverse dynamics to estimate joint torques which are compensated in part by the actuation. Other projects do use EMG signals, but in a rather basic fashion, not utilizing valuable results from researchers of the biomechanical or biomedical communities who are experts in this field. A rare exception for an EMG controlled arm reading information from two muscles can be found in [RBFA01].

This thesis presents a control system with a new biomechanical model of the human body that fuses models developed in the biomechanical and biomedical communities, and adapting them to the specific requirements for exoskeleton control. Different findings have been integrated, and complex models have been reduced to a sensible level of abstraction in context of this work, as will be described later. To the best knowledge of the author, it is the first time, that a sophisticated biomechanical model utilizing EMG signals is applied to the control of a lower extremity exoskeleton.

Furthermore, a new calibration algorithm is presented that allows the determination of parameters depending on the operator and his or her current condition through sensors mounted exclusively on the orthosis, in order to allow a more natural, predictable, and smooth control.

The ability of the system to predict the intended motion of the operator is evaluated, and the whole system is analyzed during experiments with the actuated exoskeleton. Analysis of the experiments includes evaluation of the cooperation between the human

and the machine, and the unconscious human-machine interaction during the movements.

Finally, results from experiments with dynamic models are presented. Those models can be used to estimate joint torques to: (1) predict joint angle trajectories in advance in order to integrate algorithms for postural stability, and (2) to feed the calibration algorithm with additional reference values which cannot be directly measured with the exoskeleton.

In the presented approaches it is not necessary for the operator to learn a certain language or gestures to use the interface. The system is completely intuitive. The operator has to try to perform the movement, and the support will be added almost instantly.

1.4 Overview of the Work

The work is organized as follows: Chapter 2 gives an overview of other research projects with exoskeleton devices, and describes alternative human-machine interfaces implemented for those. It also summarizes achievements from the biomechanical and biomedical communities that are utilized in this work. Chapter 3 gives the reader an overview of the human body and the human locomotor system, and summarizes the process of movement generation from the initial desire to the resulting muscle contraction. It also explains origin and some properties of EMG signals and of human muscle to motivate aspects that have to be considered and have been implemented in the body model. Chapter 4 describes the evaluation of the EMG signals to recognize the operator's behavior, the subsequent computation of support action, and the control of the actuator. During this evaluation, model parameters are revealed that need to be determined. The calibration of those parameters is presented in chapter 5. Chapter 6 describes the mechanical construction, all sensors and computer hardware of the exoskeleton, before experiments are presented in chapter 7. They show the calibration as well as experiments performed with the actuated exoskeleton, and the system behavior is analyzed and discussed. Chapter 8 describes an alternative approach to analyze the intended movement of the operator with a dynamic rigid body model, and presents a simplified model to investigate possibilities to obtain more reference values for the calibration algorithm.

This work is concluded in chapter 9 with a summary of the results and an outlook on possible future improvements.

2 Related Work

Exoskeletons that support a human operator in different tasks are not a new topic of interest for researchers around the world. Important scientific research started in the 1970's where the group around Vukobratovic played a pioneer role: They had a clear goal in mind to help patients with defects in their locomotor system to regain walking capabilities. At this time, lack of computer processor power, heavy actuators (both pneumatic and electrical), and heavy power supplies limited the realization of interesting theoretical results. But nevertheless, researchers have been far from discouraged, and continued their work that led to interesting results [VBSS90] as can be seen in figure 2.1.

A large number of scientists have sticked to upper limb devices with a focus on hand prosthesis, because the required forces are rather low and helpful devices can also be constructed with a reduced degree of freedom.

In recent years, many exoskeleton projects emerged due to increased performance of computers, actuators, and power supplies. Potential applications that have occupied the minds of scientists and engineers for a long time seemed to become realizable.

The mobility of the operator is becoming more important, and due to the reduced size and weight of the exoskeleton the operator can carry it in addition to his or her own body. By that it can also support existing muscles, in contrast to a prosthesis that replaces missing limbs.

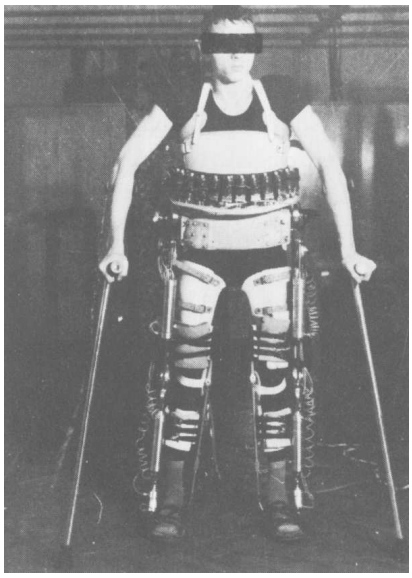

Figure 2.1: Patient with pneumatic exoskeleton with torso.

Potential applications range from military units to support soldiers in ground operations on one side, over support for factory workers, pure entertainment devices to rehabilitation aids and support for disabled or elderly people on the other side. A good overview of recent projects can be found in [Fer05].

But not only the mechanical part is an important field of research: If a lightweight and powerful exoskeleton existed, there still remains the problem of how to control the device. The interface between the operator and the exoskeleton is at least as important as the mechanical construction, since misinterpretation of the desired movement of the operator can lead to injuries or worse.

Different approaches to handle this problem exist, depending on the field of application of the exoskeleton. Generally, a good mixture of accuracy and reliability of detection, flexibility of the system and whether the operator has to adapt to the system or vice versa, has to be found.

In Section 2.1 exoskeletons from other research groups are described together with their control methods to summarize the state-of-the-art in this area. Section 2.2 summarizes biomechanical models, some of them coupled to EMG signals, in order to analyze behavior of the human body and effects of neurological injuries. From the wealth of information that is available, regarding the origin and properties of EMG signals, and of details about the mechanisms inside the human body, only those sources are selected that are related to this work. Results which have been utilized in this work are explicitly referenced in the respective sections.

2.1 Exoskeleton Research Activities

In this section, exoskeleton research activities of other groups are described. The groups are presented in separate sections for clarity. Details of the information varies greatly, depending on the published information.

Institute Mihailo Pupin, Yugoslavia: Exoskeleton Walking Aid

The primary goal of this research of Vukobratovic and colleagues was to develop exoskeletal devices that can be worn by patients with deficits in their locomotor system. Those devices were actively powered in the first versions by pneumatic actuators (around 1970), and in later versions by electrical actuators.

The first version had four actuated degrees of freedom (hip and knee joints, both legs). The ankle joint was initially passive and actuated in a later revision. The air supply for the actuators and the computer were both separated from the exoskeleton because of their heavy weight and large size.

Due to the low computational power of computers at that time, the joint angle trajectories have been computed off-line and were replayed during the experimental trials. No feedback from the patient or environment was incorporated.

A full paraplegic patient unfortunately could not walk alone with this device. He needed two people for support or a rolling aid to maintain balance.

To allow incorporation of overall stability control, the exoskeleton was extended in 1971 with a torso frame, adding two degrees of freedom to the system (in the frontal and sagittal plane). Software controllers were now responsible for moving the limbs along the desired trajectories, and overall stability was maintained by computing simplified correction terms with the zero moment point (ZMP). Those correction terms have been tailored to the task of walking on level ground. Actuation of the trunk was mainly used to maintain stability. Equipping the soles of the exoskeleton with force sensors allowed the incorporation of feedback from ground reaction forces to improve

stability and safety. It allowed the patient to walk alone, only with the aid of crutches, as shown in figure 2.1.

Figure 2.2: Patient with the electrical actuated exoskeleton.

After performing many experiments it turned out that the main drawback of the system was its heavy weight of 17*kg* (excluding air supply and computer hardware). This could be reduced in a new version to 12*kg* by using state-of-the-art actuators. But limitations still remained because of the air supply and large computer hardware: The system was confined to indoor use in a clinical environment.

A larger redesign of the exoskeleton led to a 16*kg* version with electrical actuation, that was able to follow the trajectories more accurately and more smoothly. Focusing on patients with dystrophy in the hip and thigh muscles, the degree of freedom was reduced, and the advent of microprocessors resulted in a more compact and completely portable version as shown in figure 2.2.

Controlling the different gait patterns was possible with different switches for (a) gait on level ground, (b) upstairs, and (c) downstairs. Gait pace, stride and turning to left or right was adjusted with switches. The gait cycle was always beginning with the left leg.

A 2*kg* battery allowed autonomous walking for 45 minutes on level ground or *"climbing 2-3 times the stairs to the third floor"* [VBSS90].

A good summary of the research and details of the control scheme was published in [VBSS90].

University of Berkeley, USA: BLEEX

The BLEEX project is running for several years already and has finally resulted in a company called Berkeley ExoWorks.

The focus of the Berkeley Lower Extremity Exoskeleton (BLEEX) project is to design and construct an exoskeleton for human strength augmentation. It should be used by soldiers, firefighters, and disaster relief workers to carry heavy loads faster and over longer distances in outdoor environments than would normally be possible.

Two versions of BLEEX currently exist. Some conceptual details can be found for version 1 (shown in image 2.3), whereas details of version 2 are held secret because of the U.S. military. BLEEX 1 consists of a metal frame that holds a backpack and two exoskeletal legs. Actuation is performed at the hip, knee, and ankle joint in sagittal plane, the remaining degrees of freedom in hip and ankle can be moved passively. Force sensors are attached under the soles of both feet.

It is designed for autonomous operation by a small fuel engine that supplies the onboard computer and the hydraulics with power [ZKC05].

Since the desired field of application demands a mechanically robust system, no sensors are used which are directly attached to the operator to record biological signals. Furthermore there are no sensors between the operator and the exoskeleton measuring the interaction forces since the points of contact between the two may be unknown or changing and are hard to measure.

Figure 2.3: BLEEX 1.

But nevertheless, the principle of the control scheme is to minimize the interaction forces between the human and the machine: The machine gets "out of the way" of the operator as quickly as possible, not to hinder the movement. Since the payload is attached to the exoskeleton, the operator does not feel the weight of the load [Kaz05].

To achieve this, a model of the exoskeleton was developed, and the inverse dynamics of this model delivers the positive feedback for a closed loop controller with a target value of zero. The gain is set slightly smaller than 1.0 to compensate the major part of the weight and inertia of the exoskeleton. The operator has to move the remaining part and his own body [KHS05, KS06].

There are no algorithms implemented to control postural stability to avoid unexpected forces acting on the operator. This has to be managed completely by the operator, requiring quick response of the system to operator imposed movement, so that counterbalancing movement and reflexes can be performed.

Due to the sensitivity of the model to the payload recent developments tend toward a hybrid control method using a position controller and the model based torque compensation described above, depending on the phase of gait, as published in [KSH06].

University of Michigan, USA: Powered Lower Limb Orthosis

The powered lower limb orthosis developed at the University of Michigan aims at rehabilitation of patients with neurological injuries. Investigations focus on consequences for the patient (immediate and long term), changes in movement behavior, and if certain simple control modes can be practically handled by patients.

The lightweight actuated orthosis, shown in figure 2.4, should allow more task specific training during gait rehabilitation by replacing expensive and strenuous manual assistance from a therapist. Hopefully, this will help to restore lost locomotion capa-

bilities of patients more effectively, concerning the quality of progress, and will reduce the costs of the whole process.

The orthosis is powered at the knee and ankle joint with artificial pneumatic muscles in sagittal plane. The air supply and the controller are not mounted on the exoskeleton. Since it is mainly designed as a rehabilitation device in a clinical environment, this is not a severe restriction. A detailed description of design and construction can be found in [FCH05].

Three modes of operation have been investigated [SGF05]: The first mode utilizes a foot switch and was used to study the mechanical performance of the orthosis during ankle plantar flexion[1]. This foot switch was mounted under the forefoot and maximally activated the pneumatic ankle flexor muscle when the forefoot touched the ground. When the forefoot lost ground contact during toe-off, the artifical muscle relaxed completely. Experiments showed that the artifical muscles were able to produce a substantial torque contribution to the movement.

The second mode used EMG signals of the soleus[2] as the controller input. The activation of the pneumatic ankle plantar flexor muscle was linearly related to the EMG signal of the muscle. Experiments involved thirty minutes of walking for healthy people. At the beginning, people could not benefit from the torque support offered by the actuation. But after a couple of minutes they could adapt their muscle activations properly, resulting in a kinematic gait pattern close to normal. The amplitude of the recorded EMG signal was reduced to about 50%. This is an important result, since it shows the capability of human to selectively change the muscle activations in walking to adapt to altered musculoskeletal mechanics.

Figure 2.4: Powered Lower Limb Orthosis.

The third mode was tested with partially paralyzed patients: A hand-held push button activated the artificial plantar flexor muscles proportionally while elastic cords applied the necessary torque to allow toe clearance during swing phase. The torso was supported with a harness that relieved the patient of 30–50% of the body weight. The push-button was either under control of a therapist or under control of the subject. Results revealed that soleus and gastrocnemius[3] activation was not decreased during both setups. For rehabilitation this is a useful result since the patient is not getting more passive as he or she gets support from outside,

[1] The ankle performs a *plantar flexion* when the forefoot is moving *away* from the body, in contrast to the *dorsiflexion*, where the forefoot is pulled *towards* the body.

[2] Ankle plantar flexor muscle in the back part of the calf, running from just below the knee to the heel.

[3] Ankle plantar flexor muscle. Running in parallel to the soleus.

which could hinder the rehabilitation progress. On the other hand, some patients could not use the push-button because it required too much mental effort. Subjects that were able to use it by themselves felt more comfortable being in control.

Yobotics Inc., USA: RoboKnee

RoboKnee is an exoskeleton developed by the company Yobotics, a spin-off from the Massachusetts Institute of Technology Leg Laboratoy founded in 2000.

The device is supporting the knee motion with a series elastic actuator attached to the thigh and shank as shown in figure 2.5. The control system calculates the actuator force based on the knee torque necessary for maintaining a statically stable pose. This is performed by estimating the ground reaction forces under both feet with two load cells. From the actuator length the knee angle is derived. It is assumed that the ground reaction forces are completely vertical and that the hip joint is located above the ankle joint. Through inverse computation of the dynamics of this model the knee joint torque is computed which is required to maintain a statically stable pose with the current angular configuration, even when the system is in motion. This knee torque is multiplied by a factor that defines the support ratio of the actuation, resulting in the amount of support the actuation is contributing to the motion [PKMC04].

Figure 2.5: RoboKnee.

Depending on the difference between the torque required to maintain a statically stable pose computed through this very simple model and the torque actually required to perform the desired movement, the muscle activation pattern that successfully performs the desired task with support can differ greatly from the pattern without support. In some cases, for example when climbing down stairs or sitting down, the user has to actively work against the actuation or the amplification factor must be set far below 1.0, offering less support. If the ratio is rather small, a reduction of the muscle activation will be sufficient to perform the movement. A longer training period can be necessary during which the operator learns to work with the exoskeleton.

The next steps of development involve inclusion of hip and ankle actuation and better detection of the operator's movement intent.

University of Tsukuba, Japan and Cyberdyne Systems: HAL

The Hybrid Assistive Leg (HAL) is developed in cooperation of the Japanese University of Tsukuba and the Cyberdyne Systems company. Different prototypes of the mechanical construction exist, of which two are shown in figure 2.6. Motivated by the rapidly aging — but technology-loving — society in Japan, the project focuses on supporting elderly and gait disordered people.

During the course of the project, different control strategies have been developed with the primary interface being EMG signals from the operator's muscles. Early prototypes consisted of a system with four actuated joints at the hip and knee of both legs, with passive joints at the ankles. The latest development (HAL 5) also includes actuated shoulder and elbow joints, as shown in figure 2.6.

Figure 2.6: Hybrid Assistive Leg (HAL): version 3 (left) and version 5 (right).

The first published control strategy for HAL is the "phase sequence algorithm" that was demonstrated for the stepping-up motion [KS01]. In this approach the stepping-up movement is subdivided into five phases which are handled by a state-machine: leg raising, stepping up, leaning forward, hind leg raising, torso erection. Transition to the next state is performed when the joint angles and the center of gravity measured beneath both feet meet certain criteria. Each phase has an associated predefined trajectory for all actuated joints. The EMG signal is picked up from the rectus femoris[4] to initiate the movement. After reading an increased muscle activity, the EMG signal is evaluated for 300ms and the numerically integrated postprocessed EMG signal is converted into a *hip angle* by a linear relationship that was calibrated before. This angle is used as the reference for the position controller of the system. After the 300ms interval the state machine can decide the transition based on the angle measurements, and predefined trajectories are used for the rest of the movement.

An improved version of this control structure with an extended state machine incorporating standing up, sitting down and walking can be found in [KKS03].

But this control scheme lacks flexibility and was replaced with newer versions of HAL [KS02b]: Four muscles responsible for flexion and extension in the hip and knee joints have been recorded, and support torques for the actuation in those joints have been computed in linear relation to the postprocessed EMG signal. The parameters of this relationship have been calibrated by the following setup: The operator was sitting upright on a chair without ground contact below the knee and above the hip. The actuators produced varying torques from 0Nm to 32Nm in 8Nm steps, while the operator countered the torque with his own muscles and tried to maintain the upright position. The postprocessed EMG signal was then related to the torque of the actuators. The estimated torques based on the EMG measurements are used as the target values of the control algorithm. To remove discomfort for the operator that was observed during experiments, the torque estimation had been modified: The hip torque calculation neglects the hip flexor activity during floor contact with the respective leg while walking, to make the system response more comfortable. The standing up movement uses a feedforward controller with four phases: (1) sitting, (2) hip flexion and knee extension, (3) hip and knee extension, (3) standing. During phases (1) and (4) the controller out-

[4]The rectus femoris is a knee extensor muscle.

put is 0Nm for all joints, during (2) and (3) *fixed* torques are used for each joint in each phase ($\pm$20Nm depending on direction of movement). State transitions are performed when floor reaction forces and joint angles meet certain criteria [KS02a].

To further improve the performance of the system, the exoskeleton is modelled through an inverted pendulum with gravity, inertia, and viscous friction. A compensation term is added to the supporting torque to regulate the joint impedance [LS02a, HKS05, LS02b]. Other small variances of the control schemes can be found in [LS03, KS04]

In figure 2.6 (right side) the latest development, HAL-5, is shown. Unfortunately no details have been published so far.

Kanagawa Institute of Technology, Japan: Power Assisting Suit

Researchers of the Kanagawa Institute of Technology have developed an exoskeleton for assisting nursing personnel when handling patients, as shown in figure 2.7.

The suit covers shoulders, arms, torso, waist and both legs, weighting a total of 30kg. It supports the operator at the elbows, waist and knees with pneumatic actuators.

The controller structure calculates the joint torques required to maintain a statically stable pose by computing the inverse of a rigid body model that takes into account the current joint angles and masses of the components of the exoskeleton and the weight of the patient. The weight of the patient is measured beforehand [YINH04].

The operator's own muscle force is recorded by muscle hardness sensors which consist of mini load cells with contact plates taped to the skin sitting on top of the muscle bellies, and will probably be integrated into the control in later versions.

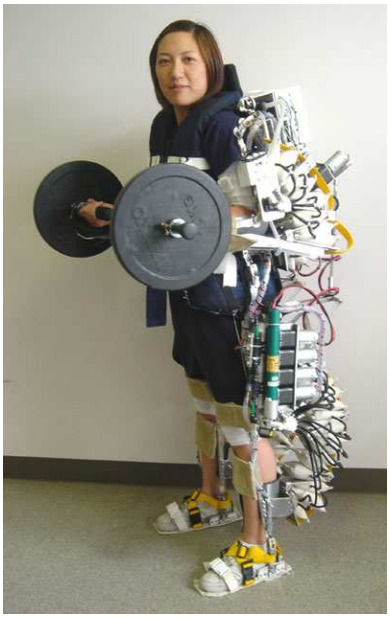

Figure 2.7: Exoskeleton to support nurses while carrying patients.

Interaction with the exoskeleton is based on the fact that the torques imposed by the operator on the joints of the exoskeleton overlay with the torques produced by the actuators, similar to the RoboKnee. Arbitrary movement patterns are possible, although not necessarily intuitively at first: Depending on the accuracy of the inverse calculation and the effects of the omitted dynamics of the system, necessary muscle activations to move in concert with the exoskeleton and the load can be very different from the intuitive activation patterns. Handling the patient with the exoskeleton may require some training.

Nanyang Technological University, Singapore: NTU Exoskeleton

The exoskeleton developed at the Nanyang Technological University is designed for performance augmentation of healthy people, like infantry soldiers or emergency personnel. It should allow the operator to carry heavy loads faster and over longer distances compared to normal conditions.

In contrast to more traditional exoskeletons, the NTU exoskeleton does not embrace the operator at the legs, except for some sensors to read current joint angles. Instead, it features two actuated legs which hold a payload frame, and the operator is standing only on the footplates of the exoskeleton, as shown in figure 2.8. The exoskeleton is completely carrying itself and the payload, and is only *guided* by the operator.

The idea of the control scheme is to follow the trajectory of the operator's foot with its own footplate during the swing phase of each leg. This allows the operator to provide information about the desired velocity and stride length of gait. The required information is taken from the operator's joint angles, and not from contact forces between the exoskeleton and the human.

Figure 2.8: NTU exoskeleton.

In theory, one would expect it to be difficulty to perform a target motion with the foot, while being rigidly attached to the footplate of the exoskeleton that should follow the motion. Unfortunately, it is not mentioned in the publications how this problem is solved.

The exoskeleton maintains balance during the motion by utilizing the concept of the ZMP: The controller moves the actuated joints in such a way that the ZMP remains within the support region. The support region is defined as the footprint, if only one foot touches the ground, otherwise it is defined as the convex area encompassing both footprints. Modification of the ZMP by the controller is performed by changing the angle of the exoskeleton "trunk", which is the payload frame. The target ZMP the controller tries to follow is the ZMP measured from the human body alone. The ground reaction forces for computation of the ZMP are measured with force sensors embedded in the feet of the exoskeleton [LLY, LL04].

Tohoku University, Japan: Wearable Walking Helper

The Wearable Walking Helper (WWH) of the Tohoku University of Japan is a lower extremity exoskeleton, covering both legs. The hip and ankle joints are both actuated

in sagittal plane with a rotatory actuator in the hip joint, and a long linear actuator connecting the hip and ankle to actuate the knee joint.

The goal of the WWH is to support the operator during walking and standing by compensating some of the body weight. The required support is calculated by an inverse model without taking into account joint angle accelerations [NSWK05a]. Joint angles of the hip, knee and ankle are measured and fed into a planar model of the operator consisting of a four link open chain. The setup used for the experiments involved only one actuated leg, the other was not regarded.

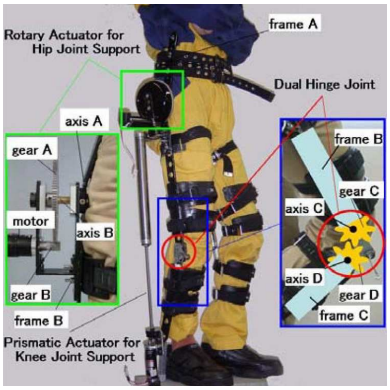

Figure 2.9: Anti-gravity system.

The support can be adjusted and is calculated through the torque required to maintain a statically stable pose multiplied by a gain. In the experiments presented in [NSWK05a] the gain was set between 0.0 and 0.5 for the knee and hip joints.

Experiments performed with the exoskeleton showed that it could add support to the knee extension task. This was tested by standing on one foot, and measuring the force acting on a sensor installed between the non-supporting foot and the floor while maximally activating the knee extensor muscles. A second experiment showed that it was possible to perform significantly more knee bends when the support was activated.

The control method was improved in [NSK05], taking into account ground reaction forces with force sensors to support walking. The system was investigated with stepping up and down, and while walking on a treadmill. The strain was measured through the heartbeat of the subject, and was shown to be reduced. In [NSWK05b] the system was enhanced with dynamic terms, and experiments included the sit-to-stand and stand-to-sit movement without taking into account external contact forces from the chair. The experiments showed a significant decrease in muscle activation revealed by EMG signals.

University of Washington, USA: Arm Exoskeleton

This project is now homed in the BioRobotics Laboratory of the University of Washington. Early work has been performed by Rosen *et al.* in the Tel Aviv University in Israel. The exoskeleton consists of one arm with actuated shoulder and elbow joints with one degree of freedom each, and is attached to the wall as shown in figure 2.10.

It is one of the rare projects that utilizes EMG signals in a similar fashion as the work presented here: by feeding them into a complex body model to calculate the resulting joint moment which is used by a torque controller.

In early work of this group a Hill-type muscle model [Hil38, Win90b] was compared to a neural network, utilized to predict the joint moments [RFA99] during elbow flexion and extension tasks while holding a load. It showed a slightly better performance of

the neural network approach. It has been assumed that the neural network adapted itself better to the specific circumstances, namely the task and operator, but would not be able to perform so well in previously untrained movements as the more general Hill-type muscle model. The Hill-type model did not contain any parameters that had been calibrated prior to the prediction experiments, aside from the normalization of the EMG signals to a maximum value, recorded during maximum voluntary contraction.

Figure 2.10: EMG controlled arm.

Those experiments led to the the EMG-controlled arm exoskeleton presented in [RB-FA01] and shown in figure 2.10. The experiments involved lifting a weight by flexion and extension of the elbow joint in cooperation with the rotatory actuation of the exoskeleton. The actuator supported the movement with additional torque, based on the estimation of the operator's own torque contribution from the EMG signals multiplied by a support ratio.

A parameter optimization of the EMG processing algorithm was presented for an improved version of the model in [CRP+05] and is based on a genetic optimization algorithm.

Latest developments in this project include the analysis of kinematic and dynamic data of daily actions [RPM+05] to design a seven degree of freedom exoskeleton arm [PR06].

The biomechanical model developed for this arm exoskeleton differs in some aspects to the model presented in this work: It is more complex, and contains more properties and parameters, and details of the modeling are different. Those details can be found in [RFA99, CRP+05] for comparison. Furthermore, the calibration algorithm as a whole is different from the approach presented in this work.

Upper Extremity Exoskeletons

Surveying the literature reveals that most of the research utilizing EMG signals to control a robotic device is performed on the upper extremities with focus on extending limbs of amputees, like replacing the hand [ZKWBH95, ITKI92, HG02, FTKO03, KOT92], and, in more recent years, to support rehabilitation. In those scenarios, classifying the recorded signals into specific patterns which are related to predefined movements is a well accepted approach. Classification has been performed with a variety of different methods, for example, with fuzzy rules for multifunctional hand prostheses [AW05, CYL+00], and with neural networks [CMM05, HC99, KOT92, AK00, KYNK04, NKYK03]. In [Whe03] evaluation of the signals was performed with a Hidden Markov Model.

A recent example of EMG evaluation to control an actuated hand orthosis has been published in [MFG05]. There, EMG signals have been evaluated continuously with a

moving average filter, and have been compared to a predefined threshold. When the threshold is exceeded, a preset hand closing motion was performed. Upon relaxation of the muscles the hand was opened again.

In [DLM04] a handexoskeleton with pneumatic actuators is tested with three different control schemes to restore dexterity of completely paralyzed hands: (a) threshold-based binary on/off control, (b) control signal is set proportional to EMG activity, (c) evaluation of the EMG signal of the biceps muscle activated during a reaching task, and learning the timing of this muscle's activation in relation to the pinch operation in the "reach and pinch"-task. In cases (a) and (b) the EMG signals have been recorded from muscles of the contralateral side, whereas in (c) upper arm muscles from the same side as the paralyzed hand have been used.

In [AAB05] a forearm exoskeleton for rotation around the axis of the forearm is controlled by mapping the muscle activation linear to the target angle, if the activation exceeds a certain threshold.

An EMG-based shoulder exoskeleton with two degrees of freedom is presented in [KIY+03]. EMG evaluation is performed with a combination of fuzzy-rules and a neural network to take into account the displacement of muscles in different shoulder configurations.

Other exoskeleton devices for shoulder, arm, and lower back support can be found in [KET+03, KS05, NNH+98, KLLK05, TC03, NKYK03].

2.2 Biomechanical Models

For the lower extremities, pattern classification and replaying predefined trajectories is not possible if the system should permit the operator to react to different circumstances in a natural environment, including obstacles, floor inclination, and steps. The EMG signals have to be evaluated in more detail, either by training a more complex black box, or by implementing a body model where the desired motion can be read from the model behavior. As a matter of fact, the question of complexity of the model arises.

Such models have been developed by researchers with a biomechanical or biomedical background [ZW90]. They have been mostly used for the study on the locomotor system of the human body to investigate how neurological signals generate movement, how this movement is controlled and how diseases affect the locomotor system. They allow, besides a detailed analysis of the operator's intention, an interesting and deep insight into the behavior of the human locomotor system. The drawback of such models is the potentially large number of parameters that need to be adjusted. But in contrast to the black box models where those parameters have to be learned with a large set of training data, many parameters can be identified by explicit measurement or can be approximated by constant values found in the literature from previous experiments.

But still, it is very easy to drown in the great number of details scientists have found out. In [Hat81] for example, chemical processes of the muscle fibers are modelled to explain muscle contraction in great detail.

A good overview and comparison of different models, for example, the molecular level versus the macroscopic level, can be found in [Zah90]. In [SBHR00, BD85] different aspects are summarized that can affect the origin, transmission and recording of EMG signals. Important work describing properties of muscle and tendon on a very useful level is published in [Zaj89].

A very important and popular biomechanical model of the human lower extremities has been published in [DLH+90]. It is in part a collection of anatomical data presented in previous work by other researchers, but it also contains new and important data of tendon pathways defined by wrapping points that are applied in certain intervals of joint angles. Those waypoints are needed for accurate modeling of skeletal muscles considering different joint angles, and to compute moment arms and resulting joint torques. Previous work mostly reported only points of origin and insertion of muscles measured from cadavers. The background of this research was to simulate how orthopedic surgeries affect muscle forces and torques around joints. Figure 2.11 shows a screenshot of the simulation software.

Modeling the behavior of individual muscles is frequently performed through Hill-type muscle models. Those models are describing the behavior of muscles with data recorded from observation during experiments (phenomenological models), not from their internal processes. They incorporate a contractile force producing element, and parallel and series viscoelastic elements modeling the passive properties of the tissue. A good overview and analysis of those models can be found in [Hil38, Win90b].

Figure 2.11: Screenshot from the simulation software SIMM, presented in [DLH+90].

In recent years modern versions of the Hill-type model have also been used to analyse human movement with respect to the neural commands that activate the muscles. Results are used to gain knowledge about strategies of muscle activation during locomotion [Nie03] and finger movement [MA04], or effects of injury and disease [MGLB02]. The implementation of a detailed muscle model to be used for a reliable controller for functional electrical stimulation is described in [BCL+00].

Such combination of EMG evaluation and muscle models have been developed for the lower back, elbow, shoulder, knee, and ankle joints. A good compilation of references can be found in [LB03]. All those models require transfer functions which relate neural activation, measured through the EMG, to muscle activation, and muscle activation to muscle force. Different EMG to muscle activation functions are suggested in for example [Zaj89, LB03, MB03], and different relationships have been observed during experiments with individual muscles [BD85].

An improved version of the lower extremity model [LB96] was utilized in [LB03],

where the knee torque was estimated based on EMG readings for different tasks including isokinetic dynamometer trials (active and passive flexion/extension under different loads and different velocities), running, crossing and cutting steps. The body model in this work consists of 13 lower leg muscles, some of which could not be measured directly. Parameter optimization was performed with inverse dynamics, fed with limb joint kinematic data that was recorded with a 3D-vision system. The data processing was performed offline, and the system was not utilized to control a device. Instead, it demonstrated the validity of the model. During calibration, the parameter set was subdivided into EMG-related parameters and geometry parameters. The EMG-related parameters are sensitive to electrode placement, skin properties and the overall condition of the subject and have to be recalibrated for every experimental session. The second group needed only to be calibrated once for every subject. Repeated trials with weeks in-between showed that it was indeed sufficient to recalibrate the EMG-related parameters, further increasing the trust in the model. The mean residual prediction error was about 12Nm.

In [MGLB02] a virtual arm controlled with EMG signals is presented. The aim of this study was investigation of neuromuscular control of arm movements. A biomechanical model for the human arm was developed, incorporating all major muscles spanning the elbow. The joint torque estimation was based on recorded EMG signals. During the experiments the subject's monitored arm was fixed and hidden from observation. The only visual feedback was provided through a computer generated 3D-visualization of the arm movement as predicted by a simulation using the estimated torque. With those experiments muscle synergies and muscle activation strategies have been examined. In a second experiment, change in muscle activation patterns in response to a simulated neurological injury was investigated.

Several other projects also investigated teleoperation with EMG signal evaluation [AK05, AK06, FTKO03, FWB+96].

Another recent development uses two different ankle models to control an ankle foot prosthesis: The first model utilizes a two-dimensional dynamic ankle model in sagittal plane with passive damping, stiffness, and the force-velocity property[5] being modelled. The second method uses a neural network to predict the resulting ankle position from the EMG signals. Experiments were performed with a below knee amputee, whose residual muscle activity from muscles moving the ankle joint was recorded with fine-wire electrodes. The subject was standing on a platform that could imitate an ankle foot prosthesis, and was asked to perform ankle movements with the residual muscles from the affected leg. This resulted in movements of the platform. Analysis of the experiments revealed that the muscle model turned out to be superior to the neural network prediction in terms of producing smoother and more natural trajectories [ABH05].

[5] The force a muscle can produce is depending on the length change per unit of time. This is explained in section 3.2.

2.3 Remarks

The previous sections have given an overview of research projects with exoskeletons and evaluation of EMG signals. Two main observation can be made:

- Control strategies without EMG signals are mainly employed where mechanically robust and reliable system behavior in unstructured environment is required, or where ease of application is needed. EMG-based control algorithms are mainly used in medical applications because of the supervised environment, or where simplified, delayed and fault-tolerant signal evaluation is possible, for example, for a hand prosthesis with a limited degree of freedom.

- Applications where EMG signals are utilized in a more elaborate fashion are developed with a biomechanical or biomedical background mainly for offline analysis to study behavior of the human body. Systems originating from robotics research groups are lacking sophisticated EMG-based models which can improve the system behavior.

Unfortunately there seems to be a big gap between the robotics research groups and the biomechanical/biomedical groups. Interesting and important results achieved in the latter two groups are not wide-spread in the robotics community, although the integration of recent findings can considerably improve the performance. One rare exception is presented in [RBFA01], where sophisticated EMG evaluation is applied to an exoskeleton system.

The reason for this may lie in the complexity of the unfamiliar topic which needs to be reduced to a practical level. Simplification of those models needs to be performed to keep the number of parameters and the computational complexity in reasonable limits. This work tries to close the gap a little by applying results from the biomechanical and biomedical communities to a robotics system.

3 Biomechanics of the Human Body

The use of EMG signals has been motivated as the main way of information transportation between the human operator and the exoskeleton in section 1.1. This chapter describes the processes in the human body from the thought in the brain to the resulting muscle activations and reflex actions during which EMG signals are generated.

The body functions described in the following sections are valid only for healthy persons, and only aspects which are directly related to this work and the implemented human body model are described. The level of detail is limited to the basics but explains the origin of modelled properties and gives insight into the simplifications that have been applied during development of the model. All descriptions refer to skeletal muscles. More detailed descriptions can be found in [KSea95, SD88, Jea90].

The following section 3.1 describes the way a thought or reflex initiates a motion, to give the reader an overview of the neural information flow in the body and the resulting motion. Section 3.2 focuses on muscle properties and how force is generated in a more detailed way. Section 3.3 describes origin and characteristics of EMG signals. Section 3.4 gives some remarks on modeling in the light of this particular application.

3.1 From the Brain to the Muscles

The motor system of the human body is responsible for transferring neural signals to physical energy: A thought initiates a motion. But not only conscious brain activity, but also input from the sensor system of the human body can initiate movements. During reflexes physical energy is converted into neural signals which in turn stimulate muscles without going through the brain.

According to [KSea95], movements can be divided into three categories depending on the influence of voluntary control:

- **Reflex responses** are the simplest form of motor behavior. Examples are the withdrawal of the hand from a hot object, the knee jerk or swallowing. Reflexes are rapid, stereotyped responses and can be performed without any voluntary control, although they can be modified with conscious effort.
- **Rhythmic motor patterns** are typically initiated and terminated voluntarily, but in-between no conscious effort to maintain the repetitive movement is necessary,

although it can be adapted to certain circumstances. Examples for this type of movement are walking, running, or swimming.

- **Voluntary movements** are the most complex movements, like playing an instrument and driving a car. Those movements are goal directed and can be improved with practice. The better those movements have been learned, the less conscious effort they require.

According to the different levels of voluntary influence on a movement, the human motor system can be divided into three levels of motor control, as shown in figure 3.1: the *spinal cord*, the *brain stem* and the *motor cortex*. Those levels are organized hierarchical and in parallel with the spinal cord being the lowest level: Reflexes and rhythmic motor patterns have local circuits which are optimized for quick responses. The brain stem is the next level of control and is divided into two parts: (1) the medial systems which are mainly responsible for controlling the body posture by integrating information from the eyes and the balance system, (2) the lateral systems, which are connected to distal muscles of the limbs, like arms and hands, to control goal-directed movements. The motor cortex is the highest level of control with the highest layer of abstraction. It is responsible for coordinating and planning complex movements. To perform this, it is connected to the cerebellum and the basal ganglia. During a voluntary movement, the cerebellum compares the actual movement through responses from the sensory systems to the desired movement, and corrects the movement if necessary. The output to the cerebral cortex is excitatory, initiating movements. The basal ganglia, on the other hand, works inhibitory on the cerebral cortex, surpressing certain movements, to allow others to be performed. The basal ganglia and the cerebellum are connected to the motor cortex via the thalamus, a relay station.

The hierarchical structure of the control system ensures that simpler movements can be performed without conscious effort. But through the additional parallel neural pathways it is possible for higher levels to modulate lower levels to adapt the movement to special circumstances, for example, changing the stride length or stepping over an obstacle.

In addition to the neural commands from the higher levels, every level is fed with sensory information that is needed for appropriate control. There is a permanent flow of information about position and orientation of the body limbs, the degree of muscle contraction, and information about events in the environment through the skin or eyes.

All pathways from the different control levels are connected in complex networks of interneurons in the spinal cord. They are ultimately converging into common pathways that lead to the motor neurons which innervate the muscles. Those motor neurons are situated in the spinal cord and connect to the skeletal muscles by axons (nerve fibers).

The signals (action potentials) sent over the axons to the muscles lead to contraction of muscle fibers, shortening the muscle. Since every muscle is connected to the human skeleton at at least two points spanning one or more joints, the shortening of the muscle creates a torque in those joints. If the torque is large enough, a motion is performed.

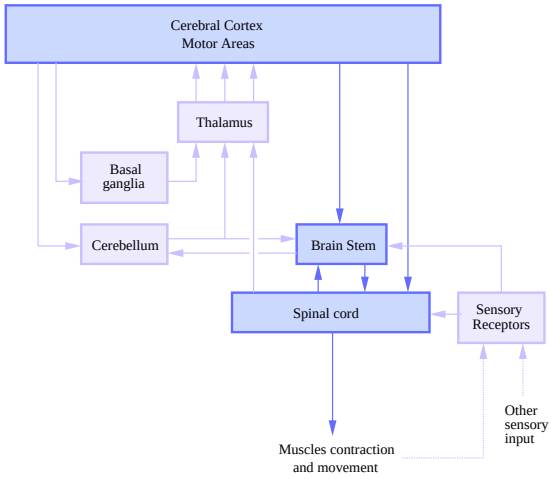

Figure 3.1: Motor system of the human body. The motor areas of the cerebral cortex are responsible for complex voluntary movements, passing control signals to the lower levels of the hierarchy: the brain stem and spinal cord. There, rhythmic movement patterns and reflex responses are generated, which can be modulated from the higher levels through the parallel pathways. The cerebellum is responsible for correcting the current movement to resemble the desired movement (refer to the text for details). Adapted from [KSea95].

Details on the control of human walking is still a matter of current research. A recent review on this topic can be found, for example, in [Nie03, KSea95].

3.2 Muscle Physiology

The purpose of muscles is to generate force between two end points either actively through contraction or passively through their resistance to stretch.

The muscle belly is connected to the bones or other muscles at points called *origin*[1] and *insertion*[2] by tendons. Muscles and tendon are surrounded by connective tissue holding them together and separating them from their neighborhood. They also allow the muscle to slide inside this hull during movement, and guide it along a predefined path preventing displacement to the side [Uhl96].

The muscle belly itself is composed of muscle fibers that are grouped into *fascicles* (muscle fiber bundles) as shown in figure 3.2. Those fibers can have a length of approximately 15cm and a diameter between 10μm and 100μm in human.

Each fiber is composed of so-called myofibrils: tightly packed filaments that go from one end of the muscle to the other. Those myofibrils are the contractile elements of muscle and have a diameter of approximately 1μm.

Each myofibril is in turn further subdivided into a chain of sarcomeres, the smallest contractile elements of a muscle. Those sarcomeres have border walls called *z-lines* to

[1] Proximal (closer to the center of the body) point of attachment of the muscle to the bone.
[2] Distal (farther away from the center of the body) point of attachment of the muscle to the bone.

which thin strands of actin filaments are attached. The distance between those z-lines is approximately 2μm to 3μm, depending on the level of contraction of the sarcomere. Located between those actin filaments are the myosin filaments.

When a muscle is activated, a biochemical process lets the actin filaments glide deeper between the myosin filaments (cross-bridge binding), so that the overlapping region increases. Since the actin filaments are attached to the z-lines, the distance between those z-lines is decreased. The sarcomere shortens, and so does the whole muscle. A sarcomere can shorten to about 57% [BD85] of its rest length. It cannot actively increase its length again. This can only be achieved through forces from outside, for example, through contraction of antagonist[3] muscles.

The force a sarcomere can produce depends on its length, that is, the distance between the z-lines: The longer the sarcomere, the smaller is the overlapping region of the actin and myosin filaments, and the smaller is the resulting force. If the sarcomere gets shorter on the other hand, filaments start to interfere, resulting in a smaller force. Inbetween an optimal length exists. Extrapolating this for the whole muscle results in a force-length relationship that has a maximum at the *optimal muscle fiber length* and declines in both directions as shown in figure 3.3, left side [GHJ66, DLH+90].

At a length above the optimal muscle fiber length, a passive force appears and steadily increases with length. This force is a result of the elasticity of myofibrils [Zaj89].

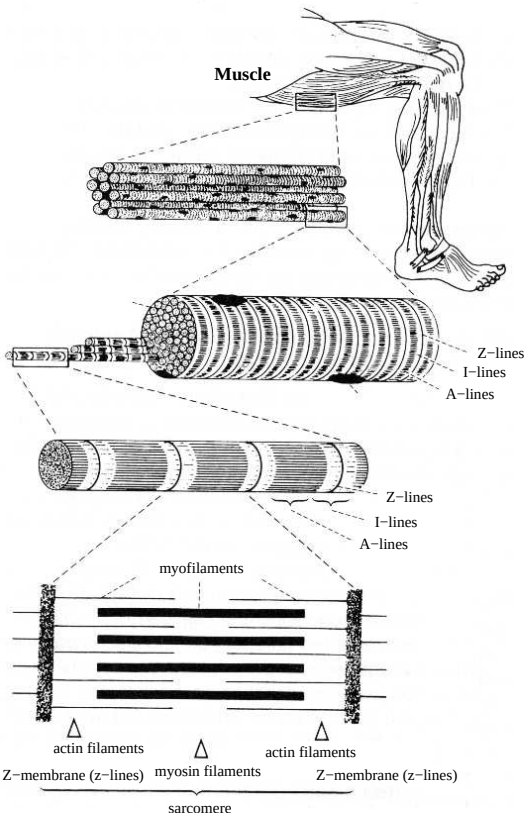

Figure 3.2: Components of the human muscle: The upper images show the whole muscle that is composed of muscle fiber bundles which are arranged in parallel. Each muscle fiber bundle in turn consists of muscle fibers, which are composed of a chain of sarcomeres. During muscle activation, a biochemical process increases the overlapping region of the actin and myosin filaments and pulls the z-membranes closer together, which results in muscle contraction (adapted from [Uhl96]).

Furthermore it has been observed, that the optimal muscle fiber length for the active force-length curve decreases with an increase of muscle activation by about 15% [BLMB04].

The muscle force is also influenced by the change of length per unit of time (muscle

[3] Antagonists act in opposition of the agonist muscle, which mainly creates the movement.

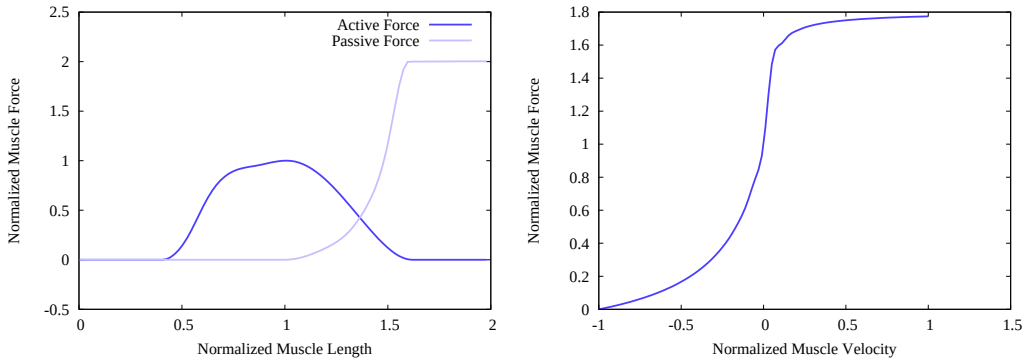

Figure 3.3: Muscle force relationships: (left) muscle force as a function of the length of the muscle fibers, normalized to optimum muscle fiber length, (right) muscle force depends on the muscle velocity, normalized to maximum muscle velocity (data from [DLH+90]).

velocity). During lengthening of the muscle, the sarcomere force is increased mainly due to stretch of elastic elements. During shortening on the other hand, the sarcomere force decreases to zero in a hyperbolic fashion. This is the case because the filament movement of actin and myosin that leads to contraction is a repeated process of binding and detachment with a limited frequency: the cross-bridge cycling. If the muscle shortens very fast (negative velocity, for example, due to external forces) the cross-bridge cycling is not fast enough to produce any force while shortening the muscle. Looking at the muscle as a whole, this introduces a force-velocity relationship of the muscle as shown in figure 3.3, right side. It is usually normalized to the maximum contraction velocity of muscle, which can be approximated through ten times the optimal muscle fiber length per second [Zaj89]. More details of the origin of the force-length and force-velocity relationships can be found, for example, in [Win90a].

Depending on the task the muscle is mainly involved in, there are differences in the macroscopic arrangement of muscle fibers: The more muscle fibers are working in parallel, the stronger a muscle is. The longer the muscle fiber, the more sarcomeres are linked in series, and the faster the contraction can be. Given a specific volume for a skeletal muscle, the arrangement of fascicles is optimized as shown in figure 3.4: When a large force production is required, the fascicles are arranged in parallel and at an angle to the direction of pull. This puts more fibers in parallel within the same volume by sacrificing a larger range of contraction. Those muscles are called *pennate muscles* [Mar98, Uhl96]. The angle between the fascicles and the direction of pull along the tendon is called *pennation angle*. This angle is not fixed but varies with the contraction of the muscle as depicted in figure 3.4e.

A measure for the strength of the muscle is the *physiological cross-sectional area* (PCA) of a muscle that takes into account the number of sarcomeres in parallel with the angle of pull of the muscle. According to [MWW83], the relationship between cross-sectional area of a muscle and its maximum force is linear. The PCA is defined

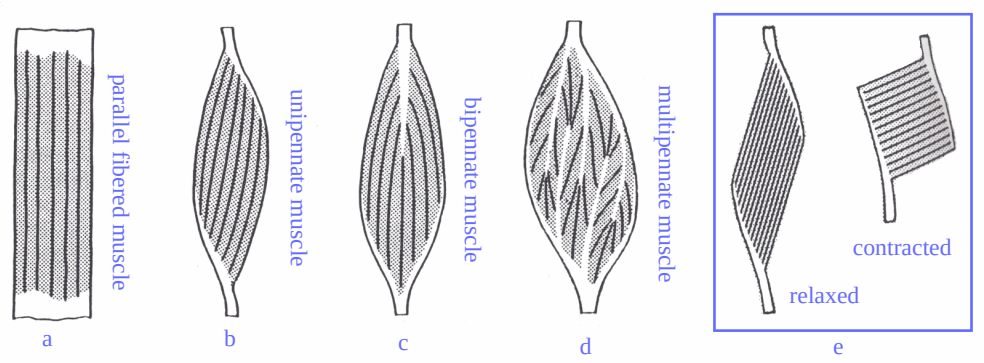

Figure 3.4: Illustration of different muscle structures (adapted from [Uhl96]). Figure e) shows the change of the pennation angle in unipennate muscles through muscle contraction.

according to [Win90a] as:

$$PCA = \frac{m \cdot \cos \phi_o}{\rho \cdot l} \tag{3.1}$$

with the pennation angle, ϕ_o, the mass of the muscle fibers, m, the density of the muscles, $\rho \approx 1.056 g/cm^3$, and the length of the muscles, l. %PCA is the cross-sectional area as a percentage of the total cross-sectional area of all muscles crossing a particular joint. Table 3.1 shows details for some muscles crossing the knee joint.

Muscle	**PCA** $[cm^2]$	ϕ_o [°]	**%PCA**	$\mathbf{F_{Max}}$[N]
Gastrocnemius	30.0	15	19	1605
Biceps Femoris (small)	6.8*	23	3	400
Biceps Femoris (long)	15.8	0	7	720
Semitendinosus	4.4	0	3	330
Semimembranosus	22.6*	15	10	1030
Vastus Lateralis	30.0	5	20	1870
Vastus Medialis	26.0	5	15	1295
Vastus Intermedius	25.0	5	13	1235
Rectus Femoris	12.5	5	8	780
Sartorius	1.9	0	1	105
Gracilis	7.5*	3	1	110

Table 3.1: Examples of muscle parameters with physiological cross-sectional area, PCA, pennation angle, ϕ_o, and maximum force, F_{Max}. Data was taken from [Win90a], except values marked with *, which have been derived from their %PCA-values.

The motor system can measure the actual muscle length and velocity through muscle spindles which are integrated in the muscles and tendons. They are linked to the spinal cord by nerve fibers to give feedback to the motor system [Uhl96, KSea95].

3.3 Muscle Activation and Electromyography

Muscle contraction is a response to signals originating from the so called α-motor neurons sitting in the spinal cord or brain stem. Those neurons create an electrical impulse that travels along axons with a velocity of 50–90m/s [BD85] to the motor endplates (neuromuscular junctions) sitting on top of the muscle fibers, usually near the middle or proximal to the middle [BD85]. Axons branch before they reach the fibers, so that every α-motor neuron can be connected to a number of muscle fibers ranging from as low as 10 for eye muscles, about 100 for muscles in the hand, and to about 2000 in leg muscles [KSea95]. The lower the number of innervated muscle fibers, the more fine grained the control of the muscle activation can be performed by the nervous system. But every muscle fiber is only controlled by a single α-motor neuron.

The α-motor neuron, together with the axon, motor endplate, and the muscle fibers that belong to this motor neuron are called a *motor unit* [BD85].

The action potential that is transmitted to the motor endplates initiates a biochemical process inside the junction to the muscle fiber, the synapse, and in the synaptic cleft between the synapse and the muscle fiber membrane (postsynaptic membrane). If the resulting depolarization at the postsynaptic membrane exceeds a certain threshold, a single muscle fiber action potential is generated that travels along the muscle fiber with a velocity of 3–6m/s [BD85] to excite all sarcomeres. This leads to contraction of the sarcomeres and to a single twitch. To achieve a *longer period* of contraction, a series of action potentials has to be generated by the motor neuron: a *motor unit action potential train*. Since a motor unit can perform only an all-or-nothing activation of the muscle fiber (the strength of a twitch cannot be modulated), the *strength* of contraction depends on the number of recruited motor units, that is, the number of motor neurons that produce an action potential at the same time. Typically, weaker motor units, innervating less muscle fibers, are recruited first if progressively increasing force is required [KSea95]. In general, motor units are firing in a random pattern and are not synchronized.

Studies on single motor units revealed that one stimulation pulse creates a single twitch response from the muscle. With increasing frequency of those pulses, the twitches start to merge and the force production of the muscle becomes continuous and increases. When the stimulation frequency is further increased, the twitches come closer to a permanent maximum contraction of the muscle at which point no further force can be generated. If this contraction is performed voluntary (no reflex, no spasm) it is called *maximum voluntary contraction*. The relationship between neural activation and force production is described of being linear, exponential or logarithmic, depending on the muscle. Results of various investigations can be found in [BD85, MB03, PNM96].

During the depolarization of the postsynaptic membrane, ion movement causes an electromagnetic field in the vicinity of the muscle fibers that overlays with fields of fibers from other motor units which are intermingled within the muscle. The resulting sum of all fields is called the electromyographic signal of the motor units and can be

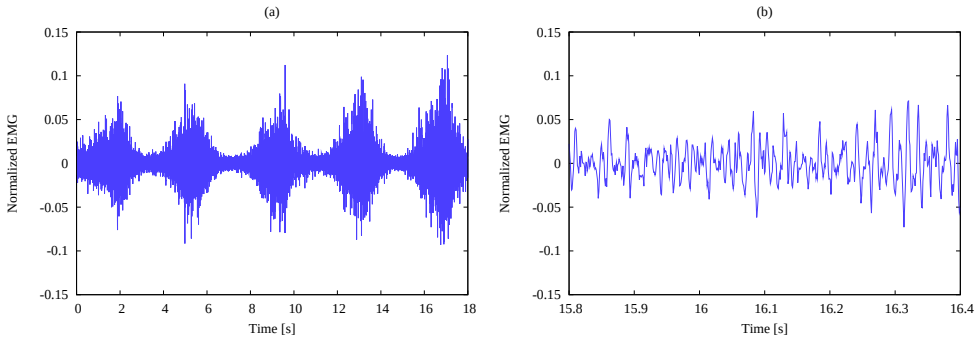

Figure 3.5: Example of a raw EMG signal as delivered by a surface electrode. The electrode has an in-built bandpass of 20–450Hz and an amplifier with a gain of 1000V/V. Diagram (a) shows a series of muscle contractions, diagram (b) shows the magnification of an interval of the same data.

directly measured invasively with needle electrodes or on top of the skin with surface electrodes. Example data is shown in figure 3.5.

Unfortunately, measured EMG signals are not always exclusively from the muscle below the electrode. Due to the conductivity of tissue and skin, signals from neighboring muscles can interfere with the muscle under observation.

On their way to the electrodes EMG signals are modified through filtering characteristics of the tissue it passes and, in case of surface electrodes, the characteristics of the connection between the skin and the electrode. Those details will not be addressed here. An introduction to this topic can be found in [BD85].

The time between the emission and detection of the EMG signal can be neglected in the context of this work. But there is also a time between emission and force production. This time, called the *electromechanical delay*, is reported to be about 50–80ms [CK79, ZLMF95, VMIS90], mainly due to low muscle fiber conduction velocity and the chemical processes which lead to contraction. It allows the signal evaluation process to start *before* the force production begins, reducing the latency of control systems coupled to EMG signals.

Furthermore, muscle fatigue has an effect on the relationship between EMG signals and muscle forces: The EMG spectrum shifts to lower frequencies and the amplitude measured by surface electrodes increases. The motor units start to fire more synchronized, resulting in a visible tremor of tension [Win90a]. Effects of muscle fatigue are not taken into account in this work. An analysis of these effects can be found in [Seg03].

In the context of this work, EMG signals are always related to *surface* EMG signals.

3.4 Remarks

In this work, muscle forces are estimated from the recorded EMG signals to analyze the desired action of the operator. For this, two main aspects have to be considered: First, a proper biomechanical model of the human body has to be developed. This model has to incorporate major properties of the muscles to deliver a good estimation of muscle forces. It does not need to be too detailed. Most complex muscle models have been developed by observation of the behavior of single muscles from animals or human cadavers, and are not used with multiple muscle systems. When performing experiments with the operator and the exoskeleton, many other factors influence the quality of the results, like attachment of the exoskeleton to the human, mechanical construction of the actuation and so on. Creating an overly complex model will not improve the overall system behavior very much. Inclusion of additional properties should always be considered in the context of the whole work and the potential improvements of the overall system behavior.

Second, recorded EMG signals depend on a variety of factors, like sweat on the skin, blood circulation and so on. Those factors unfortunately vary from day-to-day. If muscle force is to be derived from EMG signals, the EMG to muscle activation relationship has to be determined for every experimental session anew.

The implemented human body model is described as part of the control system in the following chapter 4, and the calibration of all model parameters is presented in chapter 5.

4 Intention Analysis and Support Computation

This chapter describes the control system of the exoskeleton. It is responsible for determination of the desired action of the operator and generating the support with the actuation of the exoskeleton.

In general, this system is subdivided into three distinct parts: The signal evaluation, which is responsible for analyzing the intended movement of the operator, the computation of a suitable support action, and the execution of this action through a control loop that commands the actuation of the exoskeleton, as shown in figure 4.1.

Section 4.1 describes initial considerations, and a definition of the requirements of the control system. Section 4.2 gives an overview of the whole control system, section 4.3 describes the evaluation of the EMG signals to estimate the operator's muscle forces, section 4.4 explains the appropriate determination of support, and in section 4.5 the low-level controller connected to the actuator is presented. The control scheme has been published in [FH06].

The presentation of the system is orientated towards the leg exoskeleton that was developed in this work and is presented in chapter 6 so that appropriate graphic descriptions can be given. But the algorithms are generic and can be applied to almost any part of the human body and to a wide range of exoskeletons.

4.1 Preliminary Considerations

Computation of the support action and the subsequent control of the force contributed by the actuation of the exoskeleton strongly depends on the output of the intention detection algorithm. It can be a fuzzy "idea" of the direction of movement, an accurate estimation of the movement within the next timestep, a complete movement description like "climb a stair", or the desired muscle force of the operator which he or she cannot generate alone.

From our point of view it is desirable to allow the operator full control over the exoskeleton at every time. This excludes algorithms which identify complete movements and replay pre-defined trajectories. While the latter can be useful during rehabilitation to teach the subject correct gait patterns, healthy operators can benefit from a system allowing more control: Characteristics of the movement can be modulated, for example, the stride-length, and walking in a natural environment with steps, stairs and obstacles can be performed more easily. It is also expected that the transitions between

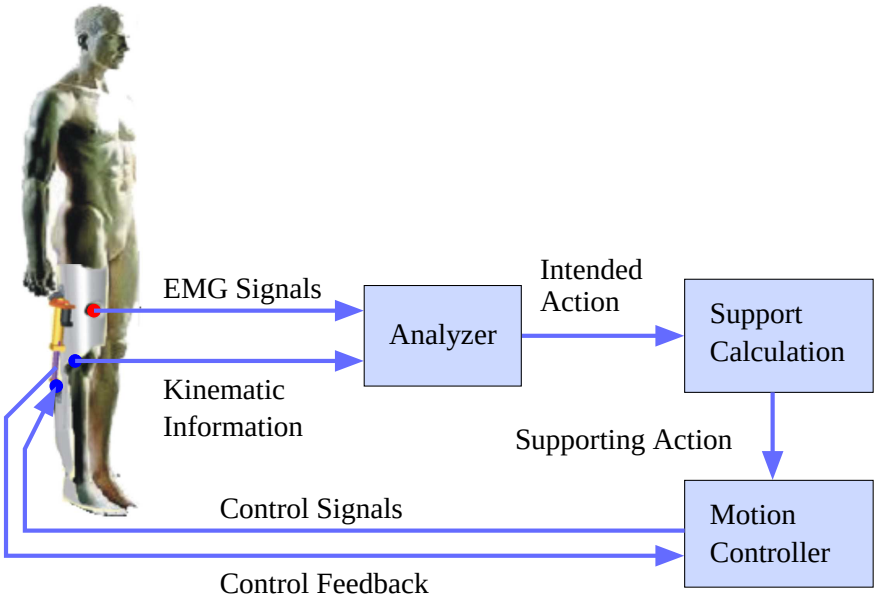

Figure 4.1: Basic concept of the interface and controller structure: The EMG signals are recorded from relevant muscles and are analyzed together with kinematic information from the exoskeleton. Output of the analyzation is the intended action of the operator, for which a suitable support is computed. This support is passed to the motion controller which is responsible for the execution with the actuation of the exoskeleton.

different tasks is performed more natural, for example, between standing-up and walking or walking and climbing a stair, and they can appear at arbitrary points in time. It is also more convenient for the first experiments, performed with healthy operators, to give less control to the machine and more control to the human for safety reasons.

In this work, two of the above mentioned approaches are explored: In the rest of this chapter an algorithm is presented that estimates the operator's own force contribution to a movement, and adds a certain amount of extra force to it. By utilizing a linear relationship between the joint torque produced by the operator's muscles and the torque created by the actuation, it is hoped that the human locomotor system can adapt easily to this external influence. In section 8.1 an algorithm is presented that predicts the desired movement of the operator for the next timestep with a dynamic rigid body model.

Both algorithms are based upon evaluation of EMG signals emitted from the muscles during their activation. The complexity of the analysis and support calculation has to be so low, that the support can be calculated continuously and very fast, but not necessarily in real-time. The loop which determines the support should run with a frequency of at least 100Hz. It is of no use to develop a detailed, complex, and accurate model that produces results with an intolerable delay. This delay could result from computational effort as well as from the structure of the signal evaluation that

has to wait for certain data to be recorded. Furthermore, no overall optimization can be performed afterwards to calculate the "optimal" estimation for every point in time. From the findings of research groups specialized in those fields results have been utilized. From the wealth of available data and models, a sensible and practical level of abstraction with a small set of parameters has been chosen. While some parameters can be taken from literature, some can be estimated. But a certain number remains and has to be calibrated for every subject. To obtain a system that can be practical used to perform experiments, the number of those parameters has to be kept in reasonable limits.

Unfortunately, some of those parameters are subject to change between experimental sessions. It should be possible to calibrate them easily. To avoid inconsistencies of computation between the calibration setup and the experiments with force support, it is best if the calibration is performed with the exoskeleton system itself, and without any external devices. But it has to be pointed out that this comfort is traded for accuracy of the calibration and the kind of parameters that can be determined. Due to the limited capabilities of the sensors mounted on the exoskeleton, not many different reference values can be accurately obtained to calibrate with. The calibration is presented in chapter 5.

4.2 Basic Concept

The concept of the system is to amplify the muscle forces the human operator is producing. Since the human is inside the control loop, he or she can regulate the muscle activations to perform the desired movement while receiving the support. Through feedback in the body he or she can take into account the external support, and reduce the own force contribution to the movement when the actuator gives support. This requires an operator that is able to coordinate muscle activations in accordance with the external support. Higher amplifications demand lower latencies of the system to remain stable and the capability of the operator to adapt his or her normal movement patterns to the modified circumstances.

The concept of the control system is shown in figure 4.2: It estimates the current joint torque contribution from the EMG signals of the operator through a simplified body model. The desired supporting torque is derived from the operator's own torque contribution and a given support ratio. The current torque contributed by the exoskeleton is calculated by a sensor integrated into the actuator and a proper model. The difference of the desired support torque and the current support torque forms the torque error that is passed to the torque controller with connection to the actuation.

The evaluation is performed continuously. No pre-defined trajectories are applied. All sensor data are recorded with 1kHz, but downsampled and evaluated with approximately 100Hz, allowing spontaneous movements. The low-level motion control loop runs at a frequency of 1kHz.

This control scheme has no knowledge about the movement that will result from

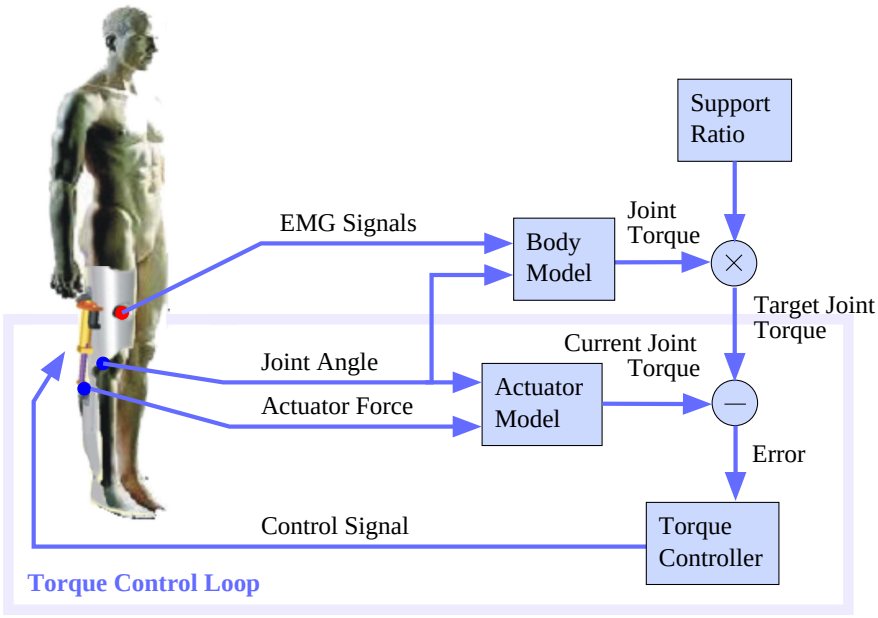

Figure 4.2: Control structure of the system: The EMG signals are evaluated by a body model resulting in an estimate of the operator's torque contribution. The support torque is computed from the operator's contribution, forming the target joint torque. This torque is compared to the current torque produced by the actuator. The resulting error is evaluated by the controller and appropriate control signals are generated.

the combined effort of the operator and the actuation. The simplicity of the general concept is traded for the possibility to include algorithms which observe the global behavior to control postural stability or suppress inappropriate movements. On the other hand it is a very fault-tolerant mechanism and gives the able-bodied operator a high degree of freedom and control.

4.3 Human Body Model

The human body model is responsible for estimating the torque of the operator from the EMG signals of all observed muscles as shown in figure 4.2. It does not take into account any movements resulting from the activation of the muscles.

Fortunately, a lot of work has been undertaken by other groups to model the human body, as summarized in chapter 2. An overview of properties and models that also includes the properties taken into account in this work can be found in [BLMB04].

In the following, the model is described as implemented. The exclusion of some well-known properties is explained, either because necessary parameters cannot be determined during calibration, or their effect is neglectable in the considered application. Properties of the human body that *are* included in the model have been introduced

with their origin in chapter 3. The effect of inclusion of those properties is analyzed during the experiments in chapter 7, justifying the complexity of the model.

The following sections describe the signal evaluation from inside to outside: from muscle details to the resulting torque contribution of a muscle, before the summation over all muscles is performed. The model is explained for the torque computation of a single joint, but taking into account multijoint muscles.

EMG Signal to Muscle Activation

First of all, the muscle activation $a(u)$ as a function of the postprocessed EMG signal, u, has to be determined. This activation is a dimensionless quantity $0 <= a(u) <= 1$ that reflects the activation of the muscle relative to the maximum voluntary contraction (MVC) of a muscle. It is obtained from the EMG signal, which is a measure for the electrical activity in muscle leading to contraction, in the following way:

1. From the time-discrete raw EMG signal $e(t)$, which is a function of time t, the moving average $\overline{e}(t)$ of the signal is subtracted, eliminating any offset from the sensor setup.
2. The offset-corrected signal is rectified.
3. The rectified signal is lowpass-filtered to form the activation envelope, $u(t)$.
4. The offset of the postprocessed EMG, u_o, which is measured when the muscle is relaxed.

This results in the following EMG postprocessing:

$$u(t) = L(|e(t) - \overline{e}(t)|) - u_o \tag{4.1}$$

where L is the low-pass filtering function, in our case a second order Butterworth low-pass filter, with a cut-off frequency of 1.6Hz. Common values are in the range of 4Hz to 10Hz [BLMB04], but experiments with the actuation have shown that a lower frequency improves the system behavior (refer to experiments in section 7.2.3). This lowpass-filtering simulates all different aspects of the lowpass-filtering in the human muscle: from the chemical processes on the way to and within the muscle fibers, the electrical transmission delays, to muscle and tendon viscoelasticities. An example of a raw EMG signal and the output of the filtering can be seen in figure 4.3.

In human body, the activation of a muscle does not happen instantaneously. It takes some time until the muscle force is generated and ceases. In literature this is modelled as the *muscle activation dynamics* [ZW90, MB03] and called the *electromechanical delay* [CK79, ZLMF95, VMIS90], which is not taken into account here. Some displacement in time between the EMG signal and the force values can be observed, but in our experimental setup it is hard to verify where this delay comes from, and the

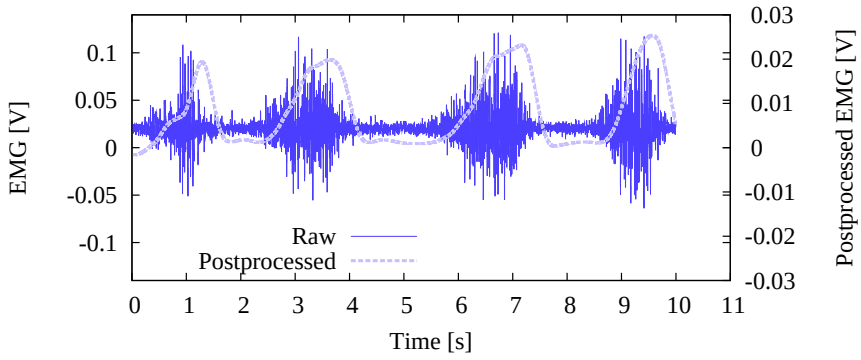

Figure 4.3: Raw and postprocessed EMG signal.

measurements are not accurate enough to calibrate required parameters. But it may have an effect upon the performance of the system.

As was explained in section 3.3, the EMG signal to force relationship is reported to be linear, exponential or logarithmic. Two transfer functions have been utilized in this work to investigate the performance of the torque prediction. The first function is based on [PNM96], using an exponential relationship:

$$a_{\text{exp}}(u) = \frac{e^{AuR^{-1}} - 1}{e^{A} - 1} \tag{4.2}$$

where u is the postprocessed EMG value, R an estimated maximum[1] of the signal $u(t)$, and A, a non-linear shape factor defining the curvature of the function, bound to an interval of $-5 < A < 0$.

For $A \to 0$ the function approximates a linear relationship.

The second activation function has been suggested in [MB03], and is slightly modified here. It consists of two portions: For EMG values below a certain threshold, u_0, with the corresponding activation, a_0, the function is approximated with a logarithmic function, whereas the other portion is approximated with a linear relationship:

$$\begin{aligned} a_{\text{pw}}(u) &= \begin{cases} \frac{a_0}{\ln(A+1)} \ln(A\frac{u}{u_0} + 1) & \text{if } u < u_0 \\ m(u - u_0) + a_0 & \text{otherwise} \end{cases} \\ \text{with} \quad u_0 &= 0.3R \end{aligned} \tag{4.3}$$

where (u_0, a_0) defines the point of transition between the two portions of the function in the EMG signal / activation space, A defines the shape of the logarithmic portion, and m the slope of the linear portion. R is the estimated maximum of the postpro-

[1] Since this function is applied online, a definite maximum cannot be determined. In contrast to the original definition, u is not normalized in advance.

cessed EMG value u. The function is modified in contrast to the original suggestion in [MB03] in such a way that the two pieces of the function are directly related through the parameters. In the original work the pieces had independent parameters which have been optimized to create a continuously differentiable function. This is not an important aspect in our work, and leads to an overall more inaccurate curve fitting with our experimental setup.

Following that, the parameters of the EMG signal to muscle activation relationship are A, R, or A, m, a_0, R, respectively, for every muscle, depending on the activation function. They depend very much on the condition of the subject and electrode placement, and have to be calibrated for every experimental session and for every muscle.

In the following text, the activation function $a(u)$ is a placeholder for one of the two functions defined above, to abstract from the underlying activation function.

Muscle Activation to Muscle Force

Once we have obtained the activation of the muscle, we can compute the resulting force using a simplified Hill-type muscle model. Hill-type muscle models abstract from internal processes of muscle in favor of a perspective from "outside": the muscle is modelled by observation of the behavior through a contractile element, and passive dampers and springs. Since the original paper by Hill [Hil38] was presented, many derivatives of the model have been published incorporating recent findings. An overview of modern Hill-type models can be found in [Win90b], and parameters of those models are readily available in literature.

In this work, a simplified Hill-type muscle model is explained, omitting some aspects which are not required in this context. This model is shown in figure 4.4. It consists of two elements: a contractile element producing the active muscle force, F_A^m, through contraction, and a parallel elastic element that produces the passive force, F_P^m, when the muscle is stretched:

$$F^m = F_A^m + F_P^m \tag{4.4}$$

The force of the contractile element is calculated by the product of the muscle activation, $a(u)$, and the maximum isometric force[2] at optimal muscle fiber length, F_o^m, and the active force-length function, $f_A(\tilde{l}^m)$:

$$F_A^m = f_A(\tilde{l}^m) F_o^m a(u) \tag{4.5}$$

$$\text{with} \quad \tilde{l}^m = \frac{l^m}{l_o^m}, \tag{4.6}$$

where $\tilde{l}^m$ is the normalized muscle fiber length, which is the muscle fiber length,

[2] Force that is produced under isometric conditions, that is, no length change of the muscle occurs.

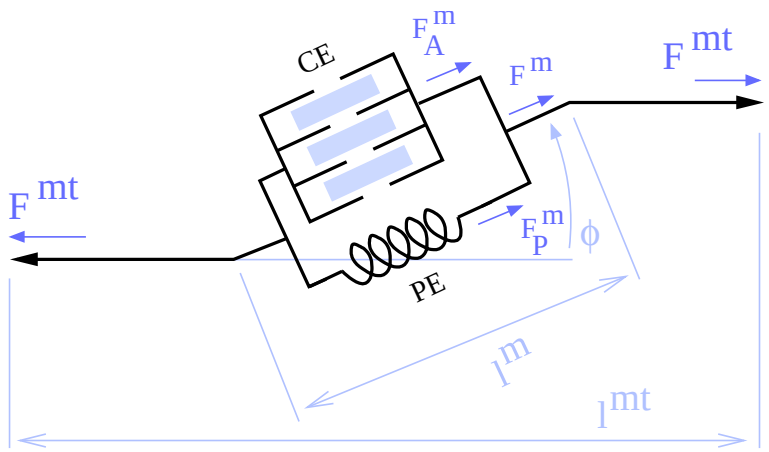

Figure 4.4: Schematic of the muscle model: The contractile element (CE) is creating the active force, F_A^m, through sarcomere shortening. The parallel element (PE) represents fiber and tissue properties resisting the stretching of the muscle through a passive force, F_P^m. The force of the muscle, F^m, is the sum of the active and passive forces and acts at an angle to the direction of pull: The pennation angle ϕ. The resulting force along the tendon is the musculotendinous force, F^{mt}.

l^m, divided by the optimal muscle fiber length, l_o^m. $f_A(\tilde{l}^m)$ describes the ability of the muscle to produce force at a certain muscle fiber length (refer to figure 3.3).

In literature it is reported that the optimal muscle fiber length changes with the level of activation [LB03, BLMB04], which is an important fact, as the optimal muscle fiber length is a crucial parameter of the muscle model. Nevertheless, this effect is neglected here to keep the number of parameters low. Further experiments have to be performed to investigate if inclusion of this property would significantly improve the behavior of the system.

The passive force is calculated as a product of the maximum isometric force, F_o^m, and the normalized passive force-length curve, f_P:

$$F_P^m = f_P(\tilde{l}^m) F_o^m \tag{4.7}$$

$f_A(\tilde{l}^m)$ and $f_P(\tilde{l}^m)$ can be found in literature [DLH+90] and are shown in figure 3.3 (left side).

The force-velocity relationship of a muscle, as shown in figure 3.3 (right side), is omitted since the movements considered in this application are rather slow, and the maximum muscle velocity that is used for normalization of the muscle velocity is reported to be about $10 l_o^m$/s [Zaj89]. The effect of including the relationship can be estimated by looking up the muscle fiber velocity for walking from diagrams 6.3 and 4.5, and retrieving values with the normalized muscle velocity from the force-

velocity curve in diagram 3.3. If desired, the force-velocity relationship as a function of the normalized muscle velocity can be included in the product of the active muscle force in equation 4.5. The omission leads to a slight overestimation of the active muscle force when the muscle shortens and an underestimation when the muscle lengthens. If handling of faster movements is desired it can be integrated.

Since f_A, f_P, and estimations of l_o^m are taken from literature, the subject-dependent parameters of this model is F_o^m for every muscle. It could be argued that the whole muscle-tendon model has to be scaled according to the size of the operator, but this is not performed. Most of this influence is compensated through the calibration of other parameters.

To be able to calculate $\tilde{l}^m$, the current muscle fiber length, l^m, has to be calculated. This requires inclusion of a complex musculotendinous model, but is necessary, since the force-length property is very important.

Initial experiments have tried to establish a force-angle relationship that implicitly takes into account the force-length relationship and the muscle length as a function of the joint angle. This relationship was calibrated with a second order polynomial. Unfortunately, the predictability of the model was small since the model was fitted strongly to the data. With inclusion of the following model, the number of parameters that are required to be optimized *per muscle* are reduced from three to one compared to using the polynomial. Less data has to be recorded to perform the calibration, since a priori knowledge is included that replaces two unknown parameters.

This musculotendinous model is a subset of the model published in [DLH+90] which is in part a consistent collection of data from other sources complemented by muscle and joint models describing the muscle paths wrapping around bones at certain joint angles where required. The model data can be found in appendix A.

The length of a particular musculotendinous complex (muscle and tendon together, that is, from the point of origin to the point of insertion) is defined by:

$$l^{mt} = \sum_{i=0}^{n-2} \|P_{i+1} - P_i\| \tag{4.8}$$

where $P_i = (x_i, y_i, z_i, 0)^T$ are the waypoints of the muscle-tendon path. All waypoints are connected to a condition, c_i, that checks the joint angles, a_k, being in certain intervals:

$$c_i = \begin{cases} 1 & \text{if} \quad \forall k : 0 \leq k < J \Rightarrow \alpha_{k,i}^{low} \leq \alpha_k \leq \alpha_{k,i}^{high} \\ 0 & \text{otherwise} \end{cases} \tag{4.9}$$

with J being the number of modelled joints. $\alpha_{k,i}^{low}$ and $\alpha_{k,i}^{high}$ are the lower and upper boundaries of the joint angle intervals belonging to waypoint i and joint k.

The waypoint P_i is inserted into the path if condition $c_i = 1$. Some boundaries are chosen in such a way that the condition is always 1.

P_i are the results of a transformation of waypoint coordinates, $\hat{P}_i$, of the body segment coordinate systems (pelvis, thigh, shank, patella) into the pelvis coordinate system with

$$P_i = \mathbf{M_i}(\alpha_\mathbf{0}, \ldots, \alpha_{\mathbf{J-1}})\hat{P}_i \tag{4.10}$$

where $\mathbf{M_i}(\alpha_\mathbf{0}, \ldots, \alpha_{\mathbf{J-1}})$ is a 4×4-transformation matrix as a function of the joint angles, α_k, with $0 \leq k < J$ of the respective body segments to which the waypoints are connected. It takes into account rotation and sliding movements of the individual segments during joint movement and transforms the coordinates into the pelvis coordinate system.

The relationship between the length of the musculotendinous complex, l^{mt}, the muscle fiber length, l^m, and tendon length, l^t, is given by:

$$l^{mt} = l^t + l^m \cos\phi, \tag{4.11}$$

where ϕ is the current pennation angle (refer to figure 4.4). Obviously, if the pennation angle would be neglected, the expression of the muscle fiber length simplifies to

$$\hat{l}^m = l^{mt} - l^t. \tag{4.12}$$

But the influence of the pennation angle on the model output has to be investigated and cannot be neglected in general.

The pennation angle changes with the muscle length with respect to the optimal fiber length and can be approximated according to [SW91] by

$$\phi = \arctan\left(\frac{l_o^m \sin\phi_o}{l_o^m \cos\phi_o - \delta}\right), \tag{4.13}$$

where δ is the length change of the musculotendinous complex, and ϕ_o the pennation angle at optimal fiber length.

According to [Zaj89] the tendon is rather stiff: The strain is only about 3% of the tendon length for maximum muscle force. It is neglected here so that the length change, δ, relates the current pennation angle to the pennation angle at optimal fiber length, ϕ_o, and muscle fiber length, l^m, through

$$l^m \cos\phi = l_o^m \cos\phi_o - \delta \tag{4.14}$$

Solving equation 4.13 for $\sin\phi$, and replacing $\cos\phi$ by the expression resulting from rearranging equation 4.14 for $\cos\phi$, yields the current pennation angle as a function of the muscle fiber length,

$$\phi = \arcsin\left(\frac{l_o^m \sin\phi_o}{l^m}\right). \tag{4.15}$$

Rearranging equations 4.11 and 4.15 yields

$$\sin\phi = \frac{l_o^m \sin\phi_o}{l^m} \quad \text{and} \quad \cos\phi = \frac{l^{mt} - l^t}{l^m} \tag{4.16}$$

with

$$\sin^2\phi + \cos^2\phi = 1 \tag{4.17}$$

it follows for the length of the muscle fibers, l^m:

$$l^m = \sqrt{(l_o^m \sin\phi_o)^2 + (l^{mt} - l^t)^2} \tag{4.18}$$

which is not depending on the current pennation angle anymore, but only on the pennation angle at optimal fiber length, ϕ_o [Onk07].

Unfortunately this equation contains the length of the tendon, l^t, which is not known exactly. But since the tendon strain is omitted in our model, l^t is approximated by the tendon slack length l_s^t:

$$l^t \approx l_s^t \tag{4.19}$$

This is the length of the tendon without any external forces applied to it. Estimations of l_s^t can be found in e.g. [DLH+90]. More complex algorithms approximate the muscle length through numerical integration of the muscle fiber velocity starting from an estimated value [LB03].

In literature it is pointed out that the model is very sensitive to the tendon slack length of a muscle which varies from subject to subject. For this reason a tendon slack length scale, s^t, is calibrated:

$$l_s^t = s^t \hat{l}_s^t, \tag{4.20}$$

where $\hat{l}_s^t$ is the tendon slack length from literature.

We bound the scale during optimization to the interval $[0.85, 1.25]$ to allow differences between subjects. The optimal muscle fiber length is not optimized to reduce the number of parameters.

We have taken values for l_o^m, ϕ_o, and $\hat{l}_s^t$ from [DLH+90]. The remaining parameters form an additional set of six subject-dependent parameters, s_i^t, one for every muscle.

Muscle Force to Joint Torque

In the previous section the calculation of the force output of individual muscles, F^m, is described. To compute the tendon force (force of the musculotendinous unit), F^{mt}, that is actually pulling at the bones, the pennation angle, ϕ, from equation 4.15 is taken into account:

$$F^{mt} = F^m \cos\phi \tag{4.21}$$

To compute the torque contribution of each muscle, the moment arm $r(\alpha)$ as a function of the joint angle, α, has to be determined. This can be performed with the tendon displacement method described in [ATHC84], based on the principle of virtual work:

$$r(\alpha) = \frac{\partial l^{mt}(\alpha)}{\partial \alpha} \tag{4.22}$$

Computation of the length of the musculotendinous unit, l^{mt}, is described in equation 4.8. If muscles are crossing more than one joint, the moment arm can depend on the angles of all joints it crosses. But in our case, due to the geometric arrangement of skeleton and muscles around the knee in the human body, the influence of the remote joints on the moment arm is small and can be neglected. As can be seen for the knee joint in figure 4.5, the length of the musculotendinous unit changes almost linearly with the knee angle, resulting in an almost constant moment arm. The values used for the moment arms are given in table A.1.

The torque contribution of muscle i in a joint is calculated by:

$$T_i = r_i F_i^{mt} \tag{4.23}$$

where r_i is the approximated constant moment arm of the i-th muscle and F_i^{mt} the force of the i-th musculotendinous unit.

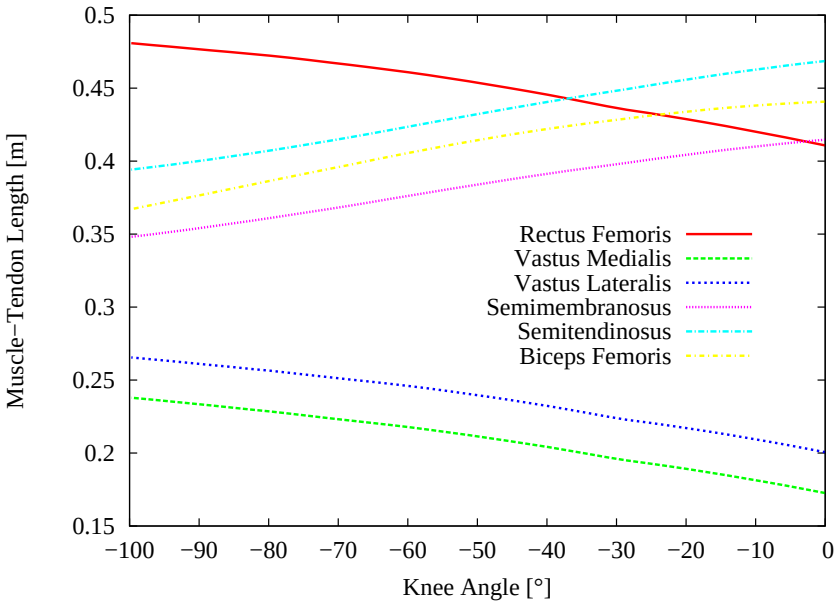

Figure 4.5: Example of the knee joint: The length of the musculotendinous units plotted over the knee angle. 0° means full extension of the knee, negative angles indicate knee flexion. The hip is assumed to be at 0° (straight).

The total joint torque produced by all muscles is the sum of the individual contributions,

$$T = \sum_{i=0}^{N-1} T_i \tag{4.24}$$

where N is the number of modelled muscles spanning the joint and T_i the torque contribution of the i-th musculotendinous unit as of equation 4.23.

Since not all muscles responsible for joint flexion and extension can be measured and due to the simplifications described above, torque T is only a rough estimation of the actual joint torque.

A summary of the computation and all parameters are given in appendix A.

4.4 Determination of Support

As previously mentioned, the exoskeleton is used as a force amplifier. That means, it does not have an explicit knowledge about the overall movement that is intended by the operator, and cannot predict the joint trajectories. Although the muscle activations are known to the system, the movement that will result is not, and cannot be determined

in advance, due to lack of information about the configuration of the human body and contact with the environment.

The operator is in charge of maintaining stability and performing the desired movement by appropriately activating his or her muscles.

To let the system act in a predictable manner to simplify the usage for the operator, the supporting torque is derived from the operator's own torque contribution to the movement by a linear relationship,

$$T_s = G \cdot T \tag{4.25}$$

where G is the gain or *support ratio*. For example, a gain of $G = 1.0$ means that the system is adding as much torque to the movement as the operator, and a gain of $G = 0.5$ means that the system is adding half of the torque the operator is contributing.

Through utilization of a linear relationship it is hoped that the overall shape of the muscle activation pattern is changed as little as possible when using the system. It is desired that only the amplitude of the activation is reduced. This should result in a short training phase to get used to the behavior of the system. This is also an advantage when regarding the exoskeleton as a device for rehabilitation: The patient would learn the correct gait pattern, and no artifical pattern which is only helpful as long as the exoskeleton is worn.

Further research has to show if other functions have any advantages over this relationship. The gain could be a function of the current state of the system, as far as known, to add increased support during slow movements (like getting up from a chair, climbing stairs, or carrying heavy load), and low support during faster movements. The operator could benefit from a more powerful support when possible, but during faster movements such a support can result in even faster movements, which the operator might not be able to control anymore.

For some applications, like rehabilitation, the responsibility of maintaining a dynamically stable pose cannot be put onto the operator. The system has to take care of that. Section 8.1 gives details on a different approach, which allows integration of algorithms controlling postural stability.

4.5 Torque Control Loop

The torque control loop is responsible for generating control signals for the actuation. The target torque of the controller equals the supporting torque, T_s, defined in equation 4.25.

The torque controller is a standard P-controller using the difference between the current actuator torque and the supporting torque as the error value to calculate the controller output S:

$$S = K_p \cdot (T_s - T_A) \tag{4.26}$$

where T_A is the joint torque currently produced by the actuator, and K_p the proportional gain of the controller. The torque controller can run with a higher frequency than the EMG signal evaluation, to achieve a better performance. In that case the target, T_s, is not updated in every iteration. Computation of the actuator torque for the exoskeleton of this work is described in appendix B.

4.6 Summary of Properties

The general behavior of the system presented here is that of a force amplifier. The simplified human body model which is described throughout this chapter is used to estimate the operator's own torque contribution to the movement in the actuated joints. This torque is multiplied with a support ratio and contributed to the movement by the actuation of the exoskeleton.

Since the support is not performed with a position controller, knowledge of the resulting movement of the cooperation between the operator and the exoskeleton is not required. While this renders the integration of algorithms for controlling postural stability impossible, it leads to a very robust and reliable system, since a dynamic body model of the operator and the exoskeleton is not required. The number of model parameters is reduced significantly, and the number of sensors to synchronize the system with the real world is very low. No global pose information is required to incorporate the effect of gravity, which is very difficulty to obtain with sensors mounted on the exoskeleton alone. Arbitrary contact forces pose no problem for the control system and are taken into account by the force or torque sensor of the actuation.

The latency of the system between the recording of EMG signals and the system response is dominated by the lowpass-filter delay depending on the lowpass cut-off frequency. The effectiveness of the support action is depending on the parameter of the controller. Those two parameters may be adapted for certain operators, applications, or specific movements to allow a quicker response or smoother movement. All other parameters influence the degree of support in relation to the operator's own torque contribution.

All the points mentioned above imply some very useful properties: Given an exoskeleton construction that can move as fast as the operator can, the exoskeleton will never hinder the movement of the operator through passivity, for example by not properly recognizing a movement. The most passive thing the presented control loop can command is to evade the leg movement of the operator. It does not matter if this leg movement is performed through the leg muscles or with support from the hands and arms of the operator positioning the leg. This behavior occurs if the target torque of the controller is zero, either by setting the support ratio to zero, or because no recorded muscles are active. It will not lock and suppress a movement as a position-controlled system. But as soon as muscle activation is detected, the exoskeleton will contribute to the movement. If the parameters of the model are determined very badly, the support

will not be linear in every joint configuration, as desired. Only during cocontraction[3] of the muscles where the resulting torque produced by the muscles is low (most of the opposing muscle forces cancel out, and the joint stiffness is increased) the exoskeleton might hinder the movement slightly, because the summation of the agonist and antagonist torques might yield a torque with a different sign than the true muscle torque. On the other hand the most active thing the exoskeleton can perform is to contribute more than linearly to the movement, because of bad model parameters. For a specific calibration the maximum deviation from the linear support can be determined.

In contrast to approaches utilizing inverse dynamics to compensate the effect of gravity regarding a statically stable pose, this approach allows larger support ratios while still working in cooperation with the operator. Increasing the support for the systems mentioned before leads to a point where the operator has to reverse his or her muscle activations and work against the exoskeleton to perform a certain movement. In the presented approach the support ratio is only limited through the reaction delay of the operator to the resulting movement.

The realization of the control system requires very few sensors: The EMG sensor for the muscles that should be recorded, a force or torque sensor (depending on the kind of actuation) to measure the current support, and a sensor to measure the joint angle for every joint that is crossed by the recorded muscles. Chapter 6 presents the exoskeleton construction and electronics which have been used to investigate the system in real world experiments. Furthermore, the algorithm scales linearly to the supported joints, and arbitrary joints can be included and are handled separately.

The described behavior, especially for worst-case scenarios, is very convenient, and especially welcome for initial experiments and experiments with patients.

The following chapter 5 describes the calibration of the model parameters.

[3] During cocontraction agonist and antagonist muscles are active at the same time.

5 Calibration of Parameters

Since the exoskeleton is in close interaction with the human operator, there are parameters in the system that have to be adapted to the individual operator and to his or her current body state. This chapter reveals all unknown parameters and explains how they are determined or optimized.

In work with even more complex biomechanical models, for example, in [LB03] the calibration algorithm is fed with reference values collected with appropriate sensors during active and passive exercises with an isokinetic dynamometer, during a straight run, a crossover-cut and a sidestep. This allowed an accurate calibration of parameters, and a larger number of parameters to be integrated. In that work, validation of the biomechanical model was the main focus.

In contrast to that, the calibration in our setup has a severe limitation: The reference values the calibration can utilize come exclusively from sensors mounted on the exoskeleton, which are also used for the control algorithm. Those are the joint angle sensor and the force sensor measuring the current force at the actuator (this could also be a torque sensor for a different actuator). No sensors connected to a global reference frame are used. This reduces the accuracy of the reference values.

Since the actuator is attached to the limbs that are connected to the supported joint, the force sensor can measure the joint torque resulting from muscle activity directly, if the actuator is locked and no external forces except gravity are applied to the leg. Unfortunately, this limits the calibration procedure to isometric tasks. But since the force-velocity relationship of muscles is neglected, this is not a drawback.

It could pose a problem if too many parameters of the human operator should be identified, because the cooperation patterns of the muscles are always similar in this configuration. It may be impossible for the optimization algorithm to distinguish between influences of the individual parameters. If different movements could be used, the pattern would change, allowing a distinction between the individual contributions and between the different parameters of the muscles. On the other hand, if an algorithm *can* be found that allows a proper optimization for the selected parameters requiring only a few isometric contractions, the application of the exoskeleton is simplified by far, reducing the setup required for the calibration significantly.

Since the much more complex model was proven to yield good results in [LB03], in terms of biomechanical analysis and not the control of an exoskeleton, we now have to show that utilizing a subset of properties and some major simplifications still delivers results that are accurate enough for our application, and that those remaining parameters can be calibrated with the given sensors to a satisfying accuracy.

In the following sections, the algorithm that is used to optimize all parameters of

the model is presented. During the description of the calibration some assumptions are made to be able to perform the calibration. While those simplifications appear very rough, it has to be kept in mind that the calibration is used for parameters of a system which controls an exoskeleton. The accuracy of the calibration is not the most important aspect, especially for the EMG-to-force function. It is rather desirable that the exoskeleton behaves in a predictable manner so that the operator feels comfortable and can take advantage of the offered support. This can only be verified in separate experiments. While it is easy to show the performance of the optimization arithmetically, for the overall system behavior this is a very difficult problem.

The following section 5.1 justifies the selection of certain parameters for optimization and explains which parameters can be taken from literature. Section 5.2 describes the procedure that has to be performed by the operator during the calibration to record useful data, and section 5.3 explains the recognition of significant values and subsequent storage. The stored reference forces are divided among all active muscles as described in section 5.4, before the geometry calibration is presented in section 5.5 and the EMG-to-force calibration in section 5.6. A small comment on cocontraction is given in section 5.7, and the calibration is summarized with its properties in section 5.8. Parts of the calibration algorithm have been published in [FH07, FKRH04b].

5.1 Parameter Selection

In the biomechanical model presented in section 4.3, a number of parameters are used: The waypoints of the muscle paths, the parameters which build the matrices used for modeling the geometric relationships between the pelvis, femur, tibia, and patella, parameters that describe the force-length-curve, the tendon slack lengths, the optimal muscle fiber lengths, the pennation angles at optimal muscle fiber length, the parameters of the EMG-to-force function, and the maximum isometric force at optimal muscle fiber length. They cannot all be calibrated. A selection has to be applied. The selection is mostly justified by experiments and results from other research groups, since they have investigated properties in greater detail, with more accurate measurement setups. It is of no use to modify parameters that are well-accepted in the community and have been validated before without a good reason. One such reason occurs, if one parameter is adapted to incorporate the effect of another, which cannot be identified separately.

Although the dimensions of the human skeleton have been identified in [DLH$^+$90] for one specific subject, they will not be calibrated in our algorithm. It can be sensible to scale the data to fit the anatomical properties of the operator more closely. But this is omitted. Investigations on the change in moment arm due to scaling is performed in [Onk07]. The linear effect on the moment arm, for example, will be compensated through optimization of the maximum isometric force, and a certain degree of this simplification will be compensated through optimization of the tendon slack length scales, which has significant influence and is not well established in literature [LB03].

The force-length-curve is widely used in literature and not tailored to a specific sub-

ject. It is modulated by the muscle activation in more complex models, which is omitted here. Initial experiments performed by ourselves optimized a force-length curve with a second order polynomial, resulting in overfitting the model to the calibration data. The model prediction was suffering, leading to the conclusion that more accurate and a greater number of reference values had to be acquired to get a more reliable solution, or the well established curve from the literature has to be used.

The optimal muscle fiber length is also a candidate for inclusion in the calibration process, but is in part compensated by the calibration of the tendon slack length scales. It is not optimized to reduce the number of parameters. The pennation angle is included into the model, although the impact on the solution with feasible values is rather small. Calibrating the pennation angle would not significantly improve the performance, thus standard values from literature are used [DLH+90, Win90a].

As motivated in section 3.3, parameters of the EMG-to-force function have to be calibrated whenever the exoskeleton is donned. Since the optimization is not necessarily performed with maximum voluntary contraction every time, the actually performed maximum isometric force needs to be calibrated.

Summarizing that, the parameters selected for optimization are:

- the shape of the EMG-to-force function, A_i,
- the expected maximum EMG signal to scale the EMG signals, R_i,
- the maximum isometric force at optimal muscle fiber length, $F^m_{o,i}$,
- the scale of the tendon slack length, s^t_i.

The subscript i denotes that all those parameters are required for every muscle.

Those parameters can be subdivided in two categories: The first category is subject-dependent and requires calibrating only once: the tendon slack length scales, s^t_i. The second category contains the parameters that are expected to be changing from one experimental session to the next. Those are: The EMG-to-force parameters, A_i and R_i, and the maximum isometric force, $F^m_{o,i}$. All other parameters can be found in appendix A.

5.2 Calibration Setup

As will be described in chapter 6, the exoskeleton developed in this work supports the thigh muscles during flexion and extension of the knee joint. The calibration setup is described for this particular exoskeleton so that proper graphic descriptions can be given. The setup can be easily adapted to other joints, and the algorithm is generic and can be applied to other configurations as well.

Reference values available for the calibration are the knee angle and the knee torque during isometric contractions. The joint angle is not changing because the actuator is locked. The basic idea is to record the subject's muscle activation and the resulting

knee torque during a special calibration procedure. The recorded torque values are used to calibrate the parameters.

Since only those sensors can be used to observe the system during calibration, effects that influence the measurements and cannot be recorded and taken into account, must be minimized in advance. A special setup has to be prepared to limit the external forces: The operator is sitting on a chair with the exoskeleton leg not having any contact with the environment below the knee joint. The thigh is supported by the chair, the knee flexed. The actuator is not powered but locked, allowing only isometric contractions. When the thigh muscles are relaxed, the force measured by the force sensor is a result of gravitation acting on the exoskeleton and the embraced leg below the knee joint.

The operator tries to extend and flex the knee with maximum muscle activation slowly in both directions a few times. The measured force is now an overlay of all muscles and the influence of gravitation. The angle remains fixed during this phase.

For the geometry calibration this isometric exercise has to be performed several times at different knee angles to measure data for different muscle fiber lengths. The hip angle is held fixed.

When the geometry parameters are available, the EMG-to-force calibration needs only one trial at an arbitrary knee angle to calibrate the desired parameters.

5.3 Data Collection

The data collection is a continuous process that runs during the whole calibration procedure. From the values that are recorded, those with significance to the calibration process have to be recognized and stored. It must be ensured that the stored data is a good representation of all muscle activations with the corresponding force values. Data of different levels of muscle activity should have the same weight in the optimization process. Making pauses or time spent with a specific level of muscle activation should not increase the weight of the data recorded during this phase.

To meet these requirements, the algorithm stores the data in tables. For every muscle a separate table is created for every angle at which a trial is performed.

Recognition of the initiation of a new isometric exercise at a certain knee angle is performed as follows: When the measured torque rises above a certain threshold while the knee angle is changed only within a small interval, due to undesired deformation of the exoskeleton, a new table for every muscle is allocated in which the data is stored. This is important for the geometry calibration, where every configuration has to be stored separately. As long as the exercise is detected (the torque remains above the threshold), data is put into the tables for all muscles at the same time. Otherwise the data is discarded.

For a particular muscle i data from the k-th isometric trial is stored in the table entry with index $h_{i,k}$, depending on the postprocessed EMG value, u_i, by:

$$h_{i,k} = \lfloor u_i S_i \rfloor \tag{5.1}$$

where S_i is the interval width of every entry of the table.

The entry contains the current data from all sensors from the current point in time, which are the postprocessed EMG signals u_i with $0 \leq i < N$ and N being the number of recorded muscles, the joint torque as measured from the sensor integrated into the actuation, T_R, the joint angles α_j with $0 \leq j < J$ and J being the number of modelled joints, and the number of former entry updates, n_u, of the same entry.

If the entry is empty, the data is stored in the selected entry. Otherwise the data is averaged on a per-element basis with the data already stored in the table. For this averaging old data is weighted with the number of former updates n_u, and the new data is weighted with factor 1. n_u is only used for this averaging.

This ensures, that during the optimization process only relevant values are used. Those are values when the muscles have been activated. All data in the tables are used with the same weight during the calibration process, independent of the activation pattern. Longer periods of, for example, rest or maximum contraction do not change the weight. Every activation level, that is, every table entry, has the same weight. This is an important advantage over standard optimization methods where all data or only every n-th value is used, and the significance of the data regarding the optimization task is not considered.

Averaging of the entries during updates ensures that the stored values are more reliable and robust, as long as no muscle fatigue appears.

The data tables are specified with the interval width S_i. The size of the table is adjusted as needed with the advent of new values.

Every muscle owns K tables after data collection, one per each angle at which an isometric exercise has been performed.

The process of data collection and sorting into tables for a specific isometric trial is illustrated in figure 5.1.

5.4 Force Determination of Individual Muscles

The calibration process described below is not a global optimization for all parameters at once over all data. The reason for this is that some muscles are cooperating during the described exercises, making it impossible for the optimization algorithm to distinguish between the individual muscle contributions. The reason for not merging all muscles into a single muscle in the model and to record only one extensor and one flexor muscle is, that during different non-isometric tasks, the muscles are behaving in different cooperation patterns. Depending on the task and the required force, different muscles are active (refer to figure 6.8 for example patterns).

In the proposed algorithm, the reference torque, T_R, is computed from the recorded torque, T_A, by eliminating the effect of gravity:

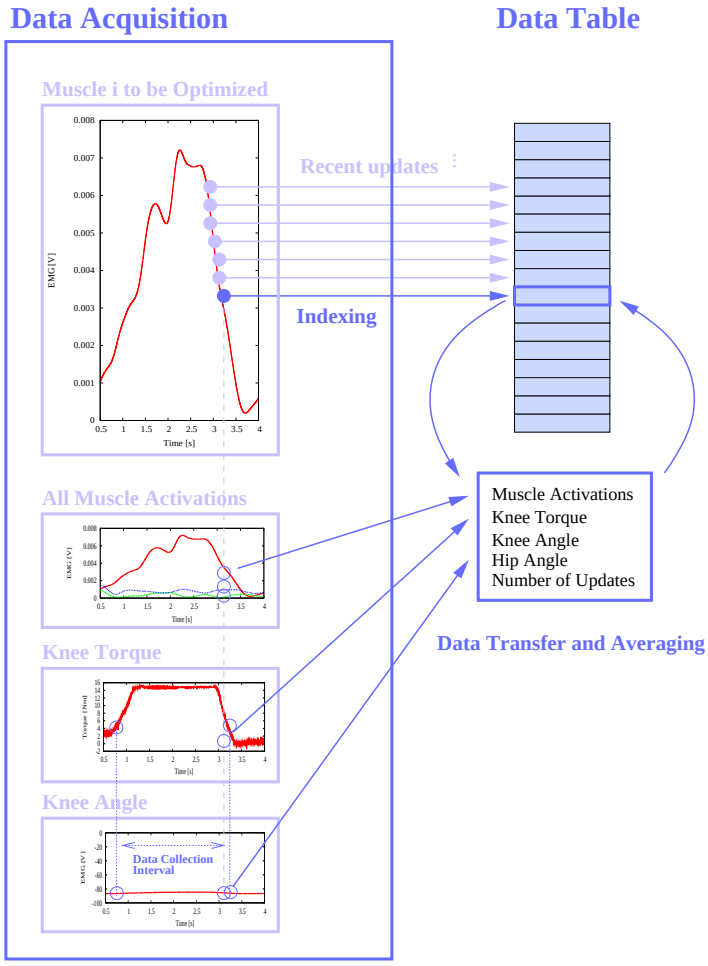

Figure 5.1: Data tables of the calibration: indexing of the table entry based on the postprocessed EMG signal, and subsequent averaging and storage of the recorded data.

$$T_R = T_A - T_g \tag{5.2}$$

where T_g is the torque measured while all muscles around the observed joint are relaxed. In that case the torque T_g is solely a result from gravity acting on the limbs, as long as no other external forces are applied, as describes in section 5.2.

The reference torque, T_R, is a result of *all* activated muscles, but it can be divided to allow the calibration algorithm to handle each muscle separately, which reduces the dimension of the parameter space significantly.

To calculate the individual muscle forces, F_i^m, the torque share, T_i, of the reference torque, T_R, has to be determined.

For this the %PCA-weight, w, of a muscle is computed by using the activation of the muscle weighted with its %PCA by:

$$w = \begin{cases} \%PCA \cdot a(u) & \text{if already calibrated} \\ \%PCA \cdot \frac{u}{R} & \text{otherwise} \end{cases} \tag{5.3}$$

where $\%PCA$ is the relative physiological cross-sectional area of the muscle, R the maximum recorded EMG signal, and u the postprocessed EMG signal. The required activation, $a(u)$ is only available if this calibration has been performed before, and parameters from the previous run are available. Otherwise the activation function is approximated by a linear relationship.

The shares are summed up for the coactivated muscles, which are the muscles from the same group as muscle i (flexor group, extensor group),

$$W_{ca} = \sum_{j=0}^{N-1} \begin{cases} w_j & \text{if muscles i, j out of the same group} \\ 0 & \text{otherwise} \end{cases} \tag{5.4}$$

where w_j is the weight according to equation 5.3 for the j-th muscle, and N is the number of muscles. Similar for the cocontracting muscles, which are belonging to the group opposing muscle i,

$$W_{cc} = \sum_{j=0}^{N-1} \begin{cases} 0 & \text{if muscles i, j out of the same group} \\ -w_j & \text{otherwise} \end{cases} \tag{5.5}$$

where N is the number of muscles.

The sum of the shares of both groups is computed with a saturation of the cocontracting shares to avoid errors during computation of the torque share in equation 5.7 for small activations:

$$W = W_{ca} + \begin{cases} W_{cc} & \text{if} \quad W_{cc} < W_{ca} - w_i \\ W_{ca} - w_i & \text{otherwise} \end{cases} \tag{5.6}$$

where w_i is the weight of the i-th muscle according to equation 5.3. This ensures that the share of the cocontracting muscles is not allowed to cancel more than the share of the muscles activated in cooperation with muscle i.

The individual torque contribution of a muscle, T_i, is computed from the reference torque by means of the estimated shares:

$$T_i = T_R \frac{w_i}{W}. \tag{5.7}$$

where w_i is the share computed according to equation 5.3 for muscle i, W the sum of shares as of equation 5.6, and T_R is the reference torque.

Substituting the force of the musculotendinous complex, F_i^{mt}, in equation 4.23 with the expression from equation 4.21 for muscle i yields

$$T_i = r_i F_i^{mt} = r_i F_i^m \cos\phi_i. \tag{5.8}$$

Solving for F_i^m results in

$$F_i^m = \frac{T_i}{r_i \cos\phi_i}, \tag{5.9}$$

where F_i^m is an estimation of the muscle force the muscle has contributed when torque T_i was measured.

We now have a relationship between different muscle activations, u_i, (through equations 5.1) and associated muscle forces, F_i^m, for every entry $h_{i,k}$ of a specific data table k with $0 \leq k < K$ of muscle i.

5.5 Geometry Calibration

The goal of the geometry calibration is to find proper values for the tendon slack length scales, s_i^t, for every muscle i. Since we are mainly interested in making the EMG-to-force relationships consistent for different joint angles, we need the relationship between muscle activation and muscle force for different lengths of the muscles.

As described above, the muscle contractions with data recording are performed under different joint angles, and the data are stored in separate tables for every angle and for every muscle. The idea is to modify the tendon slack length scales for every muscle in such a way that the computation of the muscle force based on the EMG signal of a specific muscle is consistent for all tables, and, as a result, for all joint angles.

Only if this consistency is established, the computation from the EMG signal to muscle force can be performed with a satisfying accuracy. As can be seen in figure 5.2, the left diagram shows a significant discrepancy between the EMG-to-force relationships under different joint angles, because the geometry model is not applied. Only if the geometry is taken into account with calibrated parameters the muscle force can be deducted from the EMG signal for different joint angles, as can be seen in the center diagram. The right diagram shows the EMG-to-force function fitted through the data of all trials, which establishes a consistent EMG-to-force relationship for different angles.

Expanding equation 4.4 with expressions from equations 4.5 and 4.7 yields (omitting the muscle index i):

$$\tilde{F}^m = f_A(\tilde{l}^m) F_o^m a(u) + f_P(\tilde{l}^m) F_o^m \tag{5.10}$$

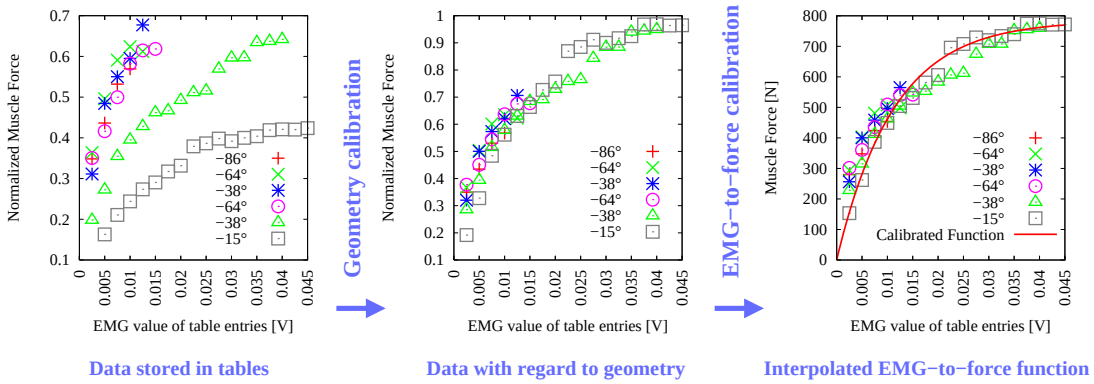

Figure 5.2: Steps of the parameter calibration for a single muscle. The left diagram shows the contents of six data tables for isometric contractions under different angles: The force output of the muscle based on the force sensor readings in each entry is plotted against the corresponding EMG activation. The middle diagram shows the same table, but the force is modified with the force-length curve after the geometry parameter s^t of this muscle has been calibrated: The EMG-to-force prediction has been made consistent for different joint angles. The right diagram shows the EMG-to-force function after calibration with data from all tables of the muscle.

where $\tilde{F}^m$ is an estimation of the muscle force based on the EMG signal u. Solving equation 5.10 for the function of the muscle activation results in

$$a(u) = \frac{\tilde{F}^m - f_P(\tilde{l}^m)F_o^m}{f_A(\tilde{l}^m)F_o^m} \tag{5.11}$$

Replacing $\tilde{F}^m$ with the force taken from entry h of table k, $F_{k,h}^m$, and canceling F_o^m yields

$$a(u) = \frac{\frac{F_{k,h}^m}{F_o^m} - f_P(\tilde{l}^m)}{f_A(\tilde{l}^m)} \tag{5.12}$$

With regard to the data tables, this equation can be interpreted as follows: For every entry h of a table k of a specific muscle, the muscle force, $F_{k,h}^m$, normalized by F_o^m, together with s^t (affecting $\tilde{l}^m$) define a point of the activation function, $a(u)$, depending on u through $u = \frac{h}{S}$ (equation 5.1 rearranged). As long as F_o^m is not known from prior calibration iterations, the term for f_P has to be omitted. In that case F_o^m is substituted by a constant value greater than zero. This introduces a linear error for all $a(u)$ that does not affect the outcome of the optimization, aside from the fact that the passive force is

not included. The consistency of this function across different tables is established if the resulting values, $a(u)$, for a given activation, u, are the same for all tables from a particular muscle. The absolute values are not important. Thus, the linear error is of no consequence.

Consistency can be established by reducing the standard deviation of the values obtained for $a(u)$ for a given activation u for all corresponding table entries of a particular muscle through optimization of s^t. The standard deviation of the force prediction of muscle i for the EMG value related to table entries with index h by equation 5.1 is:

$$\sigma_h(s^t) = \sqrt{\frac{1}{K}\sum_{k=0}^{K-1}\left(a(u_{k,h}) - \bar{a}_h)\right)^2} \tag{5.13}$$

with the activation function from equation 5.12, $a(u)$, the EMG value $u_{k,h}$ from table k and entry h, the number of tables of muscle i, K, and the average activation, $\bar{a}_h$. This computation can be performed for the entry indices h, because the scale S_i is constant for every muscle, relating the activation to the same entries for all tables of a particular muscle. It is assumed that all tables are filled.

Averaging the standard deviations, σ_h, for a particular slack length scale, s^t, over all activations is well suited to evaluate the quality of the calibration, and is computed by:

$$\bar{\sigma}(s^t) = \frac{1}{\hat{h}}\sum_{h=0}^{\hat{h}}\sigma_h(s^t) \tag{5.14}$$

with σ_h as defined in equation 5.13, and $\hat{h}$ being the highest entry index of all tables of this muscle.

The shape of the function $a(u)$ does not need to be known, which is very helpful considering the fact that different activation functions may be used for the muscles. Looking at the global scope, minimizing $\bar{\sigma}$ for every muscle delivers N optimized values s_i^t, one for every one of the N muscles.

The minimization can be performed by complete subspace search with a fixed step-size of, for example, 0.001m and an interval of $[0.85, 1.25]$ for the tendon slack length scales. This is preferred over other optimization algorithms, because local minima can exist. The error over the tendon slack length scales for an example calibration is shown in figure 7.1 right.

5.6 EMG-to-Force Calibration

In the previous step, the geometry parameters have been optimized, resulting in an improved consistency of the EMG-to-force relationship for different joint angles. The EMG-to-force calibration is closely linked to that.

In the EMG-to-force calibration, the parameters of the activation function $a(u)$ and the maximum isometric force, F_o^m, for every muscle have to be optimized in such a way that

$$a(u_{k,h})F_o^m - F_{k,h}^m \rightarrow \min. \tag{5.15}$$

for all tables k and all entries h of the specific muscle. $F_{k,h}^m$ is the force derived from the reference torque in entry h of table k for the particular muscle, and $u_{k,h}$ is the postprocessed EMG value. As motivated in section 4.3, two muscle activation functions, $a_{\exp}(u)$ and $a_{\mathrm{pw}}(u)$, with different parameters sets are utilized here. The calibration for both functions is described in separate sections below.

Both calibrations have in common, that the maximum expected EMG signal, R, can be directly read from the data tables: It equals the activation from the highest entry of all tables of a specific muscle. From the same entry, values for the maximum isometric force, F_o^m, could also be taken, but experiments have shown that the optimization can be improved noticeably if this value is optimized together with the other activation parameter(s).

Optimization of the Exponential Activation Function

According to equation 4.2, $a_{\exp}(u)$ is defined as

$$a_{\exp}(u) = \frac{e^{AuR^{-1}} - 1}{e^A - 1}$$

where A and R are the parameters of the activation function, and u the postprocessed EMG value. R can be determined as described before, and A is determined together with $F_o^m$by a two-dimensional optimization algorithm.

The error function of this optimization is given as

$$E_{emg}^{\exp}(A, F_o^m) = \sum_k \sum_h \left(a_{\exp}(u_{k,h})F_o^m - F_{k,h}^m \right)^2, \tag{5.16}$$

where the squared differences between forces predicted from the EMG signal, $a_{\exp}(u_{k,h})F_o^m$, and forces derived from the measurements, $F_{k,h}^m$, are summed over all entries of all tables of a particular muscle. A is bound to $-5 \leq A < 0$, and F_o^m to 100N$< F_o^m <$2500N.

Since the parameters are bounded and the search space has a low dimension, simple algorithms are sufficient. In this work, a subspace search was performed, which is described in appendix D.

Optimization of the Piecewise Activation Function

The piecewise activation function $a_{\mathrm{pw}}(u)$ is defined in equation 4.3 as:

$$\begin{aligned} a_{\mathrm{pw}}(u) &= \begin{cases} \frac{a_0}{\ln(A+1)} \ln(A\frac{u}{u_0}+1) & \text{if } u < u_0 \\ m(u-u_0)+a_0 & \text{otherwise} \end{cases} \\ \text{with} \quad u_0 &= 0.3R \end{aligned}$$

requiring three parameters: the maximum expected EMG signal, R, the shape of the logarithmic portion of the function, A, the activation at the transition point between the two portions, a_0, and the slope of the linear portion, m.

Again, R is directly taken from the top-most entry of all data tables.

Let $\hat{m}$ be the slope of the regression line of all entries of all tables of the particular muscle with signal $u > u_0$, and $\hat{a}_0$ the value (muscle force) of the same regression line at the point of transition between the two portions of the curve where $u = u_0$.

The muscle force of the linear portion can be computed by

$$F^m(u) = \hat{m}u + \hat{n} \tag{5.17}$$

where $\hat{n}$ is the y-intercept of the regression line. Now the maximum isometric force, F_o^m, can be calculated by:

$$F_o^m = F^m(R) = \hat{m}R + \hat{n} \tag{5.18}$$

Since $\hat{a}_0 = \hat{m}u_0 + \hat{n}$ it follows:

$$F_o^m = \hat{m}R + \hat{a}_0 - \hat{m}u_0 = \hat{m}(R-u_0) + \hat{a}_0 \tag{5.19}$$

Substituting $u_0 = 0.3R$ from equation 4.3 yields:

$$F_o^m = 0.7R\hat{m} + \hat{a}_0 \tag{5.20}$$

The slope of the activation of the linear portion of $a_{\mathrm{pw}}(u)$, m, can now be obtained by

$$m = \frac{\hat{m}}{F_o^m}, \tag{5.21}$$

and the activation level at the point of transition by

$$a_0 = \frac{\hat{a}_0}{F_o^m}. \tag{5.22}$$

The parameter A is determined by linear minimum search within the interval $[A_s, A_e]$ with $A_s = 5$ and $A_e = 100$ (boundaries experimentally determined). The error function for this minimum search is similar to the error function for the exponential activation

function, given in equation 5.16, but with F_o^m already known:

$$E_{emg}^{\mathrm{pw}}(A) = \sum_k \sum_h \left(a_{\mathrm{pw}}(u_{k,h}) F_o^m - F_{k,h}^m \right)^2 . \tag{5.23}$$

This function only depends on the non-linear shape factor, A.

5.7 Remarks on Cocontraction

When calibrating the EMG-to-force parameters, cocontraction cannot be neglected. It strongly affects the values for the maximum isometric contraction, as does coactivation. This is taken into account by equation 5.7 during torque distribution when the parameters are calibrated. Since the muscles are calibrated in sequential order, the EMG-to-force calibration can be repeated to apply the EMG parameters to the distribution.

If the cocontracting muscles are neglected in equation 5.6, the calibration error of the maximum force, F_o^m, can reach about 50%.

Experiments revealed that due to the linear approximation of the activation for uncalibrated muscles, a single repetition is sufficient, and should be performed to incorporate the effect of the passive muscle force in the geometry calibration. Additional iterations do not improve the results considerably. This is analyzed in section 7.1.1 with some examples.

5.8 Properties of the Calibration

The calibration presented in this chapter has a number of important properties which are summarized here for convenience.

- The algorithm has an automatic selection of relevant measurements for calibration. This keeps the number of reference values low and reduces the computational effort of the optimization algorithms.
- Storing the data in tables indexed by the activation of the individual muscle puts the same weight on all activations. If desired, the weight could be modified according to the EMG activity, emphasizing a special range of muscle activity.
- The algorithm is fast due to splitting of the whole set of parameters into several groups, reducing the parameter space for the individual optimizations.
- The algorithm uses an estimation for the computation of the individual muscle contributions. Initially, this distribution assumes a linear activation function, and the distribution is refined with calibrated activation functions for repeated iterations.

- The passive muscle force is included in the geometry optimization only for repeated optimizations.
- Because the optimization includes sequential steps of low-dimensional optimizations, in contrast to an optimization where all parameters are determined at the same time, the whole algorithms allows interesting insight into the process. The behavior of the system as well as measurement artifacts and results of the calibration can be interpreted. Local minima are avoided if the step size of the subspace search is chosen small enough without increasing the computational effort beyond limits. This assumes that the torque distribution is not too inaccurate.
- Due to the low dimension of the parameter spaces, the algorithm is well suited for optimization with a reduced number of reference recordings. Of course, accuracy is improved with more trials.
- The fixed distribution of the measured torque to the individual muscles can be inaccurate and reduce overall performance. It is not as adaptable as a complete optimization. On the other hand, an all-in-one optimization can result in a distorted distribution among the muscles if they are activated in linear relation. In that case, an all-in-one optimization cannot determine which muscles contribute which portion. Experiments have shown that a linear relation between the activations is common for muscles out of the same group (extensor group, flexor group).

Finally, it is to be noted that this calibration algorithm turned out to be very helpful during investigation of the biomechanical model utilized in this work. It allowed deep insight into the mechanics of the model and interpretation of parameter variation and resulting effects during the development of this work.

Important results from those investigations, like the performance improvement through inclusion of the geometry model, together with experimental data from calibrations are presented in chapter 7. But before that, chapter 6 presents the hardware that was developed for those experiments.

6 Exoskeleton Hardware

In the introduction the importance of mobility for people has been motivated. The variety of potential applications gave birth to the idea to develop a powered lower extremity exoskeleton. In order not to run into too many problems with the mechanical construction, the exoskeleton was designed to support only everyday movements: sit-to-stand, stand-to-sit, walking, and climbing stairs up and down.

From the joints mainly involved in those tasks – the hip, knee and ankle joints – the knee was chosen for support, because it is very important for movements which require large forces and where support is actually helpful: the sit-to-stand and stair climbing movements. During normal gait, large propulsive forces are produced in the ankle joint, but adding support for those muscles is more a mechanical engineering challenge because of more stringent size and weight constraints. Lack of hip muscle forces can be compensated in part through pelvis motion.

This chapter describes the mechanical construction and the electronic components of the exoskeleton. It is organized as follows: In the following section 6.1 general requirements of an exoskeleton to support the knee joint are specified. Those requirements lead to a design which is described in section 6.2. The actuation of this exoskeleton is described in section 6.3, followed by the sensors in 6.4, the data processing unit in 6.5, and the communication structure that connects all components in section 6.6. Safety issues are discussed in section 6.7 before the chapter is closed with a summary of the properties of the exoskeleton in section 6.8.

6.1 Requirements

This section describes the requirements of the system. The design parameters of the exoskeleton are: range of motion, velocity in the knee joint, torque in the knee joint, size and weight, and power consumption.

The range of motion can be directly measured: It should range from 0° (straight leg) to approximately -110° (knee flexion). While the natural range of motion is larger, it is sufficient for the movements which should be investigated.

The required velocities are functions of the joint angles for the particular movements. Figure 6.1 shows the velocities plotted over the knee angle for a single step of slow and normal gait, the sit-to-stand movement and slow stair climbing. For normal gait, angular velocities of 200–400/s are not uncommon, while slow walking requires velocities of about 100/s. During the sit-to-stand movement, the velocities are rather small, typically below 100/s. Figure 6.3 shows an example plot of the knee angle and

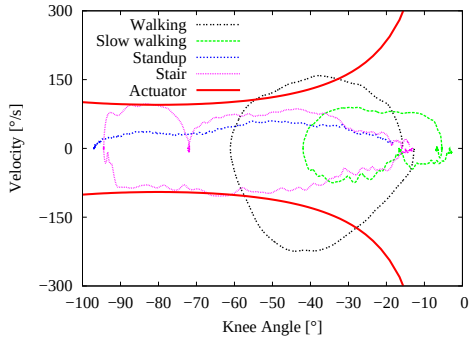

Figure 6.1: Angular velocity against knee angle for walking, sit-to-stand, and stair climbing, together with actuator maximum angular velocities (no load).

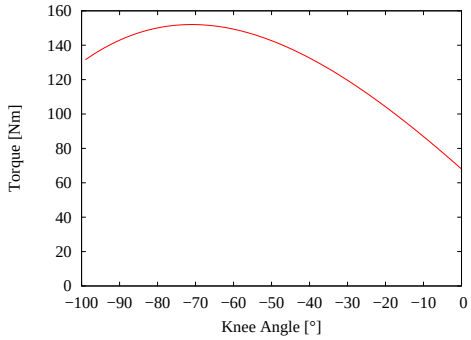

Figure 6.2: Maximum actuator torque plotted over the range of motion. The torque is largest at an angle of -75 due to the geometry of the attachment.

velocity trajectories of normal gait. It has to be pointed out, that the movements are performed rather slow, as could be expected from people who are in need of support.

The required torque in the knee joint is not so easy to define. It depends on the size and weight of the subject and how much support is desired. But a maximum torque of approximately 50–100Nm should be sufficient for the experiments intended here. It should be kept in mind that the power of the actuator determines its size, weight, and power consumption. For those parameters no definite limits can be given, since they are a matter of comfort and acceptance.

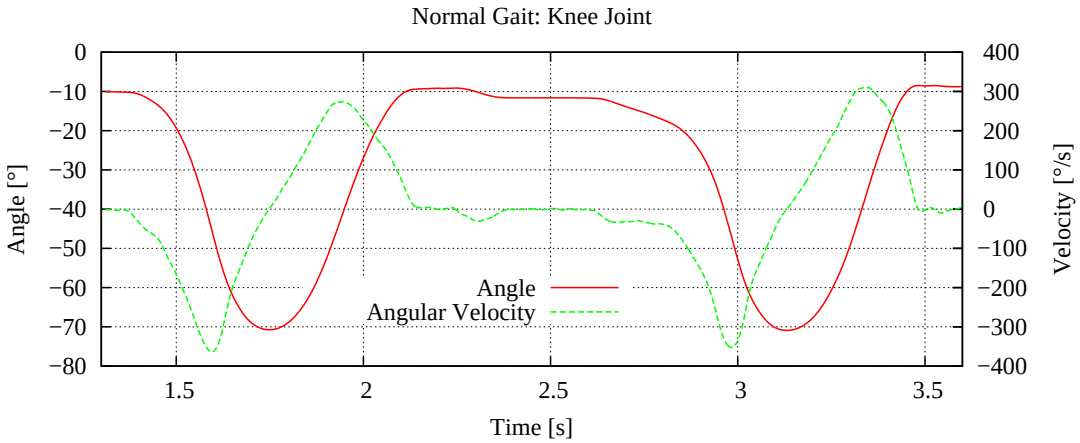

Figure 6.3: Example of normal gait: knee angle trajectory and angular velocities plotted against time.

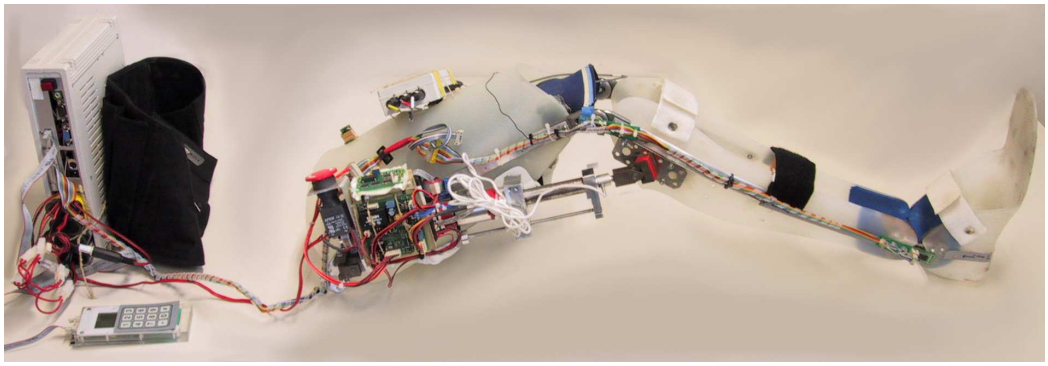

Figure 6.4: Complete exoskeleton, with the actuator connecting thigh and shank of the orthosis (right), the single board computer and power supply attached to the waist belt (left), and the display and keypad (bottom left).

6.2 General Design

The overall design of the exoskeleton system is based on an experiment orthosis manufactured by Otto Bock[1] that is normally used for patients with disabilities in their locomotor system. As shown in Fig. 6.4 the orthosis covers the thigh, shank and foot with two hinge joints at the knee and ankle. The two joints limit the motion to a single axis each, allowing movement in sagittal plane only. Support for the operator is only given at the knee joint, the ankle joint can be moved passively and allows putting the additional weight of the exoskeleton to the ground. The force support is produced by a linear actuator, shown in detail in figure 6.5, that is connected at the thigh and shank of the orthosis with two joints with two degrees of freedom each. By changing the length of the actuator the angle between thigh and shank can be modified. The force of the actuator is measured by a sensor attached between the tip of the actuator and the joint with the shank.

Embedded in a soft fabric between the orthosis and the leg of the human are six EMG sensors: three on the frontside and three on the backside of the thigh, measuring the activity of six muscles responsible for knee flexion and extension.

All sensors are connected to an SPI[2] bus that is used by a single board computer (SBC) for data acquisition and support control. The power supply can be carried on a waist belt, as can be seen in figure 6.4, allowing full autonomous operation.

6.3 Actuation

Regarding the actuation, one has to decide between several fundamental concepts: rotatory actuators (like electric motors with harmonic drives), or linear actuators (electric

[1] Otto Bock HealthCare GmbH, 37115 Duderstadt, Germany

[2] Serial Peripheral Interface bus: synchronous serial data link standard designed by Motorola.

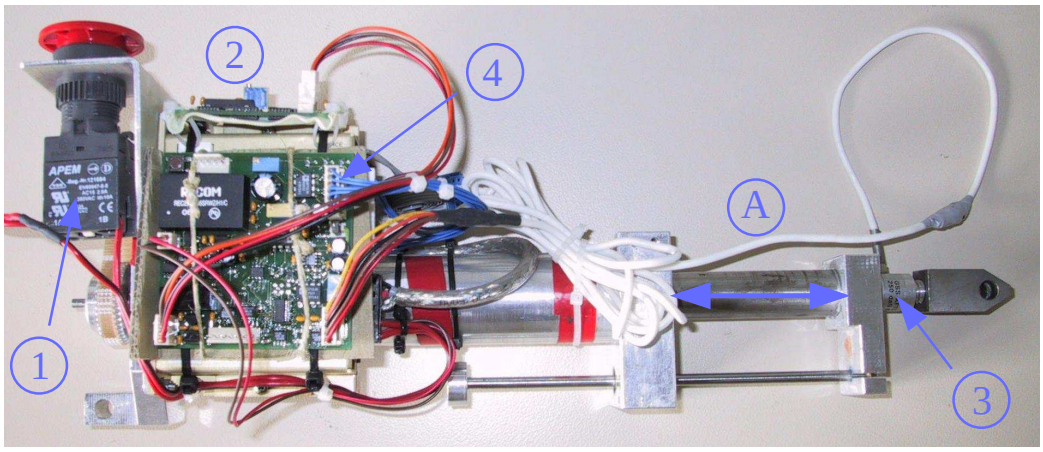

Figure 6.5: Actuator that is attached to the knee joint: (1) emergency switch, (2) watchdog, (3) force sensor, (4) hardware PID controller and signal conversion board. The pwm-amplifier and DC motor are hidden below (4). (A) Shows the direction of action of the piston.

motors coupled to ball screws, pneumatic or hydraulic pistons, pneumatic muscles). We decided to use an electric motor that is connected to a ball screw with a gear belt for the following reasons: When the actuator is attached to the thigh and shank of the exoskeleton properly, the geometry of the actuation results in a variable transmission from the linear velocity to the angular velocity and from the actuator force to the joint torque. When the knee is flexed the actuator produces a large torque with a low angular velocity, whereas in the straight-leg configuration the torque is rather small in favor of a high angular velocity. This is a very desirable property, because it resembles characteristics of human movement: For example, the sit-to-stand movement is quite slow but requires large torques during the initial phase of getting up. Walking on the other hand requires high angular velocities in the knee joint during swing phase where the leg is being extended, but only little torque. Climbing stairs is somewhere in-between: The movement itself is slower than walking but requires more torque, and higher angular velocities are found in regions where the knee is more flexed but with low torques. This is a superior property compared to rotatory actuators, since it resembles the characteristics of human movements. A common alternative approach with actuation through harmonic drives does not have this advantage: Since the geometric relationship remains unchanged in all joint configurations, the actuation has to be able to produce the maximum required torque and angular velocity under the same circumstances. Figure 6.1 shows the angular velocity plotted against the knee angle for walking, climbing stairs and the sit-to-stand movement. All those movements are performed rather slowly, as performed by people who are in need of support.

An electric actuation was chosen because the overall power to weight ratio, that is, actuation plus power supply, is lower than for the others, and electric motors allow execution of very smooth motions.

The linear actuator consists of a ball screw connected to a standard DC motor[3] by a gear belt and is shown in figure 6.5. Attached to the casing of the ball screw is the pwm-amplifier[4] which powers the actuator, a circuit board which connects the amplifier to the SPI bus, and a watch dog that takes over control in case of a computer failure.

The motor is a maxon RE35[5] with a power consumption of 90W, and a maximum power output of 206W at 42V. The amplifier is a Copley 4122Z[6] with a voltage range of 24–90V and a maximum output current of 20A. The total weight of the actuator is 2.5kg.

The actuator can change its length between the points of attachment from 300–430mm, and has a maximum force output of approximately 1700N. The points of attachment to the orthosis have been chosen in such a way that the resulting range of motion and angular velocity is sufficient for slow every-day movements. The location of those points is given in appendix B. Arranging those points is a trade-off between the angular range of motion, the maximum angular velocity, and the resulting maximum torque in the knee joint for a given actuator.

In the chosen configuration the range of motion is approximately 110, which is smaller than the natural range of motion for safety reasons. The angular velocity is depending on the linear velocity and the current knee angle. The resulting angular velocity without load for the maximum linear velocity of approximately 100mm/s over the range of motion is plotted in figure 6.1 together with examples of the movements of interest. It can be seen that for most movements the angular velocities are sufficient, because they fall in-between the curves of the actuation.

In figure 6.2 the maximum torque produced by the actuator is plotted over the joint angle. The maximum torque is produced at a joint angle of -75 due to the points of attachment of the actuator to the orthosis.

The torque that can be applied to the orthosis by the actuator is also limited by the fact that the orthosis is deformed under large forces. Not the whole force that is produced by the actuator is immediately transferred into a joint torque.

Obviously an actuator can be constructed that would be fast and powerful enough for fast movements. Limitations are only given by the additional weight that would be imposed on the operator. In this work the focus is put on the man-machine-interface and not on the mechanical construction. A lightweight actuator that is sufficient to support slower motions was used for this purpose.

[3] Electric motor that is powered with direct current (DC).
[4] Amplifier generating output signals with pulse-width modulation.
[5] maxon motor uk, http://www.maxonmotor.co.uk/, 2007.
[6] Copley Controls Corp., http://www.copleycontrols.com/, 2007.

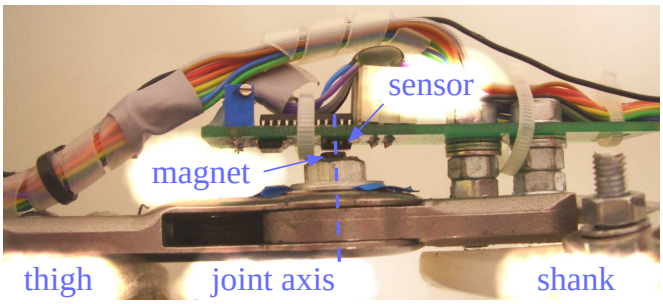

Figure 6.6: Hall sensor attachment to the knee. The magnet is mounted on the thigh part of the knee joint. The Hall sensor is fixed to the circuit board above the magnet which is connected to the shank of the orthosis.

6.4 Sensors

Three different types of sensors are attached to the exoskeleton: The first type measures the knee angle, the second type the force output of the actuator, and the third type reads the EMG signals of the operator.

Angle Sensor

The control system needs the knee and hip angles to properly predict the muscle forces. This can be performed very simply for the knee joint, since the orthosis limits the motion of the knee joint to the sagittal plane around a single fixed axis. This allows the application of a Hall sensor which is accurate and reliable.

As shown in figure 6.6, the magnet is attached to the thigh of the orthosis and the Hall sensor is placed above the magnet on the circuit board which is fixed to the shank. During joint rotation the orientation of the magnetic field below the sensor is changed, which is measured by the sensor.

The Hall sensor is a Philips[7] KMZ41, connected to a Philips UZZ9001 signal conditioning IC [DW00], which readily provides a digital output to the bus.

Due to the three degrees of freedom in the hip joint, a complex mechanical construction or other sensors, like goniometers, would have to be applied, making the application of the exoskeleton more uncomfortable. Thus, the hip angle is not measured, but determined in two different ways: During calibration it is set to 90, because it is assumed that the operator is sitting upright on a chair. During walking and climbing stairs the hip angle is set equal to the negative knee angle, which is an unconventional but sufficient approximation. Besides, the hip angle only affects the prediction of the two-joint muscles, which are the rectus femoris and the flexor muscles, but the large forces in the considered movements are contributed by the vastus medialis and vastus lateralis.

[7] Philips Semiconductors, http://www.philips-semiconductors.com, 2007.

Force Sensor

The force sensor is attached in series with the actuator as can be seen in figure 6.5. It is responsible for measuring the force that is produced by the actuator. The force sensor is a GS XFTC300[8] with a range of $\pm$2000N, a non-linearity of less than $\pm$0.5% full scale, and a sensitivity of $\pm$10mV/V. It is connected to a level adaptation circuit which outputs to the MAX1230[9] 12-bit A/D-converter which is connected to the bus.

EMG Sensors

The EMG sensors reading the muscle activations are embedded in a soft tissue of the orthosis which is holding them on the skin on top of selected muscles. The choice of muscles and sensor location is described below. The sensors are Delsys 2.3 Single Differential Electrodes[10] which have an inbuilt bandpass from 20–450Hz, and an amplifier with a gain of 1000V/V. An additional amplifier and level shifter adapts the output to the MAX1230 12-bit A/D-converter which is connected to the bus.

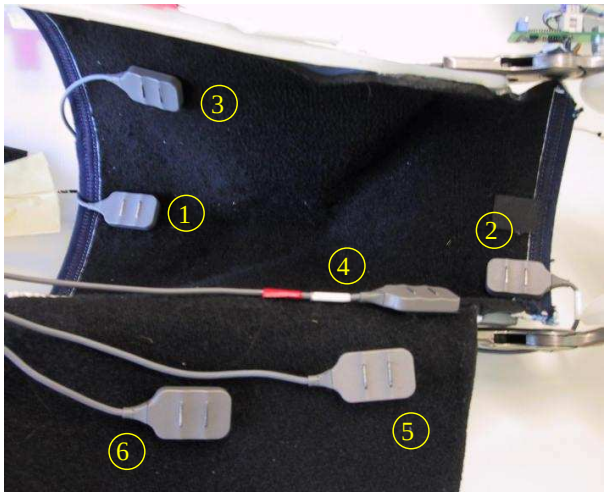

Figure 6.7: Six EMG sensors are embedded in the thigh brace of the orthosis: (1)-(3) measuring knee extensor activities, (4)-(6) measuring knee flexor activities.

Figure 6.7 shows the EMG sensors embedded in the thigh brace of the orthosis. Three sensors are measuring knee extensor activities on the frontside of the thigh and three sensors knee flexor activities on the backside.

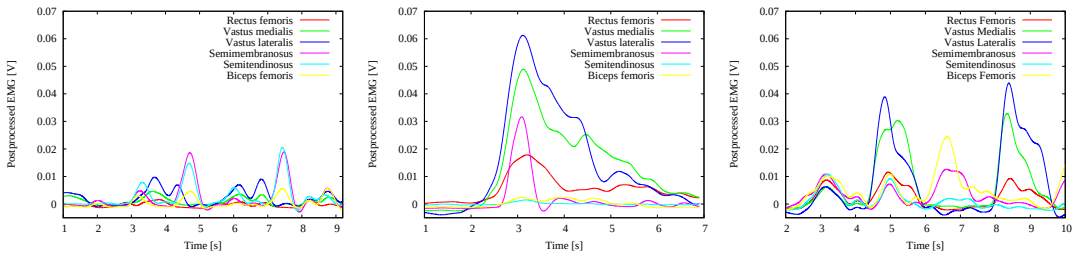

Figure 6.8: Example of postprocessed EMG patterns of walking (left), standing up (middle), and climbing a stair (right). The signal is amplified by the electrodes.

Muscle Selection and Sensor Placement

Since the exoskeleton can only offer support in the knee joint, it is feasible to try to detect the intention by reading activations of muscles which flex and extend the knee. Figure 6.9 shows those muscles.

Although all those muscles are mainly working on knee flexion and extension, some of them also have other tasks: The sartorius for example is also flexing the hip joint and can rotate the shank inwards. Stronger muscles are only activated during tasks that require more force like raising from a chair, whereas smaller muscles are activated during tasks where finer force control is necessary, for example, when positioning the foot prior to floor contact. Depending on the kind of movement that is performed, different muscles can be activated, or in a slightly different order. Following that, it would be best to be able to record all muscles to properly analyze the desired movement.

Unfortunately it is not possible to measure all muscles with surface electrodes. As can be seen in figure 6.9, some muscles are located deep within the thigh close to the femur.

It is reasonable to select muscles according to their proximity to the skin, because they can be measured by surface electrodes, and their strength, because of a potentially high contribution to the movement, to get a good estimation of the overall force production.

Deciding which muscles have to be evaluated is a trade-off between complexity and accuracy of interpretation.

The muscles selected for the exoskeleton of this work with their %PCA are: (1) the rectus femoris (8%), (2) vastus medialis (15%), (3) vastus lateralis (20%), and (4) the semimembranosus (10%), (5) semitendinosus (3%), and (6) biceps femoris (10%). Those muscles are shown in figure 6.9. They cover a total of 66% of the cross-sectional area of all thigh muscles. The remaining area is occupied by the vastus intermedius (13%), gastrocnemius (19%), sartorius (1%), and gracilis (1%) [Win90a]. While the latter two are neglectable due to their small force output, the gastrocnemius is not

[8] Distributed by GS sensors / disynet, http://www.sensoren.de, 2007.
[9] From Analog Devices, Inc., http://www.analog-devices.com, 2007.
[10] Delsys Inc., http://www.delsys.com/Products/EMGSensors_Specifications.html, 2007.

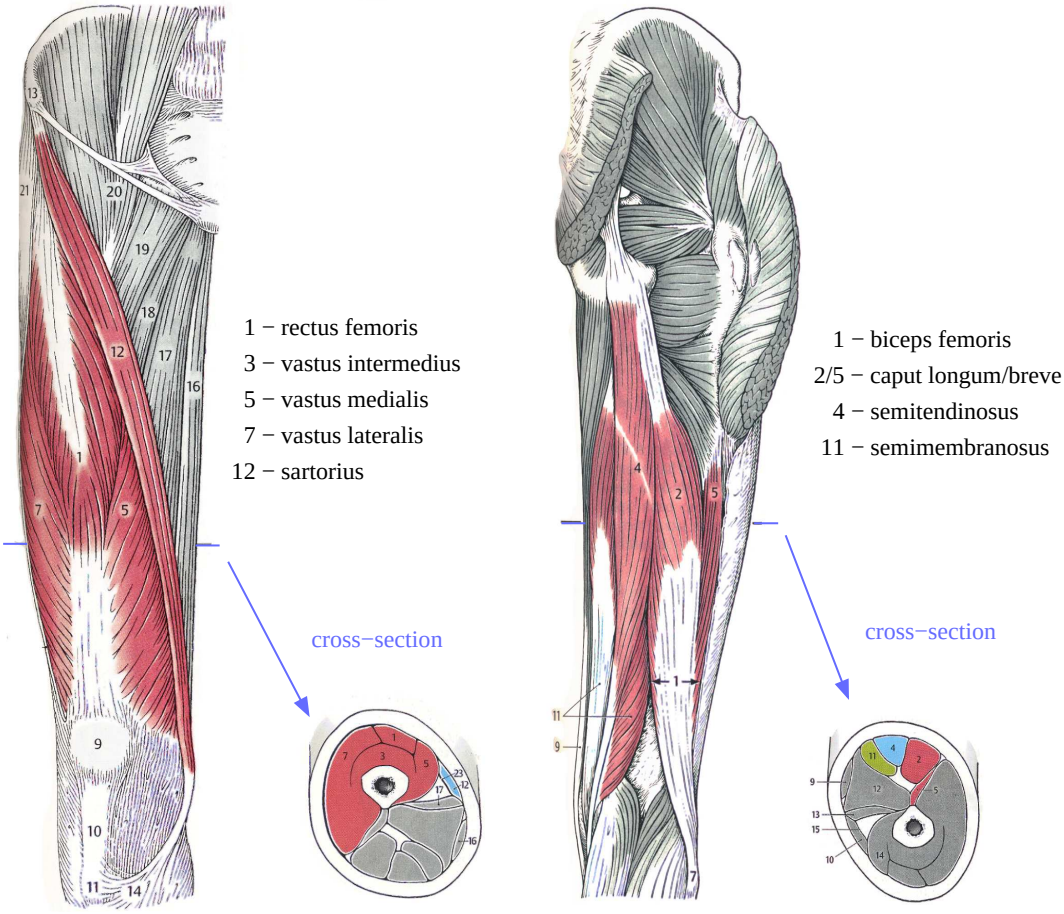

Figure 6.9: Superficial muscles of the frontside of the thigh (left) and the backside (right), together with cross-sectional views (adapted from [Pla03]). The dark colored muscles are responsible for flexing and extending the knee, the gray shaded are moving the hip and ankle joints. The cross-sectional view of the extensor muscles (left) shows the vastus intermedius hidden beneath the rectus femoris and the vasti.

recorded because it is a muscle spanning the knee and ankle joint. Muscle activations cannot simply be related to the knee joint without taking into account the ankle. The vastus intermedius unfortunately is not recordable with surface electrodes. It is located along the frontside of the femur below the rectus femoris, the vastus medialis and the vastus lateralis.

Figure 6.8 shows the activation pattern of the selected muscles for some example movements. Especially for the extensor muscles it can be seen that recording of all three muscles is required since they are active at different times.

Choosing the correct position and orientation according to the muscle fibers is very crucial to this application. Bad sensor placement results in measurements that do not reflect the force production. General placement recommendations are published for

example in [Luc07], and a guide to sensor placement for individual muscles can be found in [HFM+99, FH00].

6.5 Data Processing Unit

The single board computer is a Commel LE-370[11] equipped with a Pentium-M735 1.7GHz[12] and 1GB of RAM. The operating system of the SBC is SuSE 9.3[13], running the real-time linux RTAI[14] with kernel 2.6.15.

The realtime data acquisition system was written as part of a diploma thesis [Wal06], and the software evaluating all sensor data and computing the control signal is described in chapter 4.

In the system presented here, the torque control loop was running as a kernel module with 1kHz, the model evaluation and support computation was running in user space in non-realtime with approximately 100Hz.

6.6 Signal Flow

The hardware structure is organized around a central SPI bus that connects all components, as shown in figure 6.10. Those components are the SBC, the display and keypad unit, the sensors and the actuator. The safety system is connected to the bus as well, but only to listen for a heartbeat of the computer.

The SPI bus is a master-slave bus where the SBC serves as the master talking to all other devices. Since the SBC has no direct SPI interface, an Atmel MEGA32 microcontroller[15] acts as interface between the SPI bus and the parallel port of the SBC. All sensors are connected to the SPI-bus by A/D-converters (ADC) where necessary. The Philips UZZ9001 (UZZ) is an integrated circuit that evaluates and postprocesses the output of the Hall sensor, and performs A/D conversion. A D/A-converter (DAC) is connected to the bus to create the analog control signal for the pwm-amplifier that powers the actuator. In addition to that, a display and keypad is linked to the bus to allow simple user interaction, like starting and stopping the system and to adjust the support ratio.

6.7 Safety Concept

The safety concept is a bundle of different measures which prevent and handle system failures, and minimizes consequences for the operator on different levels, depending on

[11] Commate Computer Inc., http://www.tcommate.com.tw/manual/LE-370.pdf, 2007.
[12] Intel Corporation, http://www.intel.com/products/processor/pentiumm, 2007.
[13] SuSE Linux can be found on http://www.novell.com/linux/, 2007.
[14] RealTime Application Interface, https://www.rtai.org/, 2007.
[15] Atmel Corporation, http://www.atmel.com/, 2007.

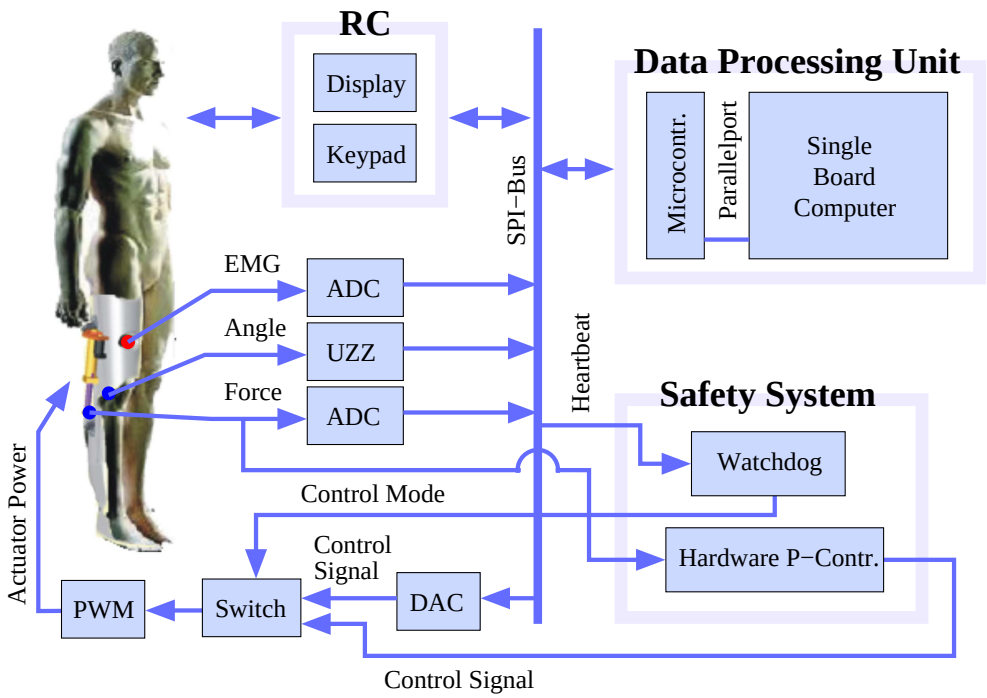

Figure 6.10: Overview of the hardware structure of the control system: All components use the central SPI bus that connects all sensors and the actuator. The SBC acts as the master and collects all sensor data over the bus. The hardware watchdog monitors the activity on the bus, and switches to the hardware P-controller as long as the single board computer does not send commands to the pwm-amplifier, assuming an SBC failure.

the layer where they occurred. This safety system allows experiments and application of the exoskeleton in life-like environments.

But it has to be pointed out that a secure fallback state does not exist for an exoskeleton. Depending on the movement in which the error occurs, the system cannot determine a safe position on its own to avoid stumbling and to maintain a stable pose. For example, extending or flexing the knee joint by default might unbalance the operator, and holding the knee angle fixed can lead to stumbling over an obstacle or a step. Nevertheless, some actions can be performed to minimize consequences of a failure.

The following subsections are arranged in order of fault-handling, explaining possible error sources and countermeasurements.

Software

In the software layer all sensor data is range-checked and clipped to sensible boundaries. The calculated desired force as well as the raw output to the D/A-converter are clipped in case of errors in the calculation of the desired support.

This minimizes bad system behavior if connection to sensors is lost or EMG sensors

are not well connected to the skin anymore. But of course, misinterpretation of valid sensor signals can result in natural movement, which can still let the operator stumble over obstacles. But since the algorithm presented in chapter 4 is very robust, and since the operator is in direct and permanent control of the performed movement, this should not happen. But it cannot be guaranteed or mathematically proven.

Hardware

The external hardware watchdog is permanently monitoring the chip select line to the D/A-converter of the actuator. If the chip is not selected for a few hundred milliseconds (adjustable), the watchdog assumes that the SBC has stopped working properly. It switches the input of the pwm-amplifier from the D/A-converter connected to the SPI bus to a hardware P-controller through a CMOS switch as shown in figure 6.10. This P-controller gets the current actuator force as feedback and controls the output signal to the pwm-amplifier in such a way that a preset force between thigh and shank is applied. This force was set to zero during experiments with a healthy operator who can stabilize himself, allowing unhindered motion with the leg if the computer is locked up or the SPI-bus is broken. No force support is generated in that case. If the SBC is sending commands to the pwm-amplifier again, the watchdog switches back to software control. This is not always a desirable solution, especially if the system fails while the operator is supporting himself only with the actuated leg. On the other hand, locking the actuator may lead to stumbling in many other cases. Due to weight and power consumption limitations, adding a second system that runs in hot-standby is not an alternative. But the target force can also be set to a value above zero so that the actuation adds some constant extension force to give the operator a chance to react properly and support himself or herself. But in any case, the movement will not be as expected by the operator and stumbling may occur.

Mechanics

If for some reason (a short circuit or something similar) the control signal of the actuator is unreasonably large or will command the actuator to drive with full power in one direction, the last safety protection for the operator are the joint angle limitations that are stricter than the natural range of motion of the knee joint. The maximum acceleration is limited through the maximum moment the motor can generate and this is well within safety limitations. Furthermore, the actuator has its own mechanical limitations. For the knee flexion this limit is reached before the human or exoskeleton joint limits are reached. The limit of the extension is reached slightly after full extension, but deformation of the orthosis protects the operator in that case. If the actuator is working with full force against its own mechanical limits, the gear-belt that connects the electric motor and the ball screw will tear apart before any harm is caused.

In case of a complete power failure, the exoskeleton cannot produce support actively. But the friction of the actuator is rather large, so that it does not immediately give way

to undesired knee flexion. On the other hand the actuator is not completely locked, and the knee joint can be moved from outside in this case.

6.8 Summary of Properties

The exoskeleton presented in this work is optimized for the desired experiments. The movements of interest are sit-to-stand, walking and climbing stairs. It limits the movements to rather low velocities, to allow the actuator limited in size, weight and power to produce enough force to support the strenuous parts of the movements. During walking the required forces are rather low, and the other movements are better suited to show the performance of the system.

The system itself is completely mobile. The autonomous running time is mainly depending on the power consumption of the actuator and the SBC. While the consumption of the first one highly depends on the performed movements and support ratio, the latter one has a permanent, rather large consumption. The presented algorithm can also work with an SBC with lower computational power requiring less energy.

The experiments presented in the following chapter 7 verify that the exoskeleton construction is suitable to perform the desired movements with adequate support to allow an analysis of the cooperation between the human operator and the machine.

7 Experiments

This chapter presents experiments with the exoskeleton. Those experiments are divided into two groups: The first group is used to perform and analyze the calibration algorithm, and the second group presents experiments with the actuated exoskeleton.

In the first group recorded data is used to calibrate the model parameters, and the performance of the model is tested with several measurements. The complexity of the model is justified by pointing out the improvements by including certain properties. Furthermore, the model prediction characteristics are quantified for data not previously used during calibration. In the second group the behavior of the whole system, that is, the human operator using the exoskeleton, is analyzed, regarding common movements like walking, climbing stairs and the sit-to-stand movement. The support for the different phases of the movements is discussed, and the resulting reaction of the human. For those experiments the performance of the system as a whole is hard to quantify. The difficult question is: How can the interface and the intention prediction be evaluated? An exact "reference desire" in a natural environment is not available to compare the prediction with. But methods applied in this work are explained as an introduction to the experiments with actuation in section 7.2.1.

For both groups, representative data is shown in greater detail to explain the behavior of the system at some crucial points. This is very important to get a good understanding of the matter. Only after that it is useful to look at the performance as a whole.

During all experiments it was tried to avoid muscle fatigue through appropriate pauses, since it is not considered in the model and can influence the quality of the results.

The chapter is organized as follows: Section 7.1 describes the calibration experiments, including the model analysis and justification, section 7.2 presents the system behavior of the actuated exoskeleton, and section 7.3 discusses the experiments and summarizes the overall system behavior.

In most of the following diagrams the knee angle is shown. A knee angle of 0 indicates full extension, and negative values indicate knee flexion.

7.1 Calibration

As described in section 5.1, the calibration is divided into determination of geometry parameters and determination of EMG-related parameters. For both operations, the operator is sitting on a chair in an upright position performing isometric contractions with extensor and flexor muscles of the knee under different angles as described in

section 5.2. The leg with the exoskeleton must not have any floor contact below the knee joint.

During every measurement, the muscles have been contracted four to five times with a large, but submaximal force. In-between the measurements short pauses have been inserted to avoid muscle fatigue.

The calibration example described in this section was performed on data from the following exercises:

1. isometric extension (trials E0-E4) at $-101°$, $-86°$, $-70°$, $-47°$, and $-27°$.
2. isometric flexion (trials F0-F4) at $-95°$, $-73°$, $-64°$, $-47°$, and $-33°$.

The geometry optimization was performed as described in section 5.5, with different properties activated to show the performance of the model. Afterthat, the EMG-to-force parameters have been optimized according to section 5.6, and optimization of the geometry calibration and the EMG calibration has been repeated to refine the solutions as described in sections 5.5 and 5.7.

Results of the calibration are presented and analyzed in the following sections.

7.1.1 Geometry Calibration

It should be pointed out onesmore that the geometry calibration is responsible for establishing consistency of the EMG-to-force relationships across different joint angles. According to section 5.5 the consistency is improved if $\bar{\sigma}$, given in equation 5.14, is reduced for every muscle. To analyze this, and to justify the use of the complex body model and some properties, the geometry calibration has been performed in five versions. Every version turns off specific features.

The first version does not include the musculotendinous model at all. The knee torque contribution of a muscle is calculated by

$$T = rF_o^m a(u) \tag{7.1}$$

where r is the moment arm around the joint, F_o^m is the maximum isometric force at optimal fiber length, and $a(u)$ the activation of the muscle.

The second version includes the musculotendinous model, but does not calibrate the tendon slack length scale of the muscle: The scale is set to $s_i^t = 1.0$ for $0 \leq i < N$, with N being the number of muscles. The third version includes the musculotendinous model, but omits the influence of the passive force, F_P^m, and the pennation angle, ϕ. The fourth version only neglects the pennation angle, and finally, the fifth version incorporates the complete model as described in section 4.3.

Table 7.1 shows the minimum averaged standard deviations as of equation 5.14 for the different versions. The resulting tendon slack length scales are given in table 7.2 (session S5). It can be seen that the complete model can reduce the values by more than fifty percent compared to the absence of the model. This is especially important

	without geometry	uncalibrated geometry	calibrated, no F_P^m, no ϕ	calibrated, without ϕ	complete model
rectus femoris	50.1	9772.7	24.8	23.5	23.3
vastus medialis	36.5	38.3	11.9	12.4	12.4
vastus lateralis	50.2	53.5	22.3	20.6	20.0
semimembran.	75.9	224.6	86.5	86.5	55.5
semitendinosus	24.1	49.3	22.4	22.2	22.3
biceps femoris	66.5	229.4	47.2	43.4	43.4

Table 7.1: Minimum $\bar{\sigma}$ of different versions of the geometry calibration for the individual muscles, as detailed in the text, multiplied by the approximated F_o^m of the individual muscles (refer to section 5.5). The unit is [N].

for the extensor muscles, since they are producing large forces during the considered movements, and bad estimations result in system behavior that is hard to predict for the operator. The results in table 7.1 also show that the inclusion of the musculotendinous model without a proper calibration can produce results that are far worse than without the model at all. This is due to the strong effect of the force-length relationship on the force output, and the sensitivity of the model to the tendon slack length and the associated scale. To show this more clearly, figure 7.1 (right) shows the individual $\bar{\sigma}_i$ as a function of the tendon slack length scale. As can be seen, the minima lie in very narrow valleys for most muscles.

Figure 7.1 (left) shows which part of the force-length curves is covered with the angles from this particular calibration. Both figures explain the results from the calibration very good: The scale for the rectus femoris is $s_0^t \ll 1.0$ resulting in a larger $\bar{\sigma}$ of the uncalibrated model as shown in table 7.1. Using the calibrated geometry model without the passive force and pennation angle reduces $\bar{\sigma}$ massively, and inclusion of the latter two improves the results even further. The $\bar{\sigma}(s^t)$ curve for the vastus medialis is not so steep for $s_1^t < 1.12$, so using default values from literature does not produce a $\bar{\sigma}$ as large as for the rectus femoris. It is similar to $\bar{\sigma}$ without the model at all. But applying the calibration reduces $\bar{\sigma}$ to 33%. Inclusion of the passive force and the pennation angle makes the result slightly worse due to small errors in the model. Leaving the geometry model out and using uncalibrated parameters for the vastus lateralis yields similar results, but inclusion of the calibration reduces $\bar{\sigma}$ to 44%, and inclusion of the passive force and pennation angle successively down to 40%. The minimum of the semimembranosus lies in a very narrow valley, resulting in a large $\bar{\sigma}$ for the uncalibrated parameters. Inclusion of the calibrated geometry model without the pennation angle does not improve the result compared to not using the model at all. The pennation angle at optimal fiber length, ϕ_o, of this muscle is 15, and including this property reduces $\bar{\sigma}$ by approximately 27% compared to not using the geometry model. Inclusion of the model for the semitendinosus reduces $\bar{\sigma}$ by approximately 10% compared to not using the model, and by more than 45% compared to the uncalibrated

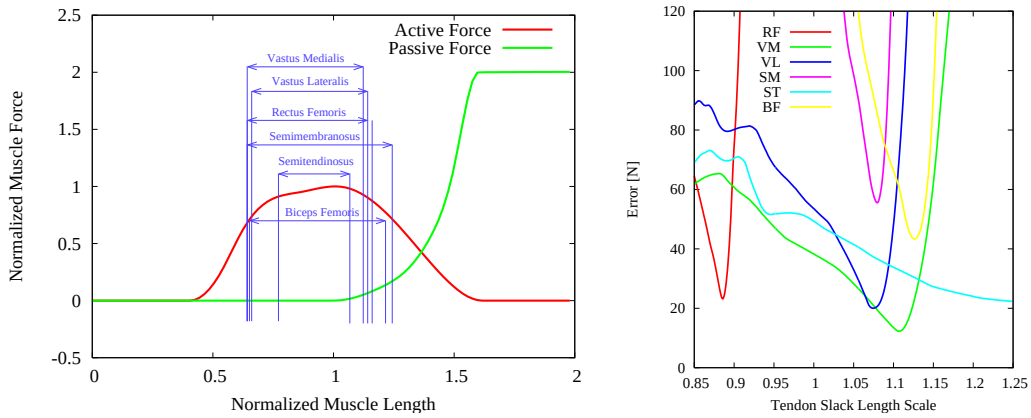

Figure 7.1: Left: ranges of the normalized muscle fiber lengths for the minimum and maximum knee angles during calibration. Right: $\bar{\sigma}$ during calibration of the tendon slack length scales s_i^t for the rectus femoris (RF), vastus medialis (VM), vastus lateralis (VL), semimembranosus (SM), semitendinosus (ST), and biceps femoris (BF). Due to simplifications in the model, the semitendinosus has no minimum within the interval.

model. The different knee angles of this calibration did not stretch the muscle significantly so only the plateau region of the active force-length curve is covered. Inclusion of the passive force and pennation angle has almost no effect. Finally, the complete model reduces $\bar{\sigma}$ for the biceps femoris compared to not using the model by 30%, and compared to the uncalibrated model by more than 80%. The passive force has a small influence here, and the pennation angle is 0°.

When looking at the minimum values of $\bar{\sigma}$ it has to be pointed out that inclusion of a calibration is definitely required if a biomechanical model is used. The inclusion of the model without a proper calibration of the parameter can produce results far worse than without the musculotendinous model at all.

The improvement of the calibrated model compared to not using the model can best be viewed with the muscle force plotted over the postprocessed EMG signal as shown in figures 7.2, for the extensor muscles, and 7.3, for the flexor muscles. The diagrams show the different isometric contractions with muscle force plotted against EMG signal. The left column shows the geometry calibration without the musculotendinous model, the middle column shows results from the uncalibrated model, and the right column shows the complete calibrated model. Obviously, the consistency is improved very much, since in the right column of both diagrams the curves have a very low divergence. This is especially notable for the extensor muscles and the trials where the leg is only slightly flexed (trials E3, E4): The effect of the muscle fiber force-length relationship has a strong influence here. According to diagram 7.1 (left), the extensor forces are modulated with values of the force-length relationship close to 0.6, because the muscle fibers are very short in this pose. If the geometry model is omitted the resulting muscle force is overestimated if the knee is extended, and underestimated for knee flexion. This becomes obvious by looking at one arbitrary diagram in the

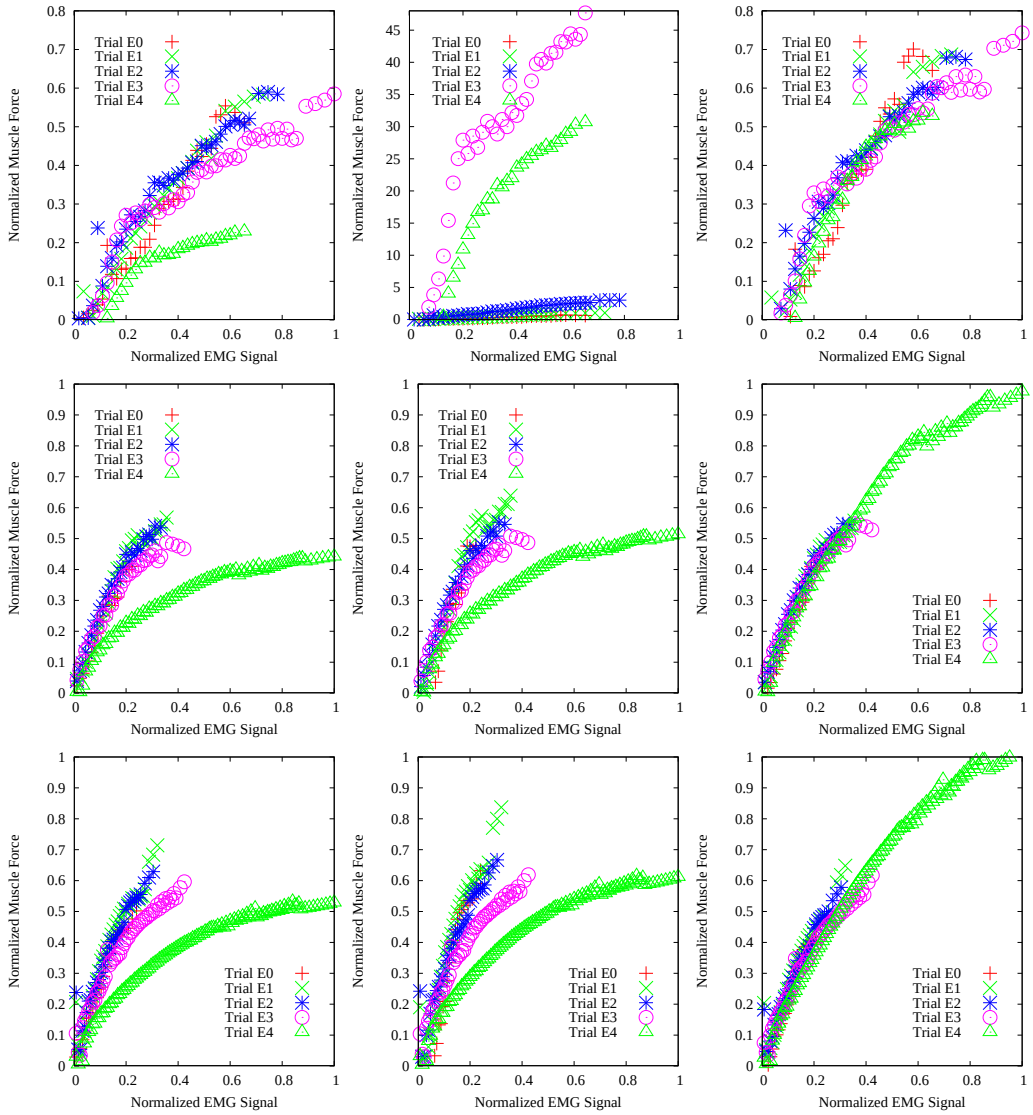

Figure 7.2: Effect of the geometry model on the EMG-to-force relationship for the rectus femoris (top), vastus medialis (middle), and vastus lateralis (bottom). The diagrams show the individual muscle forces, based on the measurements, plotted against the postprocessed EMG signal under different knee angles in a sitting position. The left column shows the relationships without taking into account the musculotendinous model. The middle column shows the model with uncalibrated parameters taken from literature, and the right column shows the complete model with calibrated parameters. It can be seen that with the calibrated model, the force prediction based on the EMG signal is much more consistent across different knee angles.

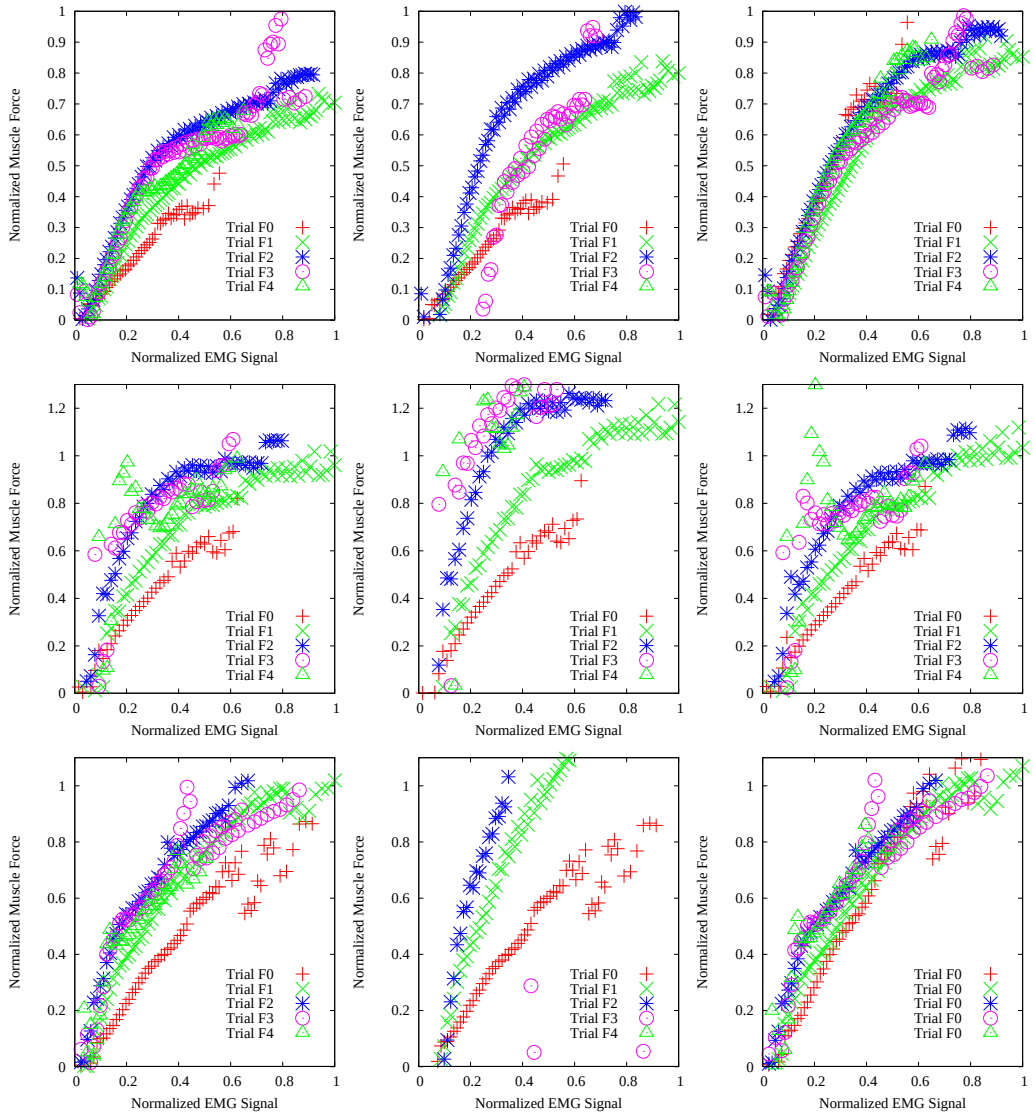

Figure 7.3: EMG-to-force relationship of the semimembranosus (top), semitendinosus (middle), and biceps femoris (bottom). Left column: no geometry model, center column: uncalibrated geometry, and right column: calibrated geometry. As can be seen, the improvement is not as significant as for the extensor muscles. It can be seen, that inclusion of the musculotendinous model without a proper calibration algorithm for the tendon slack length scales does not improve the consistency of the EMG-to-force relationship.

left column of figure 7.2. Averaging those curves would yield an EMG-to-force relationship, although a very inaccurate one. Applying this curve for the EMG-to-force computation for all angles instead of the original curves overestimates all forces for angles with corresponding curves below the averaged, and underestimates all forces for angles with curves above the averaged. This is solved by the geometry calibration as can be seen in the diagrams of the right column in the same figure.

A similar effect of the influence of muscle fiber length can be seen for the knee flexor muscles, especially for trial F0 in the left column of figure 7.3: In that case the knee is flexed and the fibers are very short. Without the geometry model muscle forces in this configuration would be overestimated.

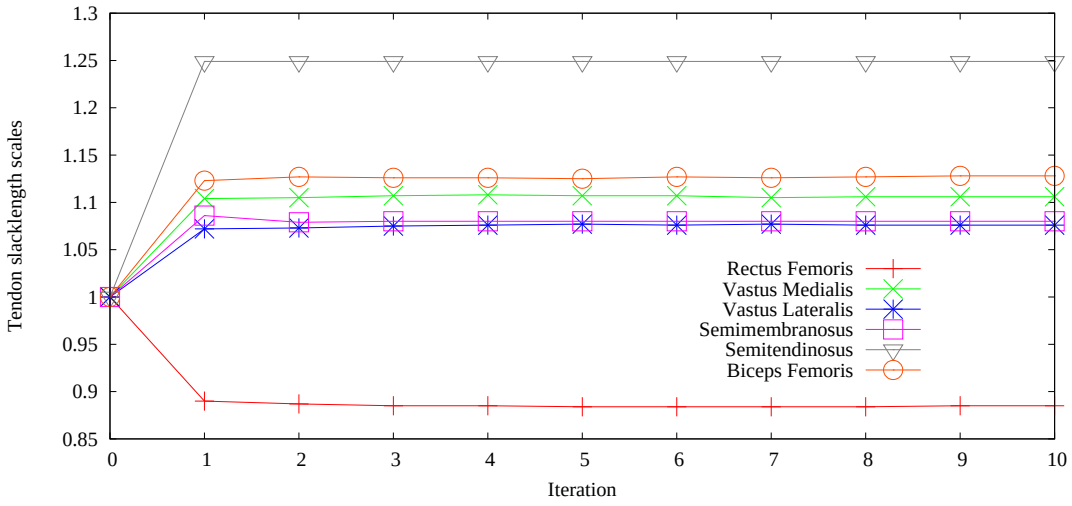

Figure 7.4: Repeated optimization of the geometry and EMG parameters results in a quick convergence of the resulting tendon slack length scales. Step 0 indicates the initial values. The scales are dimensionless.

Repeated optimization

After the EMG calibration has been performed, the geometry calibration was repeated with the same input data to refine the torque distribution with the actual activation functions and to incorporate the influence of the passive muscle force. After that, the EMG calibration has also been repeated. But this repetition has only been performed once to produce the values presented in the diagrams here, except for figure 7.4. This figure shows the quick annealing of the geometry parameters for ten iterations over both calibrations. Although they do not converge toward fixed values, one iteration is sufficient to obtain feasible values. Even a repetition to include the EMG-related parameters into the torque distribution has no significant influence. More iterations do not improve the geometry optimization.

Consistency across different sessions

As stated above, the geometry parameters are subject-dependent but do not regard the physical condition of the subject. But since the calibration of those geometry parameters utilizes the EMG-to-force relationship, it has to be investigated if the calibrated geometry parameters are consistent across different sessions or if they are influenced unintentionally by variable properties related to the EMG recordings. Experiments to investigate this have been separated by at least four days between each other. Results from five sessions are summarized in table 7.2. The table shows the scale of each muscle for every session S1–S5, together with the average of the scales, $\bar{s}_i^t$, and the standard deviation of the scales, $\sigma_{s_i^t}$, for each muscle separately. It can be seen that the scales have a very low variance across the sessions. It is especially low for the

	S1	S2	S3	S4	S5	$\bar{s}_i^t$	$\sigma_{s_i^t}$
rectus femoris	0.895	0.890	0.900	0.895	0.885	0.893	0.00570
vastus medialis	1.135	1.110	1.100	1.120	1.105	1.114	0.01387
vastus lateralis	1.100	1.075	1.085	1.090	1.075	1.085	0.01061
semimembranosus	1.085	1.070	1.070	1.080	1.080	1.077	0.00671
semitendinosus	1.250	1.250	1.250	1.220	1.250	1.244	0.01342
biceps femoris	1.130	1.115	1.105	1.125	1.125	1.112	0.01000

Table 7.2: Optimized tendon slack length scales from different experimental sessions, S1–S5, with several days in-between, with average values, $\bar{s}_i^t$, and standard deviations, $\sigma_{s_i^t}$: an obvious consistency can be seen. The scales are dimensionless.

rectus femoris and the semimembranosus. Since the minima lie in very narrow valleys of the geometry $\bar{\sigma}(s^t)$ curves, this is very important. Table 7.3 shows the EMG-related parameters of the rectus femoris of those sessions. Comparing the standard deviations to the deviations of the geometry parameters, in relation to the corresponding average values, reveals that the geometry calibration is insensitive to variances in the EMG measurements. This increases the trust in the model and confirms that the geometry needs only to be calibrated once for every subject.

	S1	S2	S3	S4	S5	avg.	std. dev.
A	-0.750	-0.606	-1.901	-1.750	-0.837	-1.169	0.607
$F_o^m[N]$	593	776	516	604	735	645	107
$R[V]$	0.026	0.024	0.028	0.037	0.027	0.028	0.0051

Table 7.3: EMG-related parameters of the rectus femoris with average values and standard deviations for the sessions. The differences of the parameters are large between sessions, taking into account the circumstances described in section 3.3. The maximum force, F_o^m, is subject to large variance because the experiments have been performed with submaximal force. The shape, A, is dimensionless.

7.1.2 EMG-to-Force Calibration

The EMG-to-force calibration was performed after geometry parameters had been obtained from the geometry calibration. It should be kept in mind that the EMG-related parameters are subject to change from session to session.

Calibration of the EMG-related parameters has been performed with the exponential activation function, a_{exp}, and the piecewise activation function, a_{pw} for every muscle. Table 7.4 shows the resulting parameters and error values. As can be seen, the piecewise activation functions performs always worse. For all further experiments the exponential activation has been used.

The actual functions corresponding to the calibrated parameters are plotted in figure 7.5, together with all entries of the tables of each muscle (compare to figures 7.2 and 7.3). As can be seen for the rectus femoris and semitendinosus the curves have a force close to zero for EMG values far greater than zero. It might be feasible to calibrate the EMG offset, u_o, of every muscle instead of measuring it when the muscle is relaxed. In that case, the curves would be shifted to the left, and the curvature could be better approximated. On the other hand this small error might be corrected through a different distribution of the reference torque among the muscles.

	A	$R[V]$	$F_o^m[N]$	$E(a_{exp})$	$a_0[V]$	$m[\frac{N}{V}]$	$E(a_{pw})$
rect. fem.	-0.837	0.027	735	14003.90	0.491	26.46	91269.79
vast. med.	-2.066	0.045	1225	7332.17	0.483	16.42	21465.34
vast. lat.	-2.174	0.062	1419	14316.69	0.417	13.32	33614.27
semimem.	-2.083	0.049	1218	38159.13	0.573	12.58	173250.67
semiten.	-3.158	0.032	251	9949.73	0.942	2.58	147191.09
bic. fem.	-2.001	0.041	852	19856.89	0.611	13.73	158541.31

Table 7.4: Calibrated parameters of the muscles from session S5: shape A (dimensionless) of the activation function, $a(u)$, expected maximum postprocessed EMG signal, R, and maximum isometric force, F_o^m. For the piecewise activation there are two additional parameters, a_0 (EMG signal at transition), and the slope of the linear portion, m.

Beside the shape of the EMG-to-force functions, the maximum isometric forces are important parameters. Comparing those values to the data collected in [DLH+90] from various sources, as shown in table 7.5, reveals interesting similarities. It has to be kept in mind that the isometric trials for the calibration have been performed with submaximal force, but the muscles in the model also take over certain shares of muscles which are not included in the model but are measured through the force sensor.

Comparing the forces to values from the literature is performed here only to check if the order of magnitude is correct. Fortunately, this is the fact. Also, the order of the strength is consistent: Weak muscles in literature correspond to muscles with low

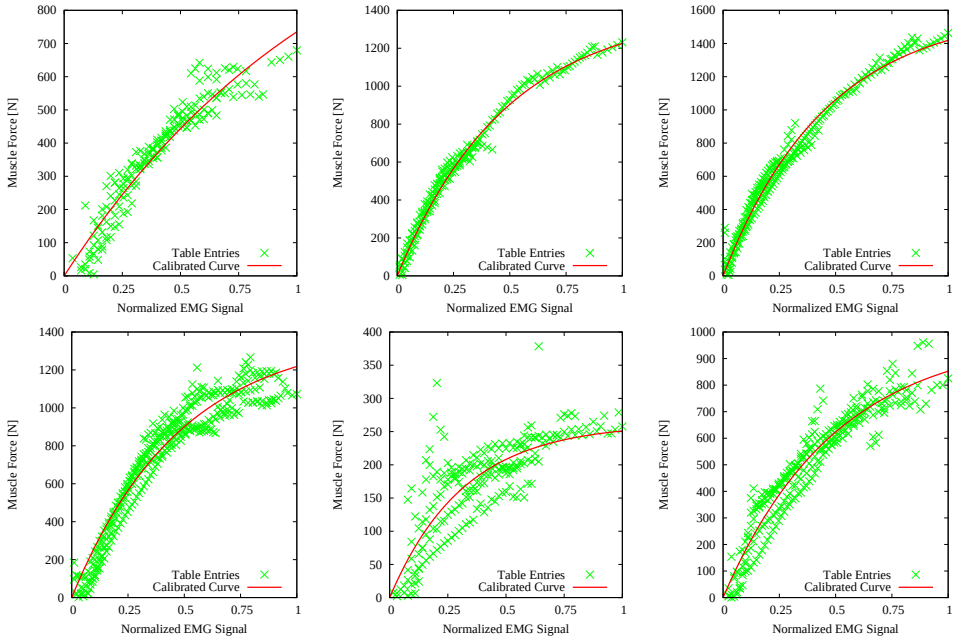

Figure 7.5: Calibration of the EMG-to-force parameters: The diagrams show the entries of all tables of the particular muscle, together with the interpolated EMG-to-force function (solid line). The muscles are from top left to bottom right: rectus femoris, vastus medialis, vastus lateralis, semimembranosus, semitendinosus, and biceps femoris. As can be seen for the rectus femoris and semitendinosus, introduction of an offset parameter could improve the calibration.

forces of this work, and likewise for the stronger muscles, as could be expected from the torque distribution based on the %PCA values.

It has to be kept in mind, that the most important goal is to make the model consistent in itself and the measurement setup through parameter optimization, but not necessarily to any external values.

7.1.3 Model Adaptation and Prediction

In this section the adaptation of the model through the calibration is examined, and if the calibrated model can be used for predicting the resulting knee joint torque for new data that was not used during calibration.

Model Adaptation The adaptation of the model can be evaluated with the torque error E_{torque}, which is the average of the difference of the torque T_{EMG}, based on EMG evaluation, and the reference torque, T_R, based on the force sensor, for all measured values,

	$F_o^m[N]$	$F_o^m[N]$
rectus femoris	735	780
vastus medialis	1225	1294
vastus lateralis	1419	1871
vastus intermedius		1365
semimembranosus	1218	1030
semitendinosus	251	330
biceps femoris	852	717, 402
gastrocnemius		1113
sartorius		104
gracilis		108

Table 7.5: Maximum muscles forces from literature compared to calibrated values. Left column: results of the calibration, right column: data taken from [DLH+90]. The biceps femoris is split into the long head and short head in the values from literature. Fields left blank indicate muscles which have not been modelled explicitly.

$$E_{torque} = \frac{1}{D} \sum_{t=0}^{D-1} \left(T_{R,t} - T_{EMG,t} \right), \tag{7.2}$$

where D is the number of samples of the trial.

Table 7.6 shows the average torque error of each trial. All those trials have also been used for the previous geometry and EMG-to-force calibration. The lower the torque error, the more accurate the model can compute the knee torque based on the EMG signals.

Two typical replays of isometric trials are shown in figure 7.6 (trial E4) and 7.7 (trial F2). The EMG signals have been filtered with a lowpass cut-off frequency of 1.6Hz. The upper diagram of each figure shows the reference torque computed from the force sensor readings together with the predicted torque based on the EMG-to-force computation. The middle and bottom diagrams of each figure show the contributions of the individual muscles to the total torque computed in the top diagram. In figure 7.6 it can especially well be seen between 12s$< t <$16s how the different muscle activation begin and end at different times but overlay to a smooth torque output which resembles the reference curve strongly. At other times of the same curve, this resemblance is not so close: For example, between 8s$< t <$12s the reference output is almost the same as during the contraction mentioned before, but the fitting of the prediction curve is not so accurate. Slightly lower activations of all extensor muscles sum up to torques lower than the reference values. This can also be seen at other times of the presented curve. Throughout the trial, all flexor muscles show a constant muscle tone slightly above the relaxed state (the activation of the relaxed state was determined as the offset and has been eliminated). Thus, no *recorded* flexor activity influences the result of the

Trial	$\bar{E}[Nm]$	$E_{max}[Nm]$	$R_T[Nm]$
E0	9.0	25.8	50.0
E1	10.8	35.0	61.8
E2	11.5	34.2	61.8
E3	7.0	25.2	58.3
E4	6.1	12.1	64.4
F0	5.4	18.8	38.2
F1	9.3	20.7	56.1
F2	7.9	24.6	57.7
F3	8.4	21.1	57.9
F4	5.9	19.5	52.5
F5	6.0	19.3	45.9

Table 7.6: The table shows the adaptation of the model to the individual trials. $\bar{E}$ is the average error of the torque prediction for the trial, and E_{max} is the maximum error of the same trial. R_T is the torque range covered during this trial.

trial. But why is the extensor torque not predicted appropriately at *all* times? There are many possible reasons for this. Some of them are:

- The EMG-to-force functions are inaccurate, and the muscle activation pattern is slightly different: The recorded muscles produce more force than predicted, and the increase of muscle activation in some muscles (while others are a little less active) is not appropriately reflected through the EMG-to-force functions because the curvature is too high (or vice versa).
- The extrapolation of the activity measured by a single electrode to the whole muscle could result in an inaccurate force prediction. This is especially true for multi-headed muscles, like the biceps femoris, which branches into a "short head" and a "long head".
- An extensor muscle that is not recorded can contribute the torque that was not predicted at certain times. This cannot be investigated with non-invasive methods.

Unfortunately, the main reason cannot be determined with the experimental setup. But it can also be a combination of all factors mentioned. It must be stated, that prediction errors in this order can occur. It will be discussed in later sections, if the resulting system behavior is negatively influenced.

During the trial F2, presented in figure 7.7, other interesting artifacts can be noticed. First, cocontraction of the flexor and extensor muscles can be seen: During the activation of the flexor muscle group that produces the main torque, the extensors are also activated. But since this is taken into account by the calibration, the predicted torque

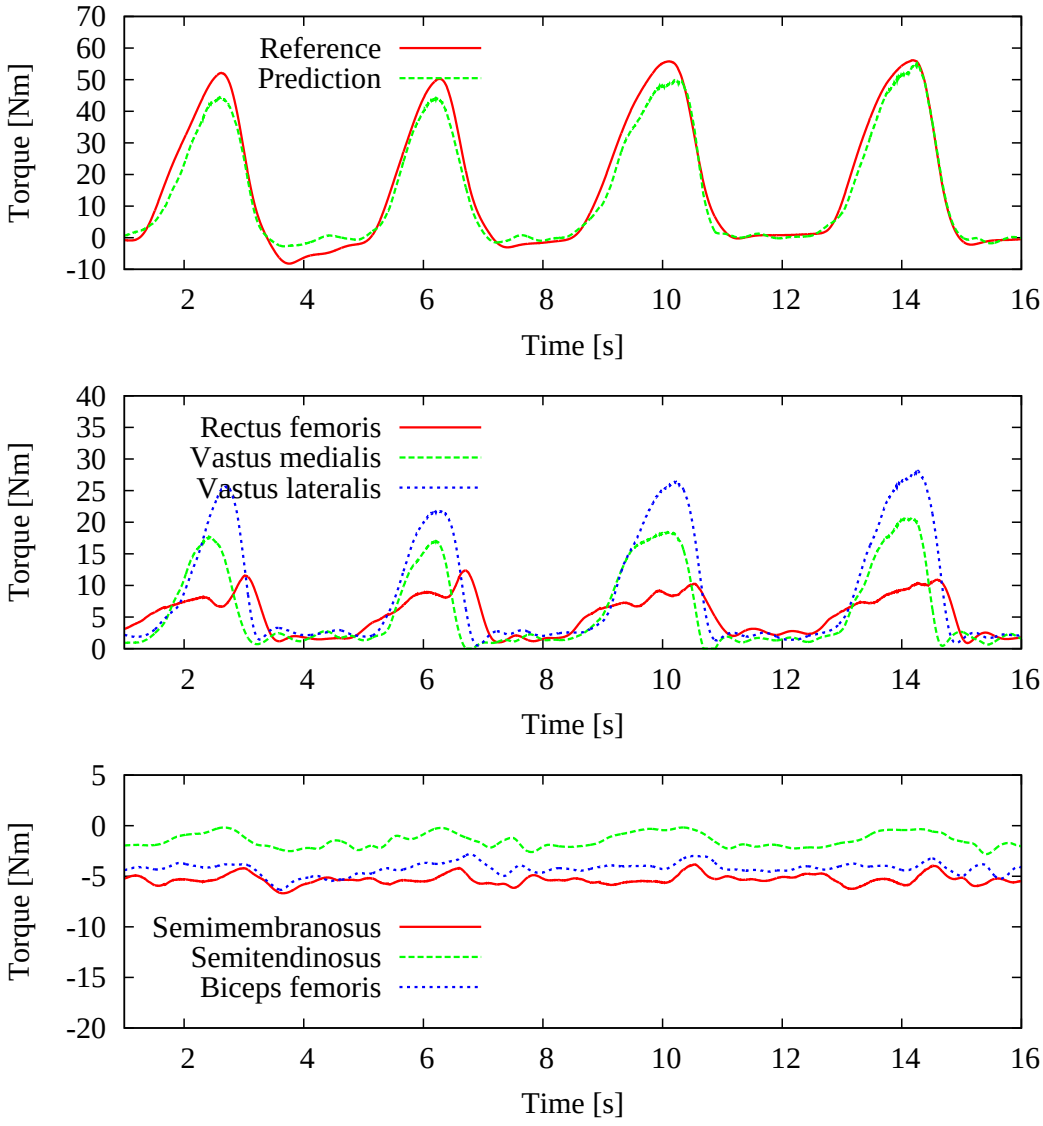

Figure 7.6: Replay of the trial E4 with isometric extensor activation. The top diagram shows the reference torque plotted against time as calculated from the force sensor and knee angle, together with the predicted torque, based on the evaluation of the EMG signals and the knee and hip angle. The middle and bottom diagrams show the individual contributions of the muscles to the prediction curve from the top-most diagram.

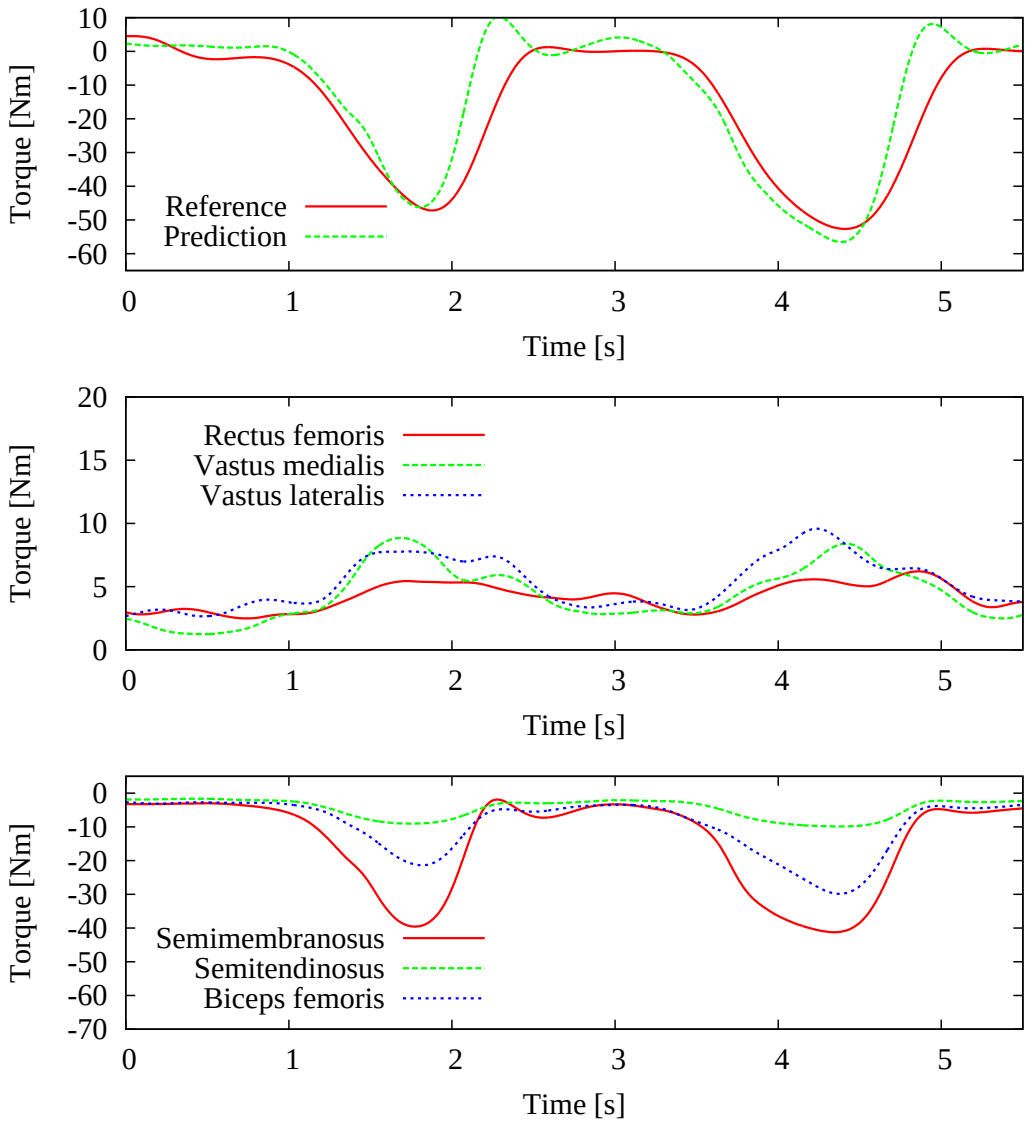

Figure 7.7: Replay of trial F2 with isometric flexor activation. The top diagram shows the reference torque plotted against time as calculated from the force sensor and knee angle, together with the predicted torque, based on the evaluation of the EMG signals and the knee and hip angle. The middle and bottom diagrams show the individual contributions of the muscles to the prediction curve from the top-most diagram.

during the increase of muscle force is predicted appropriately. But during decrease of the muscle force it can be seen that the predicted torque drops faster than the reference torque. This is even amplified through the longer lasting extensor activity. The question again is: Why is this behavior not predicted? This artifact appears often in measurements, especially for the flexor muscles, and is not a special case. At first, on may attribute this error to the neglected activation dynamics that is reported in, for example [ZW90]. But in the presented extensor measurement, and some trials with different joint angles for the flexor muscles, this effect is not visible. Thus, it is more likely to be the effect of unmodeled muscles which are especially active at certain joint angles. Since an obvious early decrease of flexor muscle activity can be noticed, it can be assumed that this muscle is slightly longer active than the others.

The adaptation errors for the different isometric trials are summarized in table 7.6. The values used for computation of the torque errors are only taken at times when the absolute value of the reference torque after elimination of the gravity offset was above 5Nm to avoid sugarcoating the errors during muscle inactivity.

Model Prediction We have seen that the model can adapt to the operator for given trials. But in real environments, the EMG curves that are evaluated are not known in advance and cannot be used during calibration. The system behavior with previously unused data has to be investigated.

Since the experimental setup only allows isometric trials when a reference torque needs to be determined, the prediction error was again performed in an upright sitting position. The knee angle was flexed to -45°, and both, extensor and flexor muscles, have been activated in a random pattern, as shown in figure 7.8. Especially of notice is the cocontraction at points of transitions between activation of the flexor and extensor group, and vice versa, as for example, at $t \approx 21.5$s.

As can be seen in table 7.7, the average prediction errors and maximum torque errors are similar to the adaptation errors in table 7.6. Again the error was only determined whenever the absolute value of the reference torque was above the threshold.

Angle $[^\circ]$	$\bar{E}[Nm]$	$E_{max}[Nm]$	$R_T[Nm]$
-45	6.3	20.4	119.9

Table 7.7: The table shows the errors that occurred during the prediction of torques *not* previously used during calibration. $\bar{E}$ is the average error of the torque prediction, and E_{max} is the maximum error. R_T is the torque range covered during this trial.

The example session presented here is not a special case. It was selected, because it features typical results of experimental sessions. It can be concluded that the model can predict the resulting knee torques based on EMG signals from the operator to a certain degree.

But some inherent problems remain which have been mentioned above. Furthermore, the unsteadiness of the EMG signal during contractions poses a potential prob-

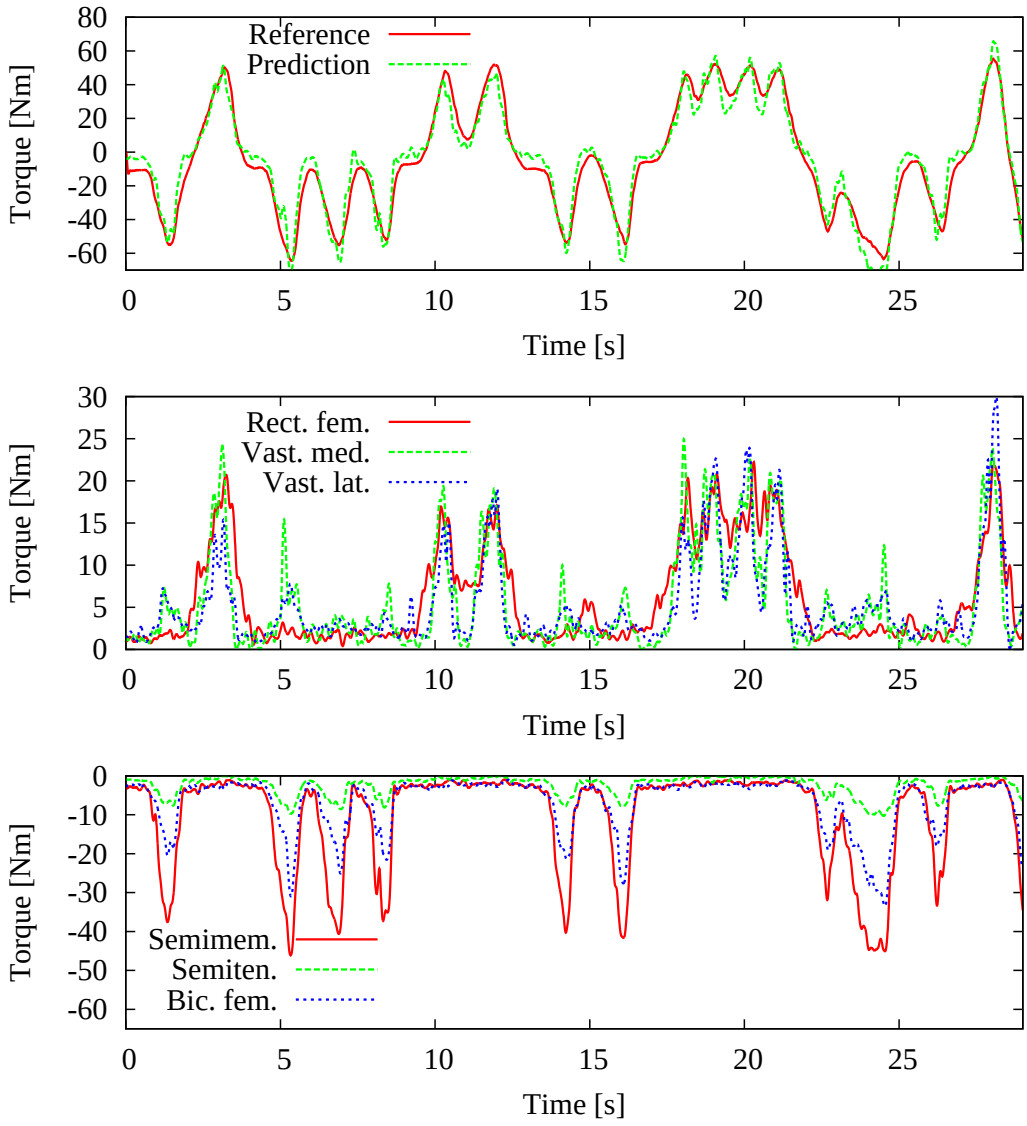

Figure 7.8: Arbitrary isometric muscle contraction pattern of the extensor and flexor groups at $-45°$. In the top diagram the reference torque based on the force sensor measurement is plotted together with the torque based on the EMG-to-force computation against time. The middle and bottom diagrams show the contributions of the individual muscles. The EMG signals are lowpass-filtered with 4Hz to show the difference in smoothness compared to figures 7.6 and 7.7. A good correlation of the reference and prediction curves can be seen.

lem: If the system reacts too quickly to those, it can vibrate in an undesired manner. This can obviously be suppressed by decreasing the lowpass cut-off frequency during EMG signal postprocessing. But since the frequency of those oscillations in the EMG signal are low, this would increase the latency of the system substantially (in the order of 500*ms* and more). The experiments presented in the following section reveal if those inaccuracies are a real problem for controlling the exoskeleton.

7.2 Torque Controlled Experiments

In this section, experiments are presented with force support from the exoskeleton. As was motivated in the introduction, a focus is put on movements of everyday life, which can be substantially supported by the exoskeleton. That is, where the knee flexion and extension is important and requires larger torques.

Each movement is discussed in a separate section, with a focus on system behavior and human-machine interaction. For the purpose of this work, the discussed movements are: free motion with the leg (section 7.2.2), sit-to-stand movement (section 7.2.3), stair climbing (section 7.2.4), walking (section 7.2.5), and an arbitrary combination of the movements (section 7.2.6).

Performance evaluation of the system during the supported movements is difficult. The following section 7.2.1 explains the methods applied here.

7.2.1 Methods of Performance Evaluation

It is very hard to evaluate the exoskeleton system with an objective criterion in a real world environment. In the context presented here, as a power amplifier, a general demand is to support the desired movement with a substantial torque while still allowing the operator full control over the movement.

Quantifying the performance regarding this demand is not possible immediately: First, the desired movement is not readily available to compare the resulting movement to. Only the task is known, but not the exact desired trajectory. And second, since the human is in the control loop, and full direct control is allowed, the outcome of large force support depends very much on the adaptability of the operator. Since the healthy operator usually has a muscle activation pattern learned that allows to perform the task without the support, he or she has to adapt to the external support, and decrease the own force contribution appropriately, as long as no additional load is carried. Both force sources, human and exoskeleton, have to work in cooperation to perform the desired movement. If the operator feels unwell because of the force produced by the exoskeleton, he or she cannot take full advantage of the support: the actuation rather disrupts the movement performed by the operator, and the operator will get tensed rather than relaxed.

In this work, the performance is evaluated with the following scheme: The resulting knee angle trajectories with various support ratios plotted against time are compared to

the trajectory without force support during which the exoskeleton evades the leg. This is not performed numerically, since durations of the different phases of the movement can be different, distorting the results. Scaling parts of the movement in time would distort the relationship between acceleration of body segments and muscle forces, due to inertia, also leading to a wrong evaluation.

Instead, the trajectories are compared for the general shape, and it is searched for unusual dents in the trajectories and corresponding muscle activations. Those dents are an indicator for unusual muscle activation which is amplified by the exoskeleton. These rapid changes in the muscle activation pattern indicate that the operator is surprised by the external force, or feels unwell and tries to counteract the force produced by the exoskeleton.

In the diagrams of the experiments the support of the exoskeleton is shown as a result of the measured torque of the actuation. It is *assumed* that this additional torque is helpful for the movement, because it is brought into the system and cannot simply vanish, and it acts in the same direction as the torque produced by the muscles, but it could, in theory, be counteracted by muscles which are not recorded. But the muscle activations of the recorded muscles are shown to be lower than without support. This seems to support the theory that the contribution of the exoskeleton relieves the operator of some torque. But again: also this reduced muscle activation could be taken over by muscles which are not recorded. Only a subjective report can reveal if the muscle activity is very unusual or feels awkward.

Experiments can be performed which measure the energy consumption of the whole body directly, but this was not performed. But also if the exoskeleton transferred load to other muscles not reducing the overall effort of the human, the exoskeleton can still be helpful, since those muscles may be more capable of performing a task, for example, the unsupported leg for motor impaired people.

As a conclusion to the above argumentation, every experiment is commented with a subjective impression of the operator. Although during the course of this project many experiments with force support have been performed, the operator can still be regarded as a novice compared to the intended everyday usage, but with some trust in the exoskeleton and control system.

7.2.2 Free Motion

This experiment is mainly presented here to justify the need of taking into account the muscle geometry to improve the consistency of the EMG-to-force relationship, which is realized in this work through the geometry model of the muscles.

The experiment was performed as follows: The operator is sitting on a chair with both feet on the ground and a knee joint angle of approximately $-90°$. Three markers are fastened to a vertical bar which is located 70cm in front of the chair, with distances of 20cm, 40cm, and 60cm above the floor. The task is to raise the supported leg, touch the lowest marker, flex the knee, extend it to touch the middle marker, flex the knee, extend it again to touch the top marker, and put down the leg. This task also involves

flexing the hip joint. It was chosen because it is a very simple movement, but requiring target oriented leg movement as during arrangement of the legs prior to standing up or positioning the foot to step over an obstacle. The task has been performed with support ratios of 0.00, 0.25, 0.50, 0.75, and 1.00. The lowpass frequency of the EMG filtering was set to 1.6Hz, which is motivated in section 7.2.3. The hip angle of the model was set to 90°. During the first trial, the complete calibrated model was used to verify if the task could be fulfilled with the system at all, and to a satisfying accuracy. The second trial was performed without taking into account the muscle geometry during computation of the support. This allowed investigation of the overall effect of the geometry model on the performance of the system for this task. Results from the experiments are shown in figure 7.9. All diagrams show the knee joint angle, the torque contribution of the operator estimated from the EMG signals, and the torque contribution of the actuation of the exoskeleton. The left column contains diagrams from the trial with the complete model, the right column contains diagrams where the geometry model of the muscle was omitted.

In all diagrams the knee joint angle starts at around $-110°$, when the foot of the supported leg is on the ground. After that, the hip is flexed and the knee is extended to touch the lowest marker. This is indicated by the first maximum of the knee joint trajectory. After that the knee is flexed and the leg is further raised, before the knee is extended again to touch the second marker, as indicated by the second maximum. This is repeated for the third marker before the foot is put down on the ground again.

In the top row the support ratio is set to zero: The actuator is not contributing any torque to the movement, minimizing the interaction force between the operator and the exoskeleton, as is shown by the torque curve of the exoskeleton being zero throughout the whole movement. In the bottom row the support ratio is set to 1.00, and the actuator torque is following the estimated torque of the operator, indicating that the actuation is able to produce the required torque during all phases of the movement. In between the top row and the bottom row, the support ratio is gradually increased, as can be seen by the increased torque contributions of the exoskeleton. As was desired, the muscle activity is reduced as a reaction to the increased support: The operator was benefitting from the support and did reduce his own muscle activations. But with increasing support, the performed trajectories are getting wavy, because the operator is not used to the support from the exoskeleton and has to adapt to it.

When comparing the knee angle trajectories of the corresponding diagrams from the two columns, it can be noticed that the quality of the performed movement is varying greatly between the trial with the complete model, shown in the left column, and the trial without the muscle geometry, shown in the right column. During trials without the geometry model, the torque is overestimated as explained in section 7.1.1 when the knee is extended before touching the marker. This leads to a behavior that is not easy to predict by the operator, let alone being taken into account unconsciously, resulting in a very unsteady muscle activation. This in turn leads to an unsteady support, and a ragged knee joint trajectory.

The subjective feeling during the experiment was that the task could be easily per-

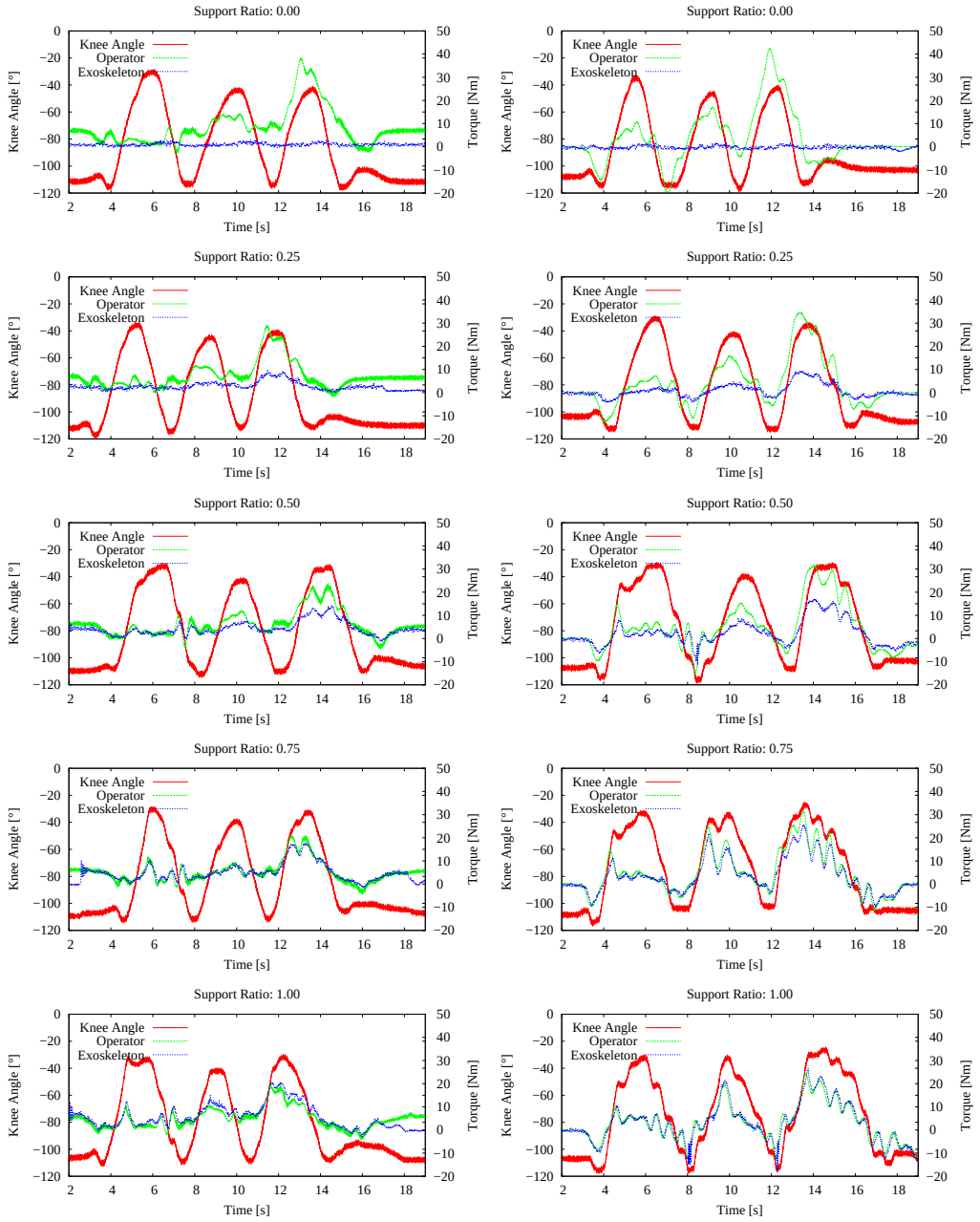

Figure 7.9: Free movement with the actuated leg. The diagrams show the knee angle, the torque contribution of the operator, and the torque support of the exoskeleton plotted against time. The support ratio was increased from top to bottom. Left: task with the complete calibrated model. Right: task with the muscle geometry model excluded. The muscle activity is reduced with increasing support in both trials, but the task cannot be performed smoothly without the geometry model, as can be seen by the dents in the knee angle trajectory in the right column. The torque estimation is poor, and the behavior of the system is hard to predict for the human locomotor system.

formed with the geometry model included. But with higher support ratios, a little more mental effort was required to perform the movement smoothly. Without the model, the mental effort was greater, and even when concentrating very hard on performing the task smoothly, this was not possible, especially with high support ratios. The actual effect of the increased mental effort on the joint trajectory was not investigated in more detail.

The results of this experiment justify the inclusion of a model which takes into account the geometry of the muscles to improve the EMG-to-force prediction.

7.2.3 Sit-to-stand Movement

This experiment is performed similar to the every-day movement when getting up from a chair, except that some additional constraints have been applied to make the results more comparable. This movement has been selected because of its relevance to daily activity, the possibility of the system to add a larger support, and because the system behavior can be tested for a relatively simple movement. It is used to determine a feasible lowpass frequency for the EMG signal postprocessing, which has a direct and strong effect on the support computation and the resulting behavior of the actuation.

The movement was started from an upright sitting position. Getting up was performed without the arms holding on to anything, like arm rests. Both feet were placed side by side on the ground, so that the legs were parallel during the whole movement. It was tried to put the same weight on both feet during each trial, to minimize the effect of different ground reaction forces on the experiments. The movement was performed as naturally as possible (leaning forward, using the arms for balancing), and as similar as possible, to reduce the effect of different postures on the required muscle activations. It can also be performed with support from the arm rests, or the feet can be placed differently. But by applying some constraints, the results are more comparable. The movement was performed a little slower than normal, as could be expected from elderly or disabled people being in need of support, because of the limited velocity of the actuator. The movement was performed with support ratios of 0.00, 0.25, 0.50, 0.75 and 1.00. The lowpass cut-off frequency for the EMG signal postprocessing was set in the first series of trials to 1.6Hz, in the second series to 4.0Hz. Results of the experiments are shown in figure 7.10. The first series of trials is shown in the left column, the second series in the right column. The diagrams show the estimated torque contribution of the operator based on the EMG signal evaluation, the torque contribution of the exoskeleton, calculated through the actuator force, and the resulting knee joint trajectory.

During the trials shown in the top diagrams the support ratio was set to zero, indicating that the exoskeleton did neither support nor hinder the movement. This can be verified by the force curve being zero throughout the whole movement. The support ratio has been increased in 0.25-steps between the trials from the top to the bottom, as can be verified by comparing the contribution of the exoskeleton to the estimated contribution of the operator for the various trials.

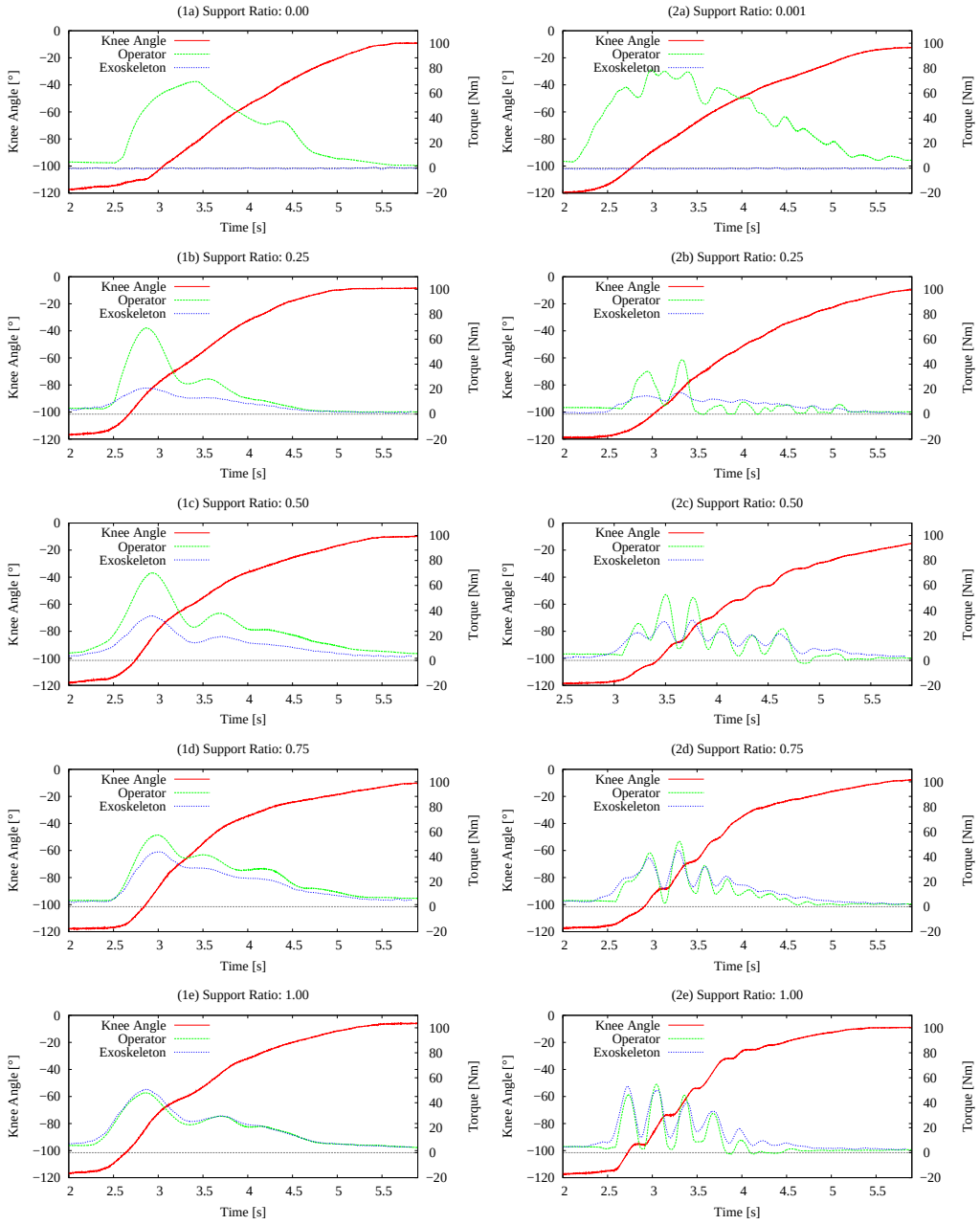

Figure 7.10: Sit-to-stand movement with support ratios of 0.00, 0.25, 0.50, 0.75, and 1.00. The torque contribution of the operator and the exoskeleton, and the resulting knee angle trajectory are shown. Left column: with a lowpass cut-off frequency for the EMG postprocessing of 1.6Hz. Right column: the same with a cut-off frequency of 4.0Hz. Muscle activation could be reduced with larger support, but oscillations can be seen in the diagrams of the right column, indicating that the operator overreacts and feels uncomfortable.

It can be seen that the shape of the knee angle trajectory is similar over all trials, indicating that the desired movement could be performed successfully, although with differences in quality: The joint trajectories in the right column show obvious bumps with increasing support. The movement has not been performed very smoothly. This originates from the waviness of the EMG signals. After the lowpass filtering during postprocessing, no other filters are applied to further smoothen the signal. A typical waviness of the postprocessed signal of the unaffected movement can be seen in diagram (2a) of figure 7.10. Since the support is directly depending on the prediction of the operator's contribution, the resulting support shown in diagrams (2c)-(2e) is very unsteady. The mechanical coupling of the exoskeleton with the operator leads to a feedback of this unsteady support, which he tried to compensate unconsciously. Unfortunately this further increased the waviness of the operator's contribution resulting in an undesired oscillation. Those oscillations are so quick that the actuator cannot always produce the required torques, as is most apparent in diagram (2e).

This effect of the feedback can also be noticed in the first series of trials in the left column: At first the operator is activating his muscles very strongly, out of long-learned experience to a degree that is required if no external support is given. This leads to a very steep inclination of the knee trajectory in the initial phase of the movement compared to the trajectory without support in diagram (1a). As soon as the locomotor system recognizes that the resulting movement is faster than expected and desired, the muscle activation is reduced to slow down the movement. Since this directly results in a decreased support which is not taken into account by the locomotor system, the movement is slower than desired which is countered by a following increase of the muscle activation. The resulting knee joint trajectory shows some small bumps as a result of this untrained interaction between the human and the exoskeleton. It is best seen in diagram (1c) and (1e). This interaction is performed without conscious effort, and cannot be simply suppressed. Additional training may reduce this effect. But with increased support from the exoskeleton, the operator could reduce the activation of his muscles, thus benefitting from the support.

The subjective feeling during the first trial was very positive. Although the feedback system of the human body is very sensitive to the accelerations which lead to the bumps in the knee joint trajectories which can be felt, but they do not cause a strong distrust in the system because they are small enough. In fact also without the support the trajectories are not always very smooth because of the activation pattern the operator is using. But this results in a feedback as expected, not causing a bad feeling. During the second series however, the accelerations created by the interaction between the operator and the exoskeleton have been so large and unexpected, that the trust in the system was very low. It was very hard to not unintentionally put all the weight on the unsupported leg to reduce the oscillations by reducing the required muscle activity. But the effect could not be omitted completely, leading to a lower muscle activation during the second series of trials.

Results of the experiment imply that cut-off frequencies lower than 4.0Hz improve the system behavior significantly. Of course a reduction of the frequency causes a

higher latency of the system, which can be a disadvantage for movements that require quicker responses. But for the experiments presented here, a cut-off frequency of 1.6Hz yields good results. It was experimentally determined, but further research may bring forward other values.

Stand-to-sit Movement

The stand-to-sit movement is investigated here, because it is also a very common movement and the interaction between the human and the system is very important.

Results are presented in figure 7.11 for support ratios of 0.00, 0.25, 0.50, 0.75, and 1.00. As for this and all following experiments, the lowpass frequency is set to 1.6Hz. The resulting curves have similar artifacts like the curves presented for the sit-to-stand movement: The estimated torque contribution of the operator is reduced with increased support from the exoskeleton. But the subjective feeling is different:

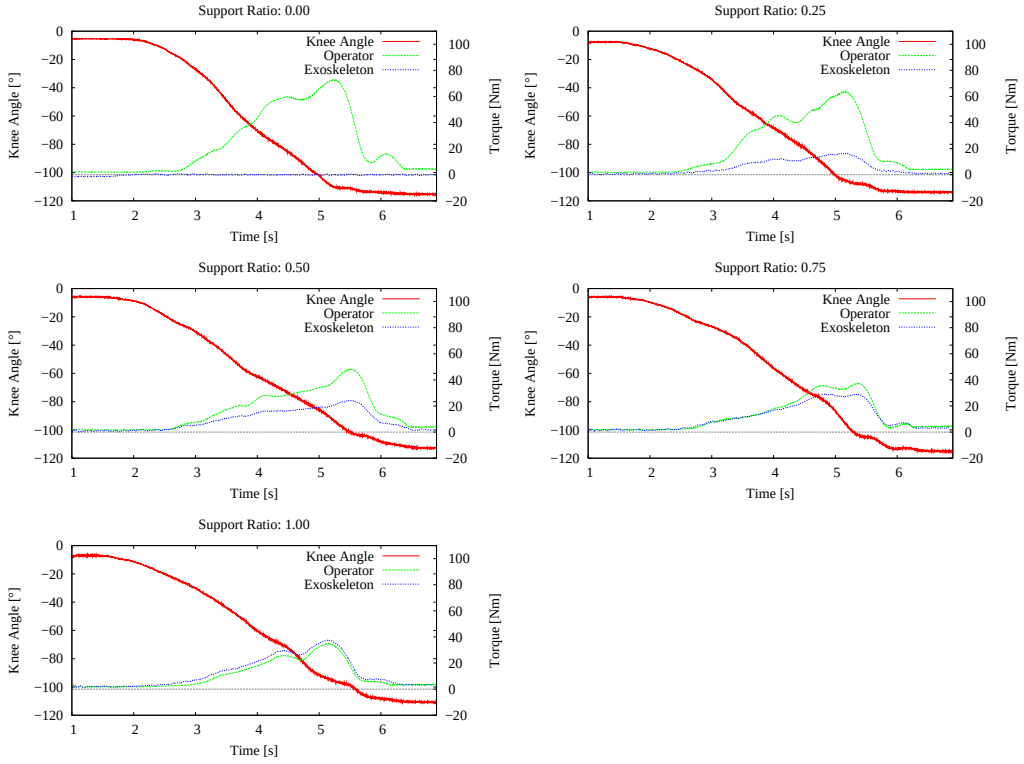

Figure 7.11: Stand-to-sit movement with support ratios of 0.00, 0.25, 0.50, 0.75, and 1.00. The torque contribution of the operator and the exoskeleton, and the resulting knee angle trajectory are shown. As expected, the muscle activation is reduced with increased support.

Although the movement itself is smooth, it is hard to reduce the muscle activation and trust the exoskeleton to take over the remaining torque. The subject seemed to perform the movement much more carefully than the sit-to-stand movement.

7.2.4 Stair Climbing

This experiment is performed similar to the daily activity of climbing a stair without using a handrail or similar support. This movement is very important because of its relevance to the daily activities, and the cooperation of the human with the machine can be analyzed in phases where higher support from the exoskeleton can be contributed, as well as smaller forces have to be applied to allow positioning the foot over the next step. The experiment involved climbing four steps, with the supported leg initiating the movement. The last step consisted of putting down the foot of the support leg beside the other foot on the platform. Again, this experiment is performed slower than normal, as could be expected from elderly or disabled persons. The experiment shows the advantages of the approach, allowing to initiate and stop the movement even with the supported leg. No handrail for support has been used to make the results more comparable, but if desired, it could be used by the operator. The support curves and knee joint trajectories from the experiments are shown in figure 7.12.

The meaning of the knee angle trajectories is explained for the unsupported movement in the top row: At $t < 2.0$s the subject is standing in front of the stair, both feet side-by-side in a natural fashion. When the knee curve starts to fall, the foot is raised from the ground through flexion in the knee and hip joints. During the following minimum at $t \approx 3.5$s the foot is at its highest point and brought over the first step. At $t \approx 4.1$s the foot is put onto the step, and the operator is leaning forward to bring his weight over the leading foot. The extensor muscles start to contract to push the subject up the stair. During the following extension of the knee, the unsupported leg is raised and put onto the second step (at $t \approx 6.0$s). The weight is moved over this foot and the following knee flexion indicates that the third step is climbed with the supported leg, in a similar fashion as the first step. The fourth step is performed with the unsupported leg, and the fifth step begins with a flexion at $t \approx 9.5$s to raise the leg and to bring down the foot onto the platform beside the other foot at $t > 10.5$s. At $t > 11.8$s the subject is standing on the platform.

The strongest muscle activation is found during the push-up phases where the extensor muscles produce large forces. The flexor muscles are very active when the foot is lifted from the ground through knee flexion and is brought above the next step. Notice that for the knee flexion during the first step almost no flexor force is required. The flexion is a result of gravity acting on the shank while the thigh is raised through hip flexion. The other two flexions have to be performed actively through the flexor muscles while the thigh is not raised very much to avoid tripping over the next step.

From the top row to the bottom row the support ratio is increased in steps of 0.25. As can be seen clearly, the support the exoskeleton contributes to the movement gradually increases accordingly. For lower ratios this support can be integrated into the movement, and the muscle activity is reduced. Unfortunately, for support ratios of 0.75 and 1.00 this support cannot be utilized comfortably. The joint angle trajectories show many bumps, for example, at $t \approx 3.0$s and $t \approx 7.5$s in the bottom diagram. Those bumps are a result of small flexor and extensor activities which can also be seen in

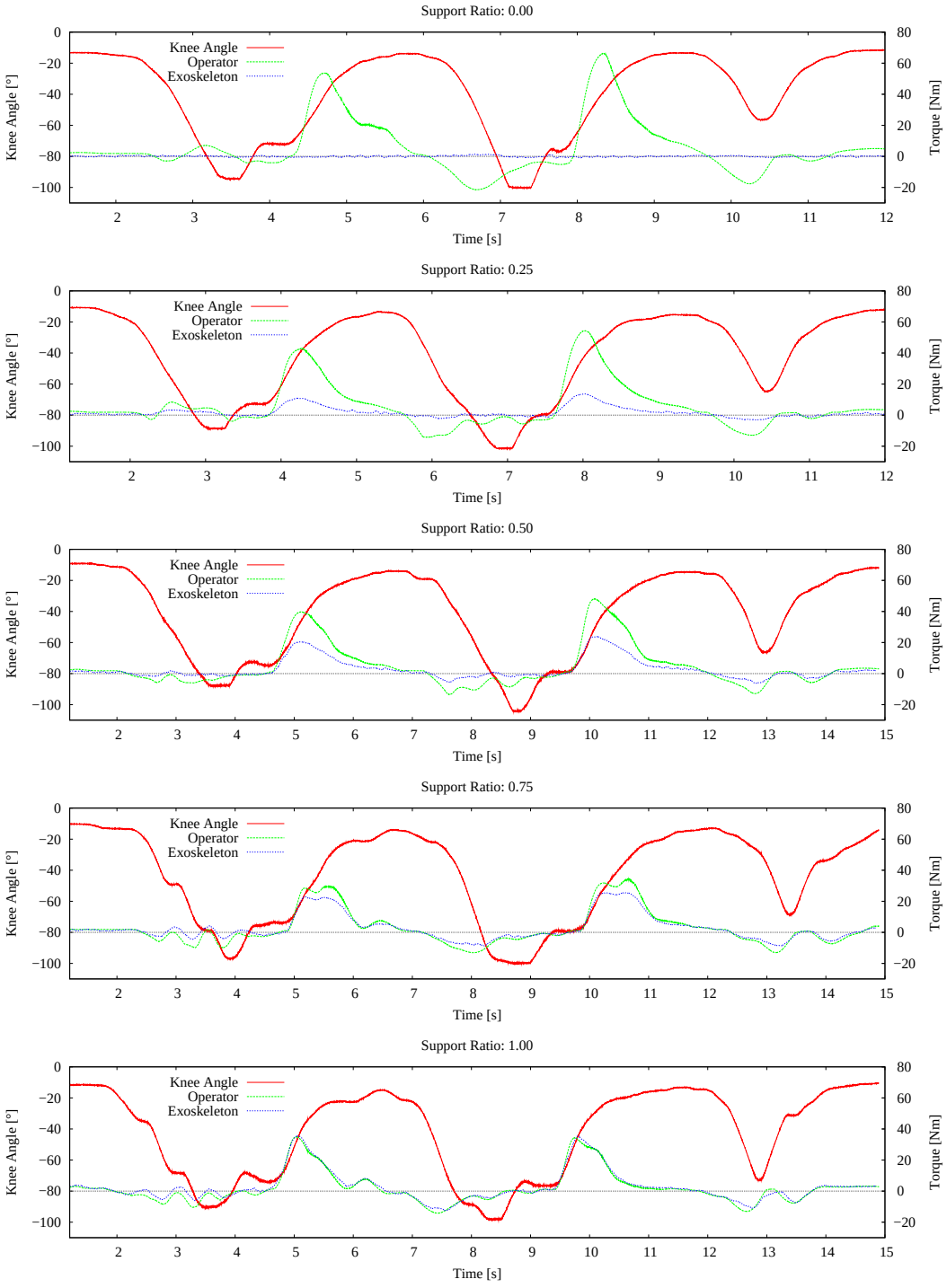

Figure 7.12: Stair climbing experiment with support ratios of 0.00, 0.25, 0.50, 0.75, and 1.00 (top to bottom). The knee angle, and the torque of the operator and the exoskeleton are plotted against time. The operator's contribution is decreased in response to the support, but high support ratios result in dents in the knee joint trajectory.

the other diagrams, but are amplified here. During those phases, the supported leg has no floor contact and small variations in the joint torques lead to relatively large accelerations. The same variations have less effect during phases with floor contact.

During the trials with lower support ratios, the task of climbing the stair could be performed easily and the operator felt safe. With higher support ratios the confidence in the system was reduced and the support could not be integrated into the movement easily, although the muscle activity is slightly reduced. But for the cost of feeling uneasy during this movement.

Small and short muscle activity seems to be hard to adapt spontaneously to external influences, like the support of the exoskeleton. Amplification of those stereotyped patterns results in undesired effects described above. During push-up phase, this support could be integrated more easily into the movement, and the muscle activity could be reduced. It seems as if the locomotor system is used to modulating the muscle activity during push-up phase because of different loads a human carries every day. The phase in which the leg is freely moved without external contact rarely needs to be adapted.

7.2.5 Walking

This task was chosen because of its relevance to the daily activities. But it is hard to verify or analyze the performance of the system with it. The reason for this are the small muscle forces that are required during walking, especially from muscles spanning the knee: During the swing-phase of the free leg, for example, the knee extension is mostly a result of the hip rotation and flexion.

The experiment was performed with support ratios of 0.00, 0.25, 0.50, 0.75, and 1.00. The resulting knee joint trajectories, and the contribution of the operator and the exoskeleton are shown in figure 7.13. At the beginning of all trials, the subject is standing upright. The movement is initiated and terminated with the supported leg, which can be seen by the smaller flexion at the beginning, and at the ending of every trial. In between the repetitive pattern of walking is shown. During phases where the knee angle is close to zero, the leg is almost straight and has floor contact while the unsupport leg is moved forward. At the end of this phase, the ankle performs the forward propulsion closely followed by the steep decrease of the knee angle indicating the beginning of the swing phase. The foot is loosing ground contact, and the supported leg is moved forward. After the free foot has passed the foot with ground contact, the knee is extended again, leading to an increase of the knee joint angles. The foot is put on the ground again, and the gait cycle is repeated.

Only during the knee flexion a larger negative torque is produced which is supported. Aside from that, muscle activity is very small, compared to, for example, stair climbing, and the output of the torque estimation for each muscle is almost zero.

Thus, the exoskeleton is following the movement of the leg passively for most of the time, not hindering the movement, although jitter of the actuation of approximately $\pm$2Nm occurred. The subjective feeling during this task was very relaxed, although the gait was affected for higher support ratios: It was noticed that the actuator produced

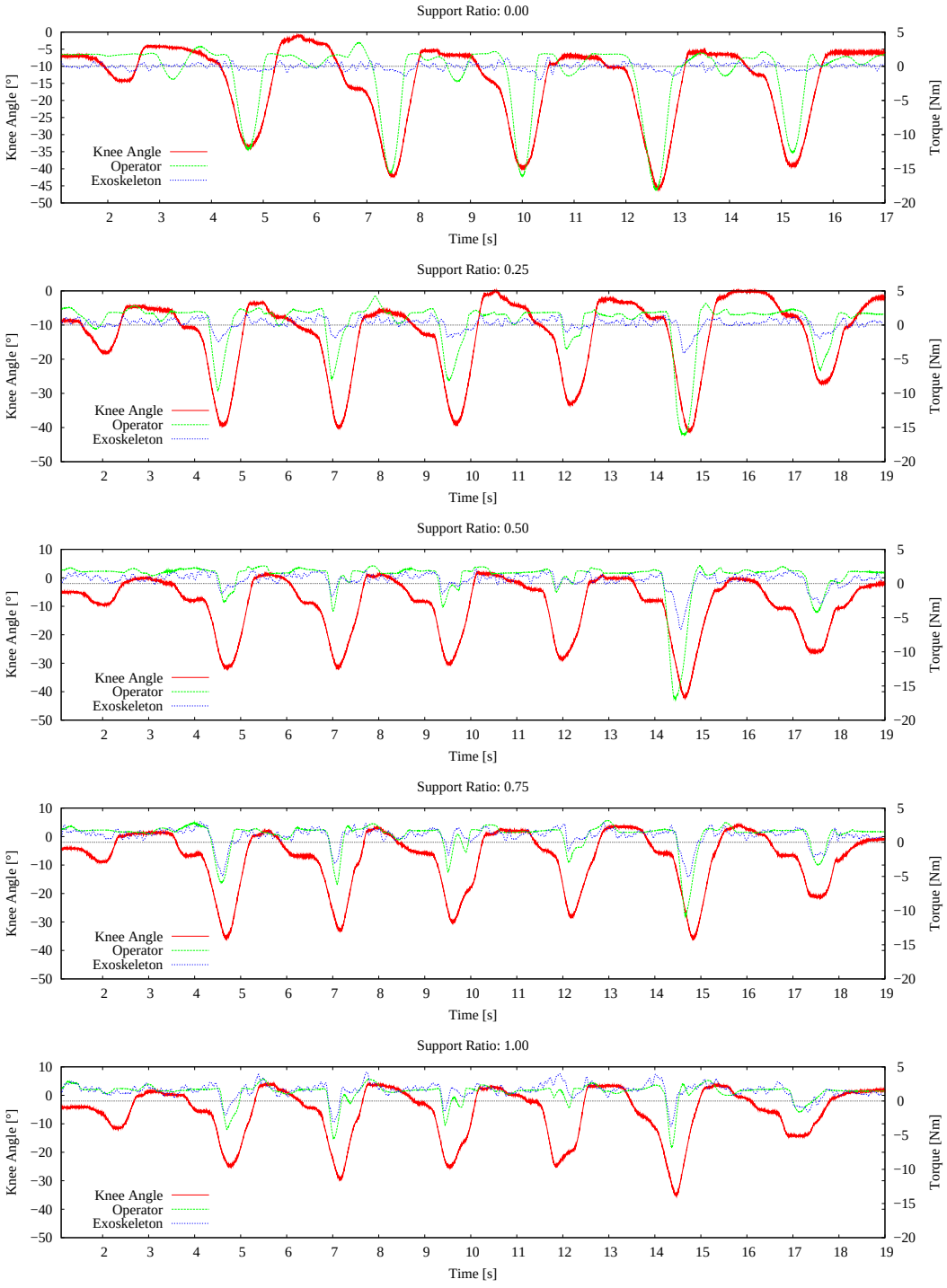

Figure 7.13: Walking experiment for support ratios of 0.00, 0.25, 0.50, 0.75, and 1.00. The knee angle and contributions of the operator and the exoskeleton are plotted against time. The recorded muscles produce very little force during walking, but still, minor activity affects the resulting knee trajectory for higher support ratios.

a torque to extend the leg, which felt a little unnatural. For higher support ratios, a constant amount of extensor torque is amplified, which can be noticed in the diagrams for support ratios of 0.50 and over, resulting in a torque offset of approximately 2Nm for the support ratio of 1.00. This is a result of permanent small activity of the extensor muscles during this movement. During calibration, an offset for all muscles in a relaxed state had already been determined and eliminated. It has to be investigated if (1) this increased activity actually produces a torque that should be amplified, (2) during activities like walking, muscles are always a little active without producing measurable torque, or (3) it is a model error that needs to be corrected.

But it is known that, for example, during and after heel strike when the leading foot touches the ground significant muscle force is required to keep the leg extended and to be able to put weight onto the foot throughout the single support phase. In those phases muscles of the flexor and extensor groups are activated at the same time, increasing the joint stiffness. In our algorithms, the opposing torques of the two muscle groups partly cancel out, but stiffness is not increased.

7.2.6 Movement Combination

The last experiment is used to show that natural transitions between individual movements, which have been presented in the previous sections, are possible. The experiment was performed with a support ratio of 0.50. It begins with the subject sitting on a chair. He (1) stands up, (2) walks three steps with each foot, (3) climbs four steps of a stair, (4) turns on the platform, (5) descends the stair, (6) walks three steps back to the chair, (7) turns, (8) and sits down. Again, this was performed a little slower than normal. Results of this experiment are shown in figure 7.14, where the numbers of the individual movements are placed at each transition.

As can be seen, the transitions between the movements appear smoothly, and significant support is contributed during the movements that require large muscle forces: sit-to-stand, climbing the stairs up and down, and stand-to-sit movements. In-between the walking can be performed in a quite normal fashion, but without the exoskeleton providing a significant amount of torque.

7.3 Discussion

In this chapter the implemented model has been justified through analysis during calibration, investigated regarding its torque prediction for isometric muscle contractions under different joint angles, and the application of the model for computing the supporting torque of the exoskeleton in experiments with the exoskeleton in common movements.

It has been shown that the implemented properties of the biomechanical model allow a consistent torque prediction based on the EMG signals. But still, a certain error remains. The torque controlled experiments showed that the error was small enough

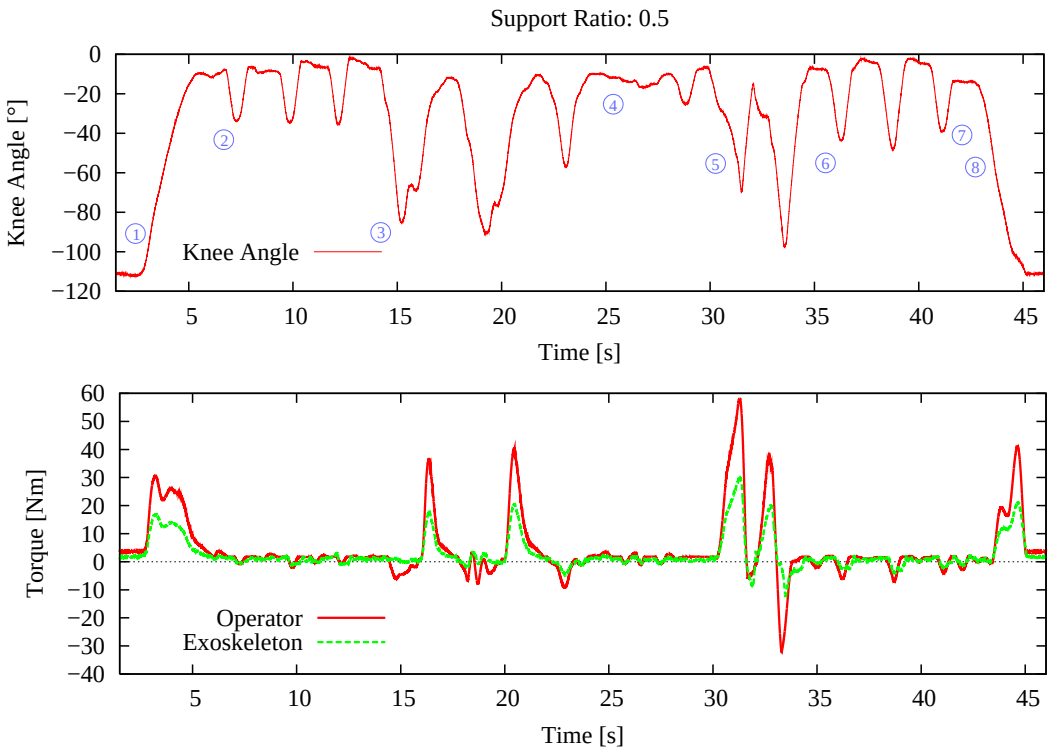

Figure 7.14: Combination of investigated movements. The movement was performed with support ratio of 0.50. Top: knee joint trajectory. Bottom: contributions of the operator and the exoskeleton. The markers indicate the beginning of the movement and the transitions: (1) standing up, (2) walking, (3) stair climbing, (4) turning on the platform, (5) climbing downstairs, (6) walking, (7) turning, (8) sitting down.

to allow the exoskeleton to add a significant support to the movement. The system behavior was so predictable by the untrained operator that he could take the external support into account and reduce his own muscle activations while performing the desired movement. During movements which require large joint torques, a significant amount of torque can be taken over by the exoskeleton, although for high support ratios, the interaction between the exoskeleton and the operator became problematic. In these cases the wavy shape of muscle activation and the resulting joint trajectory is an indication for the operator not feeling comfortable. The operator could not benefit completely from the large support and was overreacting to the feedback.

The oscillations may be reduced if the latency of the system could be reduced while still having a similar flat EMG activation envelope. Unfortunately this is a contradiction which cannot be solved easily.

The overreaction of the human to the support was performed unconsciously and could not be immediately suppressed with increased concentration on the task. It seems as if the lower levels of the locomotor system were controlling those responses,

but additional training with the exoskeleton may produce more suitable reactions to higher support from the device.

The subjective impression of all experiments with significant torque contribution and a smooth movement was that the motion felt quite natural, but the actual amount of support became especially evident after it was turned off, and the full required torque had to be produced by the subject himself again. After performing several stair climbing experiments, the operator seemed not to notice the support anymore. But after the support was turned off and the stair was climbed once more, it became obvious how much the exoskeleton did in fact contribute.

8 Miscellaneous Investigations on Body Models

Besides the algorithms presented in chapter 4 and 5, other algorithms for control and calibration of the exoskeleton have been investigated. Those algorithms are based on systems of rigid bodies, which model the operator with the exoskeleton in the environment.

In this chapter two algorithms and results are summarized, which have been developed during the course of this project. They show different paths of investigation that have been followed, but have not been included in the final system as described in chapter 4. The findings are of interest, since they illustrate general problems concerning the simulation and prediction of movement. Some of those problems could have been minimized by developing a more complex exoskeleton hardware or an external measurement setup, which is beyond the scope of this work.

Section 8.1 describes an algorithm which predicts the desired movement based on simulation of a dynamic body model, and section 8.2 describes a simplified dynamic body model tailored to a specific task: It is explicitly used during calibration of the knee extensor muscles with sit-to-stand movements.

8.1 Motion Prediction with a Dynamic Body Model

This approach was in fact the first approach to control the exoskeleton, prior to the torque control system.

The basic idea of the dynamic model approach is to simulate the behavior of a simplified dynamic rigid body model of the human body. The motion simulated for a small timestep ahead through forward dynamics computation is interpreted as the intended movement of the operator, and is executed with the actuator. The movement of the model is a result of muscle forces acting on different parts of the model as well as some selected external forces. The control system includes dynamic equations to simulate the body model and a position controller for the actuator.

This approach is well motivated by the fact that with dynamic equations at hand, which describe the system behavior, modulation of the joint torques to control postural stability as proposed in [KH03a, KH03b] could be integrated easily. Thus, the exoskeleton could not only be used to amplify the muscle forces of the operator, but also to help maintain balance during dynamic movements. Initial experiments fusing those algorithms have been presented in [FKRH04a].

But it should be noted that this is more of a theoretical consideration in the context of this work: To control postural stability it is necessary to actuate more joints than realized with the exoskeleton presented in this work.

The initial experiments for investigation of joint angle prediction based on the EMG signals have been performed on the hip joint, a revised version on the knee joint.

The following description is written with emphasize on the knee joint experiments, but short results for both experiments are presented. The dynamic model approach as presented here has been published in [FKRH04b, FH05].

The following section 8.1.1 describes the concept and the control system, and section 8.1.2 explains the properties and implementation of the dynamic body model used for the movement prediction. Details of the calibration that are specific to this body model are described in section 8.1.3, and section 8.1.4 describes the sensor system that is required in addition to the one presented in section 6.4. Results from experiments are presented in section 8.1.5, followed by a conclusion in section 8.1.6.

8.1.1 Control System

The control system of the dynamic model approach is organized in two loops which are connected: The first loop is responsible for computing the intended movement of the operator with the dynamic body model. It reads the kinematic information of the operator from the sensors, and computes the joint torques of all unsupported joints and the external contact forces through inverse dynamics. With those torques and the EMG signals the simulation of the dynamic body model is performed through forward dynamics computation. This yields the desired movement of the operator expressed through the joint angles (in our cases: hip or knee angles) that have been computed by the simulation. The simulated joint angle is passed to the inner control loop, which is responsible for executing the desired movement with the actuator. This concept is shown in figure 8.1.

8.1.2 Dynamic Body Model

During the design of the dynamic body model, several important aspects have to be considered:

- The model should be as simple as possible to keep the number of parameters low. Most of the parameters are subject-specific and have to be identified by hand.
- All sensors are mounted on the exoskeleton. The accuracy of the sensor readings, especially when measuring the current pose, may be very bad, depending on the pose and motion of the exoskeleton.

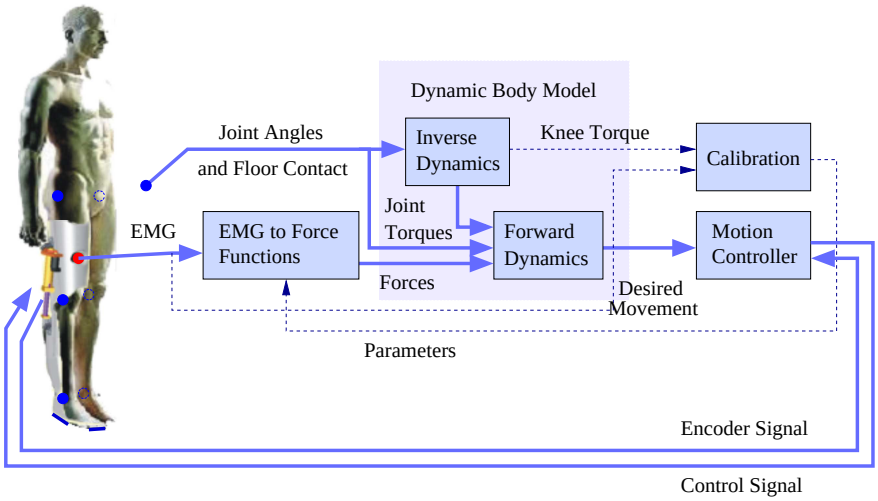

Figure 8.1: The figure shows the data flow within the system. The solid lines show the flow in normal operation mode, the dotted lines mark additional signals during calibration.

- It may be possible that some parameters or state variables cannot be measured directly. The number of those should be kept low, since indirect measurement or calculation can introduce substantial errors.

The human body model of the simulation is simplified significantly: It consists of two legs with feet, shanks, thighs, and the torso. The arms and head have not been modelled. All limbs and the torso are modelled as rigid bodies with a mass distribution of rectangular parallelepipeds. The limbs are connected with swivel joints that can rotate in sagittal plane only. Joint friction is not modelled.

Of course this simplified model is not useful for real-life stability computations, because it is planar, but the reduction of degrees of freedom helps during first investigations of the approach.

Body masses of the torso, thighs, shanks and feet are calculated as fixed fractions of the total body weight of the subject. Body dimensions are taken from our subject. All parameters are listed in appendix C.

The dynamic equations of the model were derived using Kane's formalism [KL00] [KL97]

$$\mathbf{M}(\mathbf{q})\dot{\mathbf{u}} = \mathbf{f}(\mathbf{q},\mathbf{u}) + \mathbf{g}(\mathbf{q})\mathbf{T} \tag{8.1}$$

$$\begin{aligned} \text{with} \quad \mathbf{q} &= (q^r_{hip}, q^r_{knee}, q^r_{ankle}, q^l_{hip}, q^l_{knee}, q^l_{ankle}, q_{torso}, q^x_{pelvis}, q^y_{pelvis})^T, \\ \mathbf{u} &= \dot{\mathbf{q}} \quad \text{(time derivative in the Newtonian reference frame)}, \end{aligned}$$

where

- **q**: vector of generalized coordinates, which are the joint angles of the hip, knee, ankle, and torso (with respect to the reference frame), and coordinates of the pelvis located in the reference coordinate system,
- **u**: vector of generalized velocities,
- **M** (matrix function): specifies mass distribution of the rigid bodies,
- **f** (vector function): models inertial forces and gravity acting on the system,
- **T** (vector): takes into account all torques in the joints as a result of the muscle forces applied: t^r_{hip}, t^r_{knee}, t^r_{ankle}, t^l_{hip}, t^l_{knee}, t^l_{ankle}, together with the external forces F^l_x, F^l_y, F^r_x, F^r_y applied to the left and right ankles in $x-$ and $y-$direction, F^h_x applied to the hip, and the torques applied between the reference frame and the feet T^l, T^r (refer to figure 8.2),
- $\mathbf{g}(\mathbf{q})$: nonlinear function representing the current system configuration and geometry.

The set of dynamic equations (8.1) were generated with the symbolic manipulation tool AUTOLEV[1], resulting in a system of nine equations. Those equations express the relation between the control values, which are the torques and forces acting on the system, and the resulting movement, which are the accelerations. If the current kinematic state of the system and all forces and torques acting on the system are known at any time, solving those equations for $\dot{\mathbf{u}}$ yields the resulting accelerations (forward dynamics). Double integration of those accelerations simulates the movement of all rigid bodies of the system over time from a known initial state.

On the other hand, if the accelerations $\dot{\mathbf{u}}$ are known, the equations can be solved for the torques and forces which have caused these accelerations (inverse dynamics).

As stated above, the general idea of the control system is to simulate the dynamic model for a small timestep. The result of the simulation is interpreted as the desired movement. To be able to perform the forward dynamics computation, all joint torques and external forces acting on the modelled rigid bodies have to be known. External forces could be measured by force sensors between the operator and the environment, and between the orthosis and the environment. But for the joint torques this is not possible with non-invasive methods. A different technique has to be applied: For all joints that are not covered by the exoskeleton, and their muscles not being observed with EMG sensors (in our case: all except the knee), the joint torque during the last iteration can be computed by the inverse dynamics of the model, using the kinematic information recorded with the reference system. The inverse dynamics computation requires the movements of the joints and of the reference point during the last iteration which can be determined through angle and floor contact sensors, and calculates the

[1] Kane Dynamics, Inc., http://www.autolev.com, 2007.

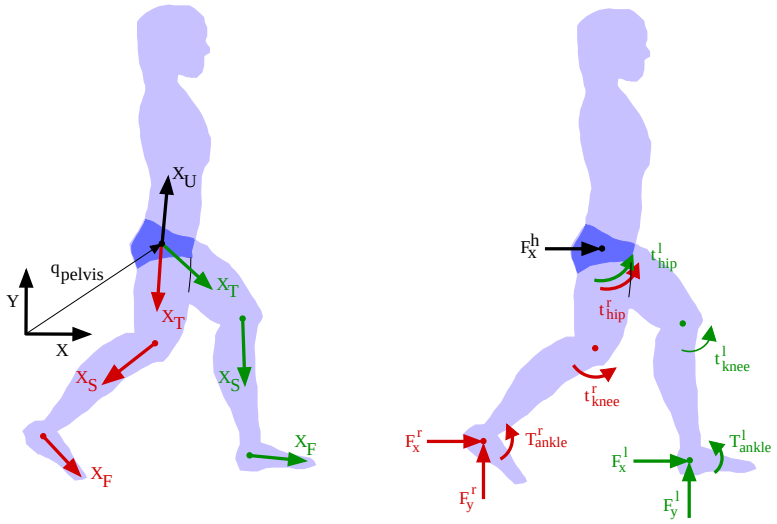

Figure 8.2: Left: coordinate systems of the reference system and the individual body segments. The *z*-axes are perpendicular to the paper plane pointing towards the reader. The *y*-axes are perpendicular to the *x*- and *z*-axes forming a right-handed coordinate system. The generalized coordinates rotate around the z-axis of the individual systems. Right: all joint torques and the modelled external forces with their points of contact.

torques and forces that must have been active to produce the recorded movement: It solves equations 8.1 for elements of **T**.

Those torques and external forces that have been active during the last iteration are assumed to be constant for the following timestep. This is a rough approximation, but we have to keep in mind that the movements which are performed with the orthosis do not contain large accelerations. For the example movements presented in figures 8.5, 8.6 and 8.7 this approximation introduces a torque error in the order of 1% to 3%.

Inverse Dynamics During the inverse dynamics computation, equations 8.1 are solved for elements of **T**. But **T** is constructed of more than nine elements, as described before, because of different external reaction forces that can contribute: contact forces and torques on one or both feet. The elements of **T** for which equations 8.1 are solved, in addition to the six joint torques, depend on the current contact information with the floor:

- only left foot: F_x^l, F_y^l and T^l,
- only right foot: F_x^r, F_y^r and T^r,
- both feet: F_y^l,F_y^r and F_x^h
  (F_x^h is symmetric for both legs and avoids singularities when feet are close to-

gether; compensates measurement errors, and is only used to be able to solve the system of equations algorithmically).

The accelerations $\dot{\mathbf{u}}$ needed to perform the inverse dynamic computation are numerically derived from the values of the pose sensors with $\Delta t = 30ms$. After this computation, the contributions of the mentioned torques and forces that result in the current motion are known.

EMG-to-Force Computing the torque is not possible for the knee joint covered by the orthosis by inverse dynamics: This joint cannot be moved without the actuator being moved, and as a consequence the inverse dynamic computation could never predict any movement of this particular knee joint as a result of the operator's intention. It would always predict the effect of the actuation, which is not desired here.

To avoid this, EMG signals of muscles spanning the knee joint are recorded, converted into muscle forces, and subsequently summed in the knee torque. The torque of the actuated knee joint, t^r_{knee}, is calculated by converting the EMG values to activations as written in equation 4.2. The resulting muscle force, F^m_i, is derived much more simple for these experiments by:

$$F^m_i = \frac{e^{A_i u_i R_i^{-1}} - 1}{e^{A_i} - 1} \cdot F^m_{o,i}, \tag{8.2}$$

with $i = 1 \ldots N$ (N: number of recorded muscles), u_i the post-processed and scaled EMG value of muscle i, and A_i the non-linear shape factor. A_i was limited to $-10 < A_j < 0$ in our setup. The scale, R_i, is the maximum recorded post-processed EMG signal during calibration with the corresponding maximum force, $F^m_{o,i}$.

Two muscles have been included into the model, one extensor and one flexor for the knee joint. The points of origin $\vec{O}_i$, and insertion $\vec{I}_i$ of the muscles are fixed and have been chosen by hand in analogy to human anatomy (refer to appendix C). This muscle model is not as elaborated as the one described in section 4.3: No waypoints have been used in this model, and no other muscle properties.

The total knee joint torque t^r_{knee} is calculated as a sum of all force contributions of the muscles spanning the knee joint with

$$t^r_{knee} = \sum_{i=1}^{N} \left(\left(\vec{I}_i - \vec{J} \right) \times \frac{\vec{I}_i - \vec{O}_i}{|\vec{I}_i - \vec{O}_i|} \cdot F^m_i \right), \tag{8.3}$$

where $\vec{J}$ is the vector to the knee joint and $\vec{O}_i$ and $\vec{I}_i$ the points of origin and insertion of muscle i in the reference frame.

Forward Dynamics Now all the joint torques and external forces are known and the simulation can be performed: The *forward dynamics* block takes the current system state $\mathbf{S}(\mathbf{t}) = (\mathbf{q}(\mathbf{t}), \mathbf{u}(\mathbf{t}))^T$ and applies all internal and external torques and forces as

calculated by the inverse dynamics and the joint torque resulting from the EMG signal evaluation. It then solves equation 8.1 for $\dot{\mathbf{u}}$, and double-integrates the accelerations to compute the new system state.

8.1.3 Calibration

In this simplified human body model, only the parameters A, R and F_o^m (from equation 8.2) have to be calibrated for all muscles.

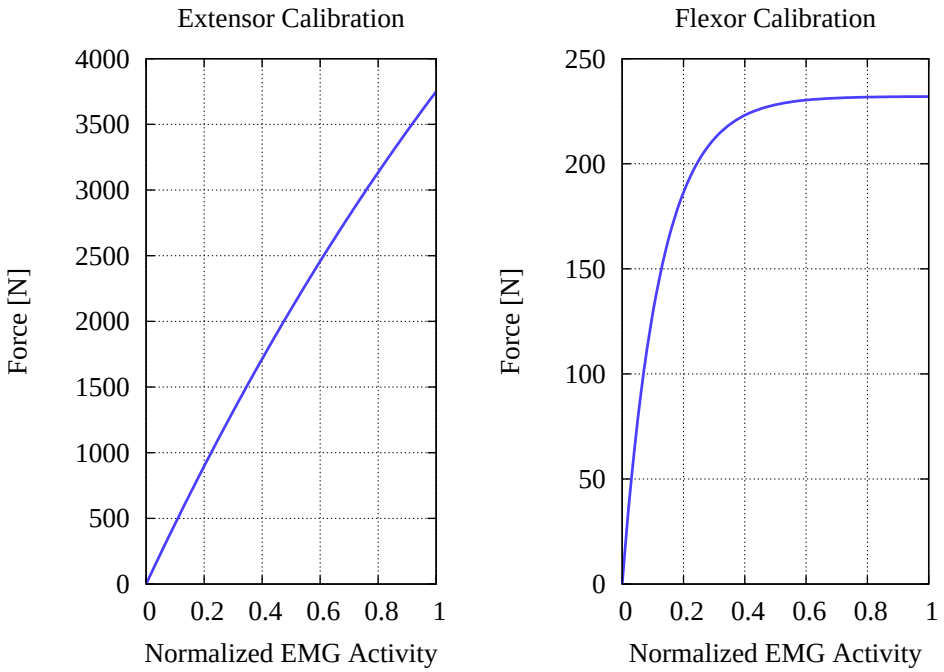

Figure 8.3: Example of the calibration with the inverse dynamic model for the thigh muscles (stair climbing experiment). The calibrated extensor muscle is a representative for the extensor group, resulting in a high maximum force output associated with the muscle. The same is true for the flexor calibration, although the calibration is not sufficient here: The sum of the flexor forces far exceeds the maximum force calibrated here.

In the setup here, a movement with the joint that should be calibrated without external contact had to be performed. That is, hip extension and flexion during early experiments, and knee flexion and extension together with climbing one step of a stair during later experiments. During the calibration, the actuator was not attached, allowing free movement in all joints.

The data was recorded and stored in tables for every muscle according to its activation as described in section 5.3. Two different optimization algorithms have been tested: The first algorithm used a black-box method for the body model, the second performs curve-fitting with the inverse model.

With the black-box method, every entry of the table contains the last recorded kinematic configuration and the resulting configuration one time-step later, together with the EMG values. This method was applied to the hip joint, and the pelvis was held fixed in the reference frame. All other joint torques have been set to zero for simplicity. During hip flexion and extension the muscles spanning the knee were all relaxed.

The error function of the black-box optimization algorithm simulates the model for every table and every entry with the current parameter set consisting of A_i, R_i, and $F^m_{o,i}$, and evaluates the predicted joint angle in comparison to the recorded resulting joint angle. The squared error is summed over all entries and all joints:

$$E_{black} = \sum_j \sum_i \left(q^{model}_{i,j} - q^{ref}_{i,j} \right)^2, \tag{8.4}$$

where j is the entry index of the table, $q^{model}_{i,j}$ is the joint angle simulated by the model based on configuration stored in entry j for the i-th joint, and $q^{ref}_{i,j}$ is the resulting reference angle of the same entry.

Optimization was performed repeatedly for all muscles to account for coactivation and cocontraction.

For this black-box method, no inverse model is required. This can be beneficial, if more muscles are incorporated and model complexity rises. But it becomes problematic with redundant muscle activations. But since the movements during this calibration are not limited to isometric exercises, other movements with other activation patterns can be included. The optimization has been performed with the Nelder-Mead Simplex Algorithm described in [NM65].

Unfortunately, this optimization is rather time-consuming because of the required model simulation. The second method calculates the inverse dynamics and stores the computed knee torque $t^{r,inv}_{knee}$ in the table entries, together with the EMG values.

The optimization of a particular muscle takes the EMG-to-force function from equation 8.2 and evaluates the result with the stored knee torque t^r_{knee}:

$$E_{inv} = \sum_j \left(t^{r,inv}_{knee,j} - t^{r,emg}_{knee,j} \right)^2, \tag{8.5}$$

where j is the entry index of the muscle table, $t^{r,inv}_{knee,j}$ the result of the inverse dynamics computation stored in entry j, and $t^{r,emg}_{knee,j}$ the torque resulting from the EMG values stored in entry j applied to the EMG-to-force function described in equation 8.3.

Aside from the reduced complexity of the optimization, both algorithms deliver equally good results. Advantages of the concept of calibration with data tables is described for the multi-muscle calibration of the torque loop control system in section 5.8. Experiments described in section 8.1.5 have been performed with the optimization utilizing the inverse model. An example calibration is shown in figure 8.3.

8.1.4 Sensor Setup

In addition to the EMG and angle sensors described in section 6.4, it is also necessary to record the joint angle configuration of the unactuated leg and the torso inclination of the operator. Ideally, also the arms and the head should be measured, but this is too complicated due to the high degree of freedom. The sensor system of the unactuated

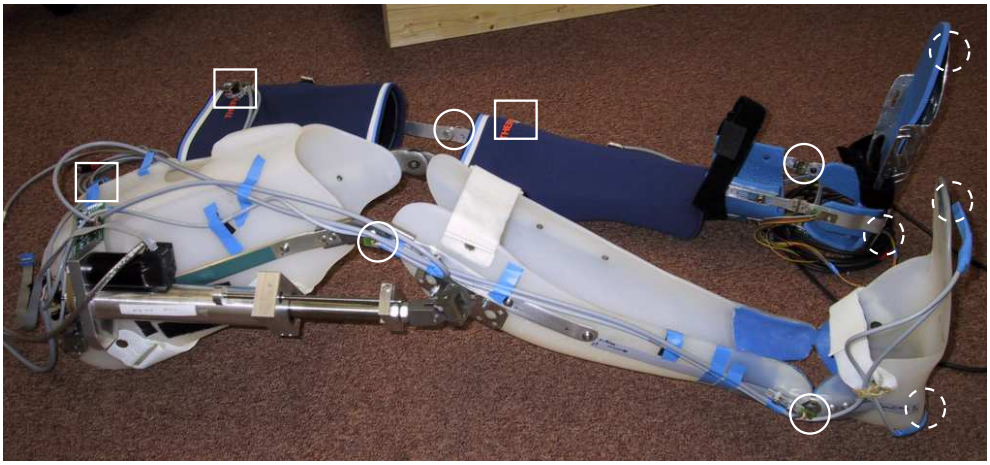

Figure 8.4: Early stage of the actuated orthosis (foreground). The leg brace used to hold the sensors for measuring the joint angle information from the unactuated leg is shown in the background. Squares indicate the position of the accelerometers, circles mark Hall sensors, and dashed circles show the location of the floor contact sensors.

leg is attached to a second, very light-weight frame. This is shown in the background of figure 8.4. The torso inclination is measured by a sensor attached to a belly plate, which is not shown in this image.

During those early experiments, two EMG sensors have been placed on top of the sartorius and gluteus maximus (for the hip experiments), and two on the semimembranosus and vastus medialis (for the knee experiments). Many other muscles cooperate during hip and knee movements, but we have chosen those, which are most clear and simple to record and have a large contribution to the resulting joint torques [Pla03]. The EMG sensors are the same as described in section 6.4 and the data is rectified and smoothed by a lowpass filter with a cut-off frequency of 5 Hz as suggested for example in [TVdZ03, BLMB04].

Ankle and knee angles are measured in sagittal plane only on both legs with Philips KMZ41 Hall sensors (refer to section 6.4), and the orientation of thigh and trunk is measured with accelerometers ADXL210 from AnalogDevices Inc., as described in [FKRH04b]. This is necessary, since no fixed axis of rotation exists to which the Hall sensor or magnet could be attached. Alternatively, goniometers[2] could be used. The joint angles of the left and right hip are calculated as the difference of the angles reported from the accelerometers of the torso and the left thigh, and the torso and

[2]For example, from BioVision, http://www.biovision.eu, 2007.

right thigh, respectively. The accelerometers have been placed as close as possible to the rotation axes of the hip to reduce the inertial acceleration resulting from limb movement.

In addition to that, force sensing resistors (FSR sensors) are attached under the heel and footpad on both feet to detect floor contact. All sensors are sampled with 1kHz.

Since no sliding on the floor and no ballistic flight phase is considered, it is sufficient to record all joint angles for determination of the current kinematic state of the operator. The position of the reference point in the pelvis is computed through the contact points with the floor and evaluation of the joint angles with the corresponding lengths of the body segments. The angular velocities are computed by numerical derivation of the joint angles. This could be improved by integrating velocity and acceleration sensors on every body segment with additional filters to maintain consistency across all sensors.

8.1.5 Experiments

The experiments presented here are divided into two groups. The first group deals with simulating the hip joint movement during free leg movements, the second group with climbing a step.

The first experiments have been performed as follows: The subject is standing upright, but only on the left foot. The right leg is free to move in sagittal plane, and the actuator is not attached. The shank should point roughly down to the ground. Calibration is performed offline on a set of recorded data: The left side of figure 8.5 shows a replay of the data used for the calibration. The right side of the same figure shows the prediction of an arbitrary movement pattern with the same posture. Both diagrams show the reference hip angle and the predicted hip angle plotted against time. During this experiment, the model was synchronized with the reference system only at the beginning. After that the knee angle is computed based on the forces predicted from the EMG signals. As can be seen, the model can adapt the parameters quite well during calibration. Unfortunately the calibrated EMG-to-force function has a strong curvature ($A \approx -3.5$), thus omitting a force production that is required to reach angles above 70° as shown during the prediction on the right side.

One could argue that this experiment is an exercise in curve-fitting only, but it should not be forgotton that the data is a result of the simulation of an underlying dynamic model. On the other hand it is true that the model features limited predictability because of the low number of integrated muscles, and the abstraction from muscle and tissue properties.

The second group of experiments which is presented here is very much optimized on the task of climbing one step of a stair for several reasons: First of all, climbing a stair is a prominent example where large force support in the knee joint can be applied for good, in contrast to normal walking where the thigh muscles are only activated during certain short phases, and additional support is not sensible for healthy subjects. Second, it omits some problems which complicate the experiments unnecessarily: When

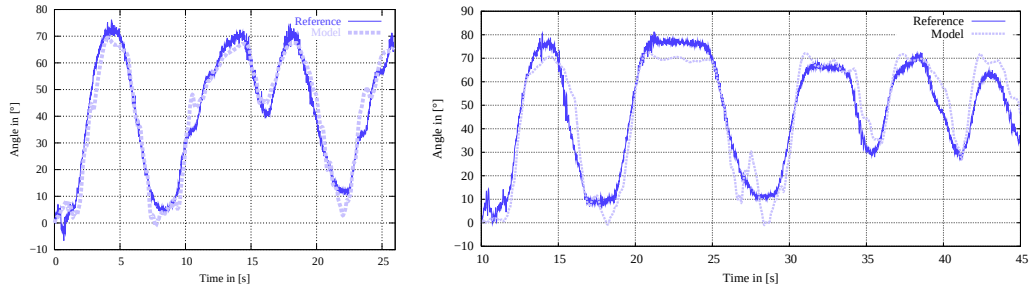

Figure 8.5: Results from early experiments: The subject was standing in an upright position. The recorded reference hip angle is plotted together with the hip angle prediction of the model based on the EMG signals (no actuation). Zero degrees indicate a hip in neutral position, pointing down. A positive angle means hip flexion (raising of the knee, torso remains upright). Calibration had been performed with the data on the left side. The right side shows the prediction for previously unknown data.

considering the sit-to-stand movement, for example, additional contact forces have to be detected at other locations. And since both feet are set side by side during standing up, the ground reaction forces for the individual feet cannot be estimated by a planar model in sagittal plane.

This experiment consists of two movements: During the first one the subject is standing upright and flexes and extends his knee and hip joints. In the second movement the subject is climbing one step of a stair, with the right leg leading. During the movements the actuator was detached to allow unhindered motion. The kinematic information as well as the EMG signals are recorded. Data of both parts are utilized to calibrate the flexor and extensor muscles (as shown in figure 8.3).

This simple experiment tests the most important aspects of the algorithm: motion of all limbs, various points of contact during single- and double-support phase, swing-phase of the right leg, cocontraction of knee flexor and extensor muscles and coactivation with other muscles that are not recorded.

The calibration of the muscle parameters is divided into three parts: The first part is performed after the backward motion with the knee flexors, the second part after climbing the step, and the third part performs the calibration again for both muscles without the need to acquire new data. Figure 8.6 shows a replay of the data used for calibration to show the model adaptation. Applying the EMG signals to the body model results in a torque-curve very similar in shape and magnitude to the torque-curve calculated by the inverse dynamics as described in section 8.1.2. The offset of the torque curves is partly a result of measurement errors, and not modeling the passive forces of the muscles and tissue: When the muscles of the free leg in an upright standing position are relaxed, the knee of the human is not completely extended, in contrast to the modelled knee, due to passive forces of the muscles. This leads to an angular displacement resulting in a different knee torque. In addition to the vertical displacement, a horizontal displacement exists as a result of the delays through the numerical derivation of the

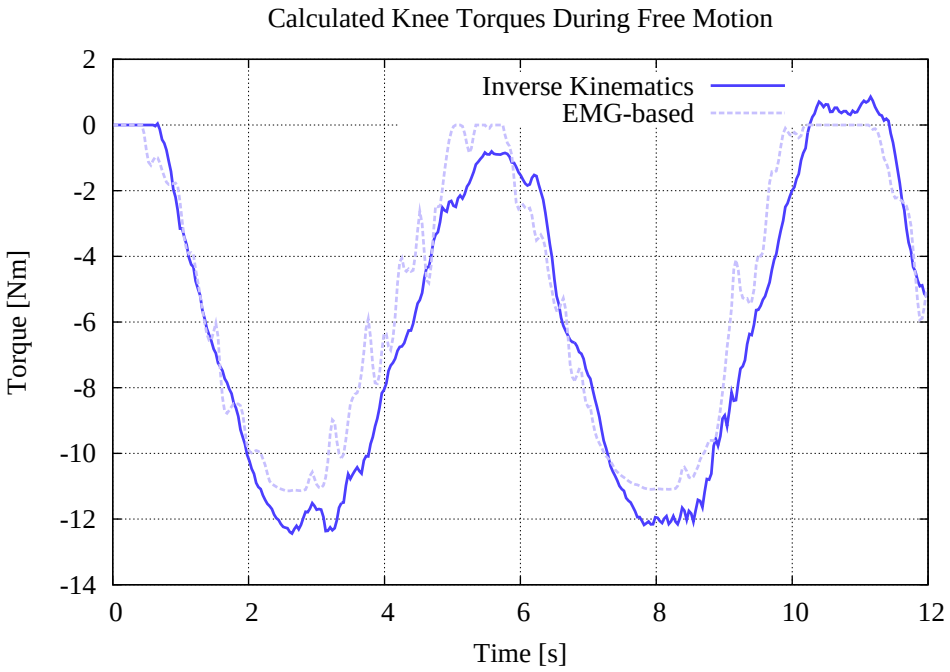

Figure 8.6: This diagram shows the knee torque as calculated through inverse dynamics compared to the torque resulting from the EMG signal evaluation (after having calibrated the EMG-to-force parameters of the knee flexor). A negative torque indicates knee flexor activity. The vertical offset is a result from the unmodeled passive muscle force and errors in the angular measurements of the thigh and shank.

joint velocities and joint accelerations. This can be compensated for an offline replay, but not for an online experiment.

Since the body model will be synchronized with the reference system during every iteration, it is sufficient to display the torque plot of the actuated joint to analyse the short-term behavior of the system. The overall fitting of the joint angletrajectory is not so important, since the human is inside the control loop and can compensate a divergence from the desired trajectory.

Step two is performed after stepping up the stair, as shown in figure 8.7. The data begins when the right foot is lifted from the ground. A little flexor activity with co-contraction indicates the interval where the knee is bend to raise the right foot. The section between the dashed lines indicates the double support phase, during which the weight is shifted forward from the left to the right foot. After the dashed lines, the left foot is raised and also put on the same step.

As can be seen in the lower part of the figure, both muscle groups are active during this motion resulting in the calibration of the knee extensor parameters using the parameters of the knee flexor.

In the third and final step, parameters of both muscles have been optimized repeatedly without the need to acquire new data. This was necessary since results modify

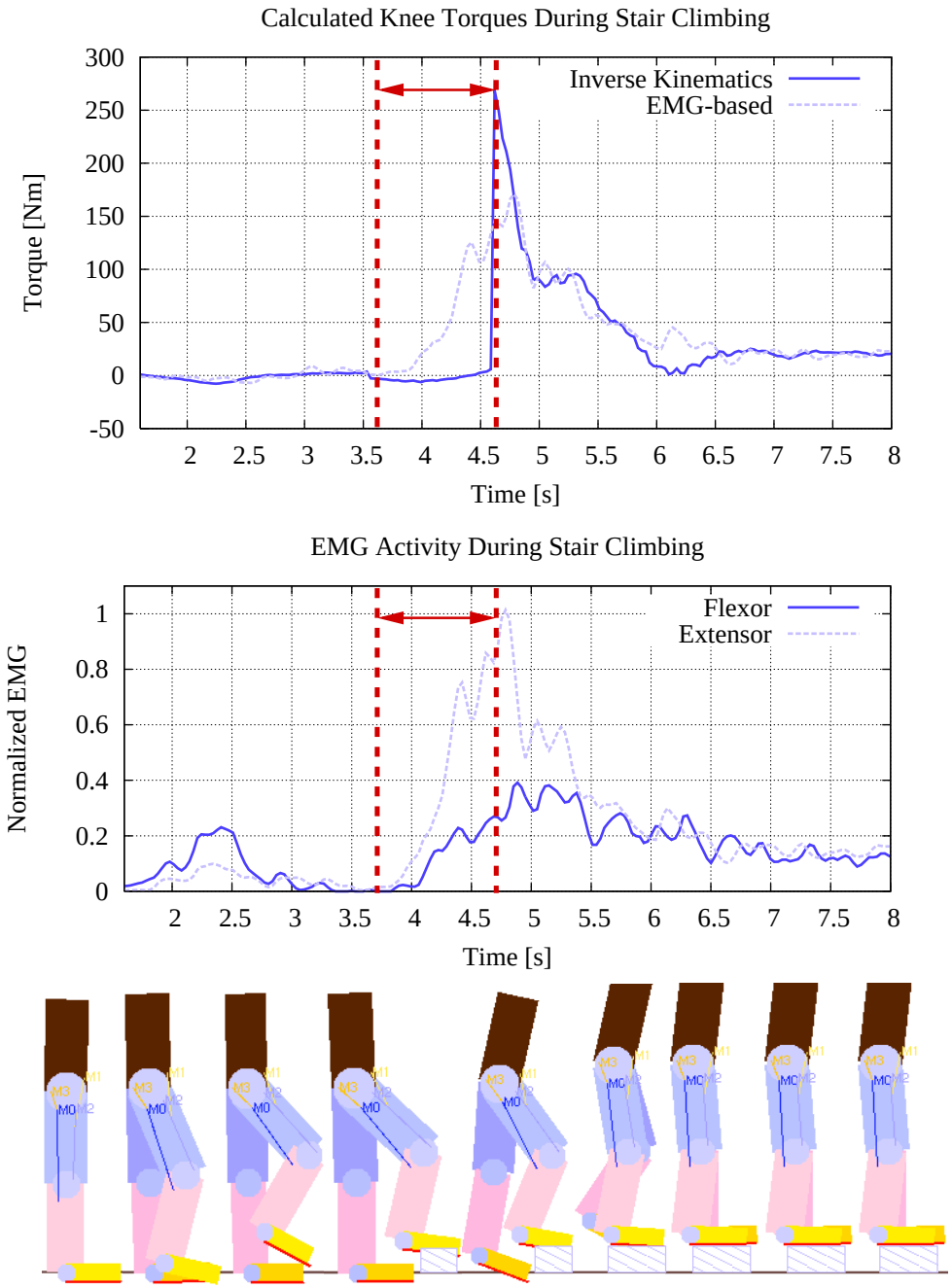

Figure 8.7: Top: torque prediction with a dynamic body model during stair climbing. The torque computed by the inverse dynamics is plotted over time, together with the torque derived from the EMG signals. The dotted lines mark the double support phase, in which deficits of the model can be seen. Middle: Postprocessed EMG activity of the observed muscles. Bottom: Visualization of the reference sensor information.

each other due to cocontraction. This procedure was terminated when the change in parameters was sufficiently small.

The upper part of figure 8.7 shows the torque curves during stair climbing after the calibration was completed (a replay of the recorded data), and figure 8.3 shows the final calibration curves for both muscles. When examining those curves, the high force output of the knee extensor muscle attracts attention. But it should be considered, that the vastus medialis recorded during this experiment represents a whole muscle group with a sum of peak forces of over 5000N [DLH$^+$90]. But climbing one step of a stair requires not maximum muscle force. Thus it can be said that the order of magnitude is correct. This is different for the knee flexor muscle that also represents a muscle group with a sum of peak forces over 2000N. For that, it should be noted, that the movement chosen for the calibration is nowhere near the maximum force the knee flexor can produce. But this does not explain the strong curvature of the function, prohibiting the production of large forces during extrapolation for higher muscle activations. This could be a result of inaccurate modeling, or a result of the misalignment of the EMG signal and the torque computed by the inverse dynamics. It reduces the predictability of the model across different movements, but nevertheless allows a good prediction for the setup it was calibrated for (task-dependent).

Examining the upper part of figure 8.7 more closely reveals the most important problem of the control system: The measurement of the operator's kinematic configuration is inaccurate, so that when the floor contact configuration is changed (the left foot is raised from the ground), a large discontinuity in the torque prediction at $t \approx 4.62$s can be observed. In-between the dashed lines, the operator was leaning forward to bring his mass forward over the leading foot. Unfortunately, the torso angle was determined not accurately enough (amplified by the unmodeled arms and head) to reflect this in the data. Instead, the data suggests that the center of mass of the human is behind the supporting foot, leading to an abrupt increase of the computed knee torque at the transition to the single support phase. Such a large knee torque is possible, because during this phase the foot with floor contact is rigidly connected to the floor in the model, creating a large supporting ankle torque to establish consistency with inaccurate sensor readings.

In theory, if the motion is completely tracked with head, arms and upper torso (or the torso has to be stiff), and if the pose sensors are accurate enough, an abrupt change should not occur. Unfortunately this is not the case with our experimental setup. Influence of unmeasured and unmodeled body parts, unmodeled degrees of freedom, motion artifacts due to inertial accelerations, and errors in calibration of the accelerometers attached to the torso and thighs result in inaccurate angle readings. Especially for the heavy torso this leads to wrong torque calculations in the joints for some configurations.

Before and after the double support phase, a good correlation of the two torque-curves can be seen expressing the performance of the body model and the consistent calibration for both muscles in those configurations.

8.1.6 Results

Figures 8.5, 8.6, and 8.7 show results of the model adaptation and intended motion prediction. The shape of the curves correlate very well, although sometimes the amplitudes of the curves differ. This is not a major problem for the desired application: Since the subject wearing the orthosis is inside the control loop of the system, he or she can increase or decrease the muscle activity a little to adapt to the circumstances.

The major problem of this approach occurs during the double support phase and at the transitions between contact configurations: The torques computed by the inverse dynamics cannot be computed reliably and continuously. Feeding those torques into the simulation of the body model may result in an unexpected target joint angle, which is not desired. Without a solution to this problem, experiments cannot be performed safely. In order to solve those problems, the system and model can either be simplified, hoping to get a more robust and reliable system, or made more complex, addressing all drawbacks directly. Similar problems have been investigated during the KONDISK research project: In [SB98] the theory of a state-based controller is proposed that handles hybrid discrete-continuous dynamic systems. It was applied to the simulation of a multi-fingered robotic hand during grasping and regrasping tasks, and later investigated and extended in experiments with a robotic hand [BS00]. Problems of contact state errors due to inconsistencies between the model and the real world have been addressed in [Sch03]. Applying such a control system to the exoskeleton can improve the system behavior.

For most of the deficits or simplifications that have been mentioned above an appropriate solution or replacement may be found that improves the results. For example, the complex biomechanical model described in section 4.3 can be applied, the model can be three dimensional, more EMG sensors can be evaluated, and joint friction and passive elements can be included. But this does not solve the inherent problem of this approach which is the sensibility of the inverse dynamics computation to disturbances, and inaccuracies in the sensor readings and modeling. Some of those problems could be reduced by increasing the complexity of the sensor system: Recording the angular velocities and acceleration directly can reduce some artefacts. In addition, the upper torso, arms and head could be equipped with sensors to improve the consistency between the model and the real world. But most importantly, the ground reaction forces have to be determined properly, and the pose in the global reference system has to be determined accurately due to the effect of gravity. Even with an array of 64 FSR sensors from Medilogic[3] the acquired data was not sufficiently accurate. Besides, extending the system with, in theory, redundant sensor information adds the problem of consistency across different sensors, and an appropriate calibration has to be implemented.

Some of those problems disappear if the exoskeleton is extended to a full-body suit.

[3] T&T medilogic Medizintechnik GmbH (Germany), http://www.medilogic.com/, 2007.

In that case, the joint angles could more accurately be determined, and more limbs can be integrated into the model.

On the other hand, the system and dynamic model can be simplified, relying on less sensors, and performing some estimations. Such approaches are presented in chapter 2, where the RoboKnee [PKMC04] is one example of them: Ground reaction forces under the feet are measured, and the knee torque that is necessary to maintain a statically stable pose is computed through a very simple model. A certain percentage of this torque is added by the actuator. The drawback of this approach is that it does not regulate the support depending on the task, and it does not "listen" in any way to the operator for his or her desired movement.

For the BLEEX mentioned in chapter 2 a more complex model was developed that computes the support torques required to relieve the operator of the weight and inertia of the exoskeleton and payload. But the sensitivity of the model to the payload led to a control algorithm using a position controller and a model based torque compensation, depending on the phase of gait, as published in [KSH06].

As a conclusion to the experiments presented in this chapter it can be said that the theoretical model is too complex for application in this particular exoskeleton. If the dynamic body model is applied properly it would offer some advantages: The desired movement can be computed in advance and can be modified according to constraints defining stable movements, or can be inhibited completely for safety reasons. But those features begin to make sense only with a more complex exoskeleton hardware, in terms of more actuated degrees of freedom. Furthermore, the favorable behavior of the torque controlled system presented in section 4.6 cannot be integrated: The robustness to external contact forces wherever they appear cannot be achieved, and it is not possible to override the predicted "desired" motion or pose through additional forces from unmeasured muscles, or, for example, the hand helping to move the leg. The system always sticks to its simulated results.

For the exoskeleton hardware presented here, a more simple and reliable approach was sought and found. This approach has been presented in chapter 4.

8.2 Knee Torque Prediction with a Simplified Body Model for Calibration

This section discusses the application of simplified body models to be used for specific tasks. To analyze the behavior of such systems, the special case of a system modeling the sit-to-stand movement is developed and analyzed. If the system proves to be useful, new models can be developed for the exoskeleton control.

During the calibration movement described in chapter 5 it turned out, that not all extensor muscles are equally active during isometric exercises at all knee angles, namely the vastus medialis and vastus lateralis. Those muscles are activated during tasks where larger muscle forces are required, for example, during standing up from a chair

or during knee bends. The simplified model here produces reference values for the calibration of the EMG-to-force parameters. By analyzing the model behavior in this context, it can be evaluated in how far this model shows consistency with the real world.

A simplified version of the body model described in section 8.1 was developed, tailored to the task of standing up from a chair. This model is used to calculate the knee torque to obtain the reference torques for the optimization process.

Recording of the data is started after losing contact with the chair, and stopped when standing in an upright position. No transitions between contact configurations has to be considered. The body model is simplified in such a way that little extra sensors are required. The algorithm has been published in [FH07].

8.2.1 Model Simplifications

To estimate the knee torque the muscles are producing during getting up from a chair without hindering the movement, it is necessary to track the movement and compute the torque by inverse dynamics. The advantage of using a rather simple movement is the possibility to apply major simplifications to the model. Without those, the problem cannot be solved satisfyingly in a real world environment or only with many additional sensors.

For the sit-to-stand movement the body model uses the following simplifications:

- Both legs are merged into one, and a two-dimensional model is used.
- After losing contact with the chair, the operator is not allowed to support himself with his arms to omit unmeasured and unpredictable external force input.
- Only the trunk, thigh, and shank are modelled (as rectangles). The arms and head are approximated through modifications of the trunk properties. Excessive movements with the arms have to be avoided.
- The ankle is rigidly attached to the floor, the foot is not modelled.
- Joint friction and passive joint stiffness is neglected (typically 2–5Nm/rad for most major joints in the mid-range of motion [ZW90]).
- Joint accelerations are small and can be neglected, especially because the phase when losing contact with the chair is not regarded due to reaction forces from the seat.
- Joint velocities, typically below 50/s, during the considered movements contribute only about 1% to 3% of the knee joint torque, and are neglected.

Following the model description from above, the parameters of the model are:

- The total body mass of the human: m_{total} (must be measured from the subject),
- Masses of the body segments as a fraction of m_{total} for the trunk, thigh and shank taking into account the combination of limbs as described above.
- Length and width of the trunk, thigh and shank: (L_u, W_u), (L_t, W_t), (L_s, W_s) must be measured from the subject.
- The location of the center of mass as a fraction of the length of the body segment from the proximal end for each body segment, r_t (thigh) and r_s (shank), taken from literature [Win90a]. The mass center of the trunk r_u is determined separately later on. It also incorporates the arms and head.
- The location of the balance point of the foot: $b_x = 0.04$m from the ankle joint towards the distal end of the foot (see remarks below).

The individual values used in the experiment are given in appendix C. The model includes three joints: ankle, knee, and hip, with corresponding generalized coordinates q_1, q_2, and q_3, which are defined as shown in figure 8.8. The third angle can be computed as a result of the other two angles by introducing an additional constraint: The center of mass (CoM) of the body projected onto the ground must be on a specific point within the region of the foot, the balance point $\vec{B} = (b_x, 0)^T$. The ankle angle is measured in addition to the knee angle, because a sensor can be easily attached. By computing the hip angle as described below, it can also integrate effects of the unmodeled head and arms.

The x-coordinate of the center of mass of the model can be computed by:

$$\begin{aligned} CoM_x &= \big(L_u r_u m_u \cos(q_1+q_2+q_3) + L_s(m_t+m_u+m_s(1+r_s))\cos(q_1) \\ &\quad + L_t(m_u+m_t(1+r_t))\cos(q_1+q_2)\big) \cdot \big(m_s+m_t+m_u\big)^{-1} \end{aligned} \tag{8.6}$$

The angle of the hip is calculated by solving equation 8.6 for q_3:

$$q_3 = \begin{cases} -q_1 - q_2 & \text{if} \quad C > +1 \\ \pi - q_1 - q_2 & \text{if} \quad C < -1 \\ \arccos(C) - q_1 - q_2 & \text{otherwise} \end{cases} \tag{8.7}$$

with

$$\begin{aligned} C &= \frac{A}{B} \\ A &= b_x m_{total} - L_s(m_t+m_u+m_s(1+r_s))\cos(q_1) \\ &\quad - L_t(m_u+m_t(1+r_t))\cos(q_1+q_2) \\ B &= L_u r_u m_u \end{aligned}$$

and

$$\begin{aligned} b_x &= CoM_x && \text{(balance condition)} \\ m_{total} &= m_s + m_t + m_u && \text{(total body mass)} \end{aligned} \tag{8.8}$$

If $C > +1$ or $C < -1$ the balance condition is violated: $CoM_x \neq b_x$, and the arc cosine of C cannot be computed. To allow calculation of an approximated hip angle, C is replaced by the boundary it has exceeded.

8.2.2 Human Body Model

The equations with the simplifications justified above (joint accelerations and velocities are neglected: $\dot{u}_1 = \dot{u}_2 = \dot{u}_3 = u_1 = u_2 = u_3 = 0$) have been computed with the tool AUTOLEV, yielding:

$$\begin{aligned} 0 &= -T_a - L_s m_s (1+r_s) g \cos(q_1) - m_t g (L_s \cos(q_1) + L_t (1+r_t) \cos(q_1+q_2)) \\ &\quad - m_u g (L_s \cos(q_1) + L_t \cos(q_1+q_2) + L_u r_u \cos(q_1+q_2+q_3)) && (8.9) \\ 0 &= -T_k - L_t m_t (1+r_t) g \cos(q_1+q_2) - m_u g (L_t \cos(q_1+q_2) \\ &\quad + L_u r_u \cos(q_1+q_2+q_3)) && (8.10) \\ 0 &= -T_h - L_u r_u m_u g \cos(q_1+q_2+q_3) && (8.11) \end{aligned}$$

The knee torque T_k can be easily obtained by rearranging equation 8.10:

$$\begin{aligned} T_k &= -g(L_t m_t (1+r_t) \cos(q_1+q_2) + m_u (L_t \cos(q_1+q_2) \\ &\quad + L_u r_u \cos(q_1+q_2+q_3))) \end{aligned} \tag{8.12}$$

Assuming that $-1 \leq C \leq +1$ and substituting q_3 in equation 8.12 with the expression from equation 8.7 yields:

$$\begin{aligned} T_k &= -g(L_t m_t (1+r_t) \cos(q_1+q_2) + m_u L_t \cos(q_1+q_2) + b_x m_{total} \\ &\quad - L_s (m_{total} (1+r_s)) \cos(q_1) - L_t (m_u + m_t (1+r_t)) \cos(q_1+q_2)) \end{aligned} \tag{8.13}$$

Interestingly, the knee torque is not depending on r_u or q_3, meaning that there is no need to measure the torso angle or any upper limbs. But this implies proper knowledge of the balance point. If q_3 should be computed, the mass center of the trunk, r_u, must be chosen in such a way that the balance condition from equation 8.8 is fulfilled throughout the sit-to-stand movement. Argument C from equation 8.7 only exceeds the upper boundary $+1$ when the CoM cannot be brought over the balance point due to the knee and ankle configuration. The lower boundary -1 is never under-run during correct measurements.

Evaluating equation 8.7 for r_u in one important extreme configuration of the movement yields the required relative position of the mass center of the trunk. The extreme

configuration is taken from the initial phase when losing contact with the chair: The body is bent maximally forward to bring the center of mass almost over the knee joint (over the balance point). Solving equation 8.6 for r_u yields:

$$\begin{aligned} r_u &= -[L_s(m_t+m_u+m_s(1+r_s))\cos(q_1)+L_t(m_u+m_t(1+r_t))\cos(q_1+q_2) \\ &\quad -b_x(m_s+m_t+m_u)][L_u m_u \cos(q_1+q_2+\tilde{q}_3)]^{-1}+r_\Delta \end{aligned} \tag{8.14}$$

To take into account that the body is maximally bent forward, $\tilde{q}_3$ is set to an extreme, resulting in a horizontal trunk configuration:

$$\tilde{q}_3 = -q_1 - q_2 \tag{8.15}$$

The contribution $r_\Delta \approx 0.2$ moves the mass center a little towards the head to be on the safe side for repeated measurements. It has to be pointed out, that r_u, b_x, and q_3 are directly related: Modifying one of those quantities results in a change of at least one of the other two.

Unfortunately, the x-coordinate of the balance point, b_x, which is considered to be a parameter, appears in equation 8.13 multiplied by the total body mass m_{total}. As a consequence, variation of the balance point has significant influence on the computed knee torque.

8.2.3 Experiments

Prior to the calibration with the sit-to-stand movement, four of the six muscles used for the torque loop approach had been calibrated as described in chapter 5: all, except the vastus medialis and vastus lateralis. After that, another calibration step was performed, with a sit-to-stand movement as described in section 8.2.1. The reference torques have been computed from the inverse dynamics of the simplified body model, and the parameters of the last two muscle have been optimized.

Figure 8.9 shows the results of a calibration: At $t \approx 1.6$s the movement was recognized due to a sufficient change in the knee angle. For $1.6\text{s} < t \leq 4\text{s}$ the prediction correlates with the reference very well. For $t > 4$s a discrepancy can be seen: The predicted torque is smaller than the torque based on the inverse dynamics. Due to the balancing condition the thigh and trunk is not upright, but the knee and hip are slightly flexed. This results in a residual torque which is not present in the human. This could be omitted, if the balance point would be allowed to move on a trajectory, and if this trajectory was known. Unfortunately it is not, which decreases the performance of the model: Since all sit-to-stand movements are performed slightly different, the true balance point is deviating from the point of the model leading to an error in the estimation. This can be observed if the calibrated parameters are applied to data from a different trial: The torques computed from the inverse dynamics and derived from the EMG signal show a considerable error of 20% or more. By adjusting the balance point the reference data can be manipulated to fit the predicted data. A trajectory for

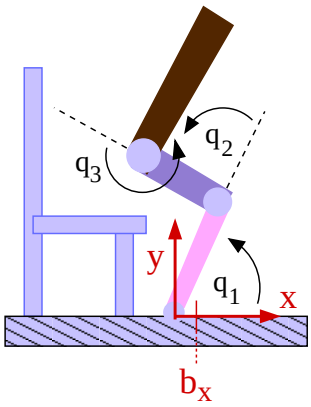

Figure 8.8: Simplified model for calibration: definition of the angles, balance point and reference system.

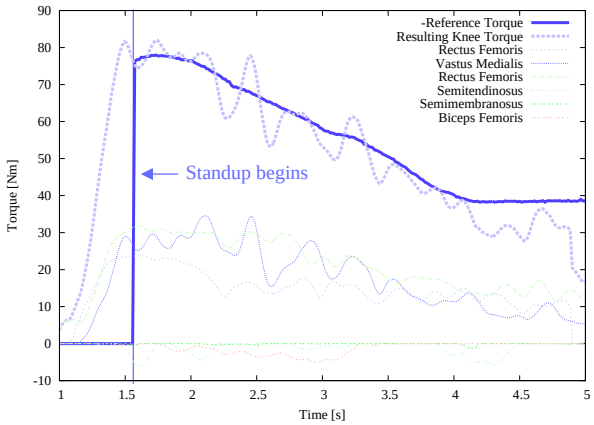

Figure 8.9: Replay from the sit-to-stand experiment: The knee torque calculated with the inverse dynamics of the simplified model can match the calibrated EMG-based biomechanical model.

the movement of the balance point could be found for every trial, leading to a good calibration. But this trajectory was different from trial to trial, reducing the predictability of the model significantly.

8.2.4 Results

In this section, a simplified rigid body model was proposed to be used to produce reference values for calibration of the EMG-to-force parameters. In addition, the feasibility of such simplified models in connection with the exoskeleton was investigated.

Unfortunately, the output of the simplified model is not accurate enough to be used for a reliable and accurate calibration. But it can be used for a rough estimation of the joint torques for this particular task with the suggested simplifications. Also, if a trajectory for the balance point is established successfully, a quantitative analysis of the torque during this movement can be performed. This can be achieved by either integrating more sensors, or by calibrating parameters of a balance point trajectory that are determined together with the EMG-parameters for several sit-to-stand movements. In that case, the number of parameters must be small and bound to feasible values to not overfit the model to a specific data set.

With slight modifications, this model could also be used in a similar fashion to the algorithms presented for the RoboKnee or BLEEX, as described in section 2.1. In those algorithms, the controller compensates a certain percentage of the torque as computed by the inverse model of the operator with the exoskeleton. But as was shown above, those estimations are very rough, and even more simplified for the RoboKnee. As a consequence, the actuation of the exoskeleton takes over a varying amount of torque

in relation to the total joint torque. This leads to a system requiring some training by the operator to adapt movement patterns, and to react properly to the support.

8.3 Conclusions on using Rigid Body Models

Utilizing rigid body models for the prediction of movements or joint torques as well known from simulation in industrial applications opens a wide range of possibilities. If successfully applied, interesting quantities can be computed through the dynamic equations, allowing modification of joint torques for stability control, checking the movement on feasibility to suppress dangerous trajectories and much more, in combination with a position, velocity or acceleration controller.

Unfortunately, in our context it is very difficult to establish consistency between the real world and the model, namely the human body, which is highly non-rigid in the trunk and possesses a large number of degrees of freedom in the joints and between the vertebrae of the spine. And since the torques and forces in the joints of the human body cannot be measured directly non-invasively, the kinematic state of all limbs of the operator and all objects having contact with the operator and exoskeleton have to be determined to incorporate the effect of gravity and inertia. Contact forces include the ground reaction forces, forces from a chair the operator is sitting in, or from a handrail that is used during stair climbing.

While this may be achieved with external sensors observing the operator and the exoskeleton from a fixed reference frame, this is almost impossible with sensors mounted on the exoskeleton and operator alone, which is required for a mobile system that should not be confined to a special indoor environment.

Most of the projects described in chapter 2 using inverse dynamics of a model are coupled to force or torque controllers, which take over a certain share of the torque required for a certain task. The question arises, what performance such systems can achieve. Unfortunately, this is not easy to answer, and depends on the model complexity and reliability. But depending on the accuracy of the system, the contribution of the actuation has to be rather small especially for control systems which rely on adding a fixed torque share in relation to the statically stable pose. Otherwise if the support is large, and the computed support torque is larger than the torque required for the task, for example, when the operator wants to sit down while the system tries to maintain a statically stable pose, the operator would have to actively work against the support to perform the desired movement. Furthermore, in those systems the resulting movement of the cooperation of the operator and the exoskeleton is also unknown, preventing the inclusion of additional stability and safety algorithms as described above.

9 Conclusion and Future Work

In this work an exoskeleton system for supporting the operator with extra force in the knee joint is presented. The interface between the operator and the exoskeleton is based on the evaluation of electric signals emitted by the muscles during their activation.

The main focus of this research was put on the interface between the human and the exoskeleton and the recognition of the intended action of the operator.

Two algorithms have been investigated for the purpose of controlling the support of the actuation: The first algorithm estimates the operator's own force production from the EMG signals and contributes a linear share by the actuation. The second algorithm takes the muscle forces estimated from the EMG signals, and simulates the dynamics of a rigid body model of the operator and the exoskeleton. The resulting motions of the rigid bodies is interpreted as the desired movement of the operator.

The evaluation of the EMG signals for the first algorithm have been performed with a body model which is based on complex models developed in the biomechanical and biomedical communities. The parameter calibration of this model uses a novel approach to select relevant reference values based on the muscle activations and distributes the measured torque among the active muscles with respect to their activation and physiological cross-sectional area.

Both control algorithms have conceptual advantages and disadvantages: The second system allows incorporation of a variety of algorithms to modify the movement because the trajectory of the exoskeleton is known in advance, but experiments have shown that the system is very sensible to inaccurate sensor readings, making a practical application very complex and difficult. This approach begins to make sense, if the exoskeleton construction is more complex, like in a full-body suit. The first system on the other hand is very robust and reliable, requiring only a minimum of sensors, because the complete kinematic state does not need to be known. This simplicity is traded for the possibility to include certain algorithms, for example, to enforce postural stability, because the resulting movement is not known in advance.

The mechanical construction of the exoskeleton and actuation that was developed to investigate the system behavior in real world experiments was not the main focus of this work, but performed very well and allowed evaluation of the human-machine interaction during the movements of interest. The architecture is designed in such a way that it can be easily extended with more joints.

In the introduction many different potential applications have been pointed out that can take advantage of exoskeletons like the one presented in this work. With the ex-

periments it was shown that for healthy operators the desired movements can be successfully performed in cooperation with the exoskeleton to receive support.

But with the end of this thesis, the research is far from finished. It rather opens a door for further interesting research: Details of the body model can be further optimized, for example, inclusion of activation dynamics, and the torque distribution during calibration can be further investigated. A small redesign of the exoskeleton can allow faster movements with lower support to investigate the human-machine interaction for more dynamic movements. For this, the model can be easily extended to incorporate the force-velocity relationship of muscle. It can also be analyzed if the support ratio can be adapted on-the-fly to avoid oscillations in the human-machine interaction, and the controller can be modified to simulate joint stiffness and friction depending on the degree of muscle cocontraction to smoothen the resulting joint trajectories.

Looking at disabled people and patients opens a different challenging field of research: Since no two patients are equal, the quality of EMG signals and the contained information have to be investigated with respect to the presented algorithms. More signal processing stages may be introduced, and additional safety measures have to be incorporated to react on unskillful behavior and spasticities of patients.

This is all interesting and challenging work for the future. The motivation for this research is further increased by the positive feedback on the publications of the research results from industrial companies, rehabilitation institutes, and patients, all showing great interest in the development of the device.

List of Main Symbols

α_i	angle of the i-th joint
$\bar{e}(t)$	moving average of the raw EMG signal
$\hat{l}_s^t$	tendon slack length from literature
$\hat{P}_i$	i-th waypoint of a musculotendinous pathway in the local coordinate system it is linked to
$\mathbf{f}$	vector function that models inertial forces and gravity
$\mathbf{g}(\mathbf{q})$	nonlinear function representing the current system configuration and geometry
$\mathbf{M}(\mathbf{q})$	matrix function that specifies mass distribution of the rigid bodies
$\mathbf{q}$	vector of generalized coordinates
$\mathbf{T}$	vector of joint torques and external forces
$\mathbf{u}$	vector of generalized velocities
ϕ	pennation angle
ϕ_o	pennation angle at optimal muscle fiber length
$\tilde{l}^m$	normalized muscle fiber length
A	shape parameter of the exponential activation function, and of the logarithmic portion of the piecewise activation function
$a(u)$	general neural activation function
a_0	activation at point of transition between the two portions of the piecewise activation function
$a_{exp}(u)$	exponential neural activation function
$a_{pw}(u)$	piecewise neural activation function
$e(t)$	raw EMG signal
E_{emg}	error of the EMG-parameter optimization

E_{geom} error of the geometry parameter optimization

F^m force produced by a muscle

F_A^m active muscle force

F_o^m maximum force of a muscle at optimal muscle fiber length

F_P^m passive muscle force

$F_{k,h}^m$ force share of a muscle in entry h of calibration table k

F^{mt} force of the musculotendinous unit

F_A force measured at the tip of the actuator

$f_A(\tilde{l}^m)$ active force-length curve

$f_P(\tilde{l}^m)$ passive force-length curve

$L(e(t))$ Lowpass filtering function applied to signal $e(t)$

l^m length of the muscle fibers

l_o^m optimal muscle fiber length

l^t length of the tendon

l_s^t tendon slack length

l^{mt} length of the musculotendinous unit

L_s, W_s length and width of the shank rectangle

L_t, W_t length and width of the thigh rectangle

L_u, W_u length and width of the trunk rectangle

$M_i(\alpha_0, \ldots, \alpha_{J-1})$ transformation function for the i-th waypoint from the local coordinate system in the pelvis coordinate system

m_s mass of both shanks of the operator

m_t mass of both thighs of the operator

m_u mass of the trunk of the operator

m_{total} total body mass of the operator

$P_i(x_i, y_i, z_i)^T$ i-th waypoint of a musculotendinous pathway in the pelvis coordinate system

R	range of the postprocessed EMG signal
s^t	scale of the tendon slack applied to value from literature
T_A	joint torque derived from F_A and the knee angle
T_g	joint torque as a result of gravitation
$u(t)$	postprocessed EMG signal
u_0	postprocessed EMG signal at point of transition between the two portions of the piecewise activation function
u_o	postprocessed activation offset
$u_{k,h}$	postprocessed EMG signal of a muscle in entry h of calibration table k

A Biomechanical Model

This section gives a quick overview of the necessary equations for the biomechanical model used in chapter 4. The complete description is given in section 4.3. The estimated knee torque is calculated by:

$$T = \sum_{i=0}^{N-1} r_i F_i^{mt}$$

with

$$F_i^{mt} = (F_{A,i}^m + F_{P,i}^m)\cos\phi_i, \qquad \text{(force of the musculotendinous complex)}$$

$$F_{A,i}^m = f_A(\tilde{l}_i^m) F_{o,i}^m a_i(u_i), \qquad \text{(active muscle force)}$$

$$F_{P,i}^m = f_P(\tilde{l}_i^m) F_{o,i}^m, \qquad \text{(passive muscle force)}$$

$$a_i(u_i) = \frac{e^{A_i u_i R_i^{-1}} - 1}{e^{A_i} - 1}, \qquad \text{(muscle activation)}$$

$$\phi_i = \arcsin\left(\frac{l_{o,i}^m \sin\phi_{o,i}}{l_i^m}\right), \qquad \text{(pennation angle)}$$

$$\tilde{l}_i^m = \frac{l_i^m}{l_{o,i}^m}, \qquad \text{(normalized muscle fiber length)}$$

$$l_i^m = \sqrt{(l_{o,i}^m \sin\phi_{o,i})^2 + (l_i^{mt} - s_i^t \hat{l}_{s,i}^t)^2}, \qquad \text{(muscle fiber length)}$$

$$l_i^{mt} = \sum_{j=0}^{n-2} \|P_{j+1,i} - P_{j,i}\|, \qquad \text{(length of musculotendinous complex)}$$

$$P_i = \mathbf{M_i}(\alpha_\mathbf{0}, \ldots, \alpha_{\mathbf{J-1}})\hat{P}_i \qquad \text{(muscle waypoints)}$$

The order of computation is from the bottom to the top. Input of the system are the values of the joint angles, α_j, with $0 \leq j < J$, and J being the number of joints in the model, and the postprocessed EMG signal, u_i, from every muscle. Required constants are presented in the following sections.

A.1 Muscle Parameters

The parameters which have to be determined by a calibration routine for every muscle i are: s_i^t (tendon slack length scale), A_i (shape of the EMG-to-force function), R_i (maximum EMG signal), and $F_{o,i}^m$ (maximum muscle force at optimal fiber length).

The remaining parameters are given in table A.1.

Muscle	i	$r_i[m]$	$l_{s,i}^t[m]$	$l_{o,i}^m[m]$	$\phi_{o,i}[deg]$
Rectus Femoris	0	-0.039	0.346	0.084	5
Vastus Medialis	1	-0.037	0.126	0.089	5
Vastus Lateralis	2	-0.037	0.157	0.084	5
Semimembranosus	3	0.038	0.359	0.080	15
Semitendinosus	4	0.042	0.262	0.201	5
Biceps Femoris (long)	5	0.042	0.341	0.109	0

Table A.1: Muscle index, moment arms, r_i, tendon slacklengths, $l_{s,i}^t$, optimal muscle fiber lengths, $l_{o,i}^m$, and pennation angles at optimal muscle fiber length, $\phi_{o,i}$, of the three extensor and three flexor muscles used for the biomechanical model. Data taken from [DLH$^+$90], except the moment arms, which have been derived from own computations.

A.2 Limb Segment Transformation

To compute the waypoints of the muscle-tendon units in a reference frame, the individual limb segments have to be transformed into the same reference frame according to the hip and knee joint angles. The segments considered here are the pelvis, femur, tibia, and patella.

The model relating the joint angles to the segment transformation matrices is published in [DLH$^+$90], and summarized here for convenience. Some simplifications have been applied.

The transformation matrices needed here are homogenous 4×4-matrices. The translation of frame B in frame A is defined by:

$$ {}^{\mathbf{A}}\mathbf{T}_{\mathbf{B}}(x,y,z) = \begin{pmatrix} 1 & 0 & 0 & x \\ 0 & 1 & 0 & y \\ 0 & 0 & 1 & z \\ 0 & 0 & 0 & 1 \end{pmatrix} \tag{A.1} $$

The rotation of frame B in frame A around the z-axis with angle θ is defined as:

$$ {}^{\mathbf{A}}\mathbf{R}_{\mathbf{B}}(\theta) = \begin{pmatrix} \cos(\theta) & -\sin(\theta) & 0 & 0 \\ \sin(\theta) & \cos(\theta) & 0 & 0 \\ 0 & 0 & 1 & 0 \\ 0 & 0 & 0 & 1 \end{pmatrix} \tag{A.2} $$

The transformation from the pelvis segment to the femur segment is defined by the concatenation of a translation and a rotation, which takes into account the hip joint angle, α_1,

$$ {}^{\mathbf{pelvis}}\mathbf{M}_{\mathbf{femur}}(\alpha_1) = {}^{\mathbf{pelvis}}\mathbf{T}_{\mathbf{H0}}(-0.0707, -0.0661, 0.0835) \cdot {}^{\mathbf{H0}}\mathbf{R}_{\mathbf{femur}}(\alpha_1) \tag{A.3} $$

where H0 is an intermediate frame. Hip adduction and rotation is neglected here.

The transformation from femur to tibia is defined by a translation and a rotation, which takes into account the knee joint angle, α_0,

$$ {}^{\mathbf{femur}}\mathbf{M}_{\mathbf{tibia}}(\alpha_0) = {}^{\mathbf{femur}}\mathbf{T}_{\mathbf{H1}}(f_x^t(\alpha_0), f_y^t(\alpha_0), 0.0) \cdot {}^{\mathbf{H1}}\mathbf{R}_{\mathbf{tibia}}(\alpha_0) \tag{A.4} $$

where H1 is an intermediate frame. $f_x^t(\alpha_0)$ and $f_y^t(\alpha_0)$ are functions of the knee angle and take into account the small displacement in *x*- and *y*-directions, which occurs during knee flexion, because the knee joint is not an ideal swivel joint. The functions are defined through a series of interpolation points, given as pairs of the knee angle and the corresponding displacement.

For $f_x^t(\alpha_0)$ these are:

$$ \begin{aligned} P_{f_x^t} = \{ \quad & (-2.09, -0.0032), (-1.74, 0.00179), (-1.39, 0.00411), \\ & (-1.04, 0.00410), (-0.69, 0.00212), (-0.35, -0.0010), \\ & (-0.17, -0.0031), (0.000, -0.00525) \quad \} \end{aligned} $$

And for $f_y^t(\alpha_0)$:

$$ \begin{aligned} P_{f_y^t} = \{ \quad & (-2.09, -0.4226), (-1.22, -0.4082), (-0.52, -0.3990), \\ & (-0.35, -0.3976), (-0.17, -0.3966), (0.000, -0.3960) \quad \} \end{aligned} $$

The transformation from tibia to patella is defined by a translation and a rotation, which takes into account the knee joint angle, α_0,

$$ {}^{\mathbf{tibia}}\mathbf{M}_{\mathbf{patella}}(\alpha_0) = {}^{\mathbf{tibia}}\mathbf{T}_{\mathbf{H2}}(f_x^p(\alpha_0), f_y^p(\alpha_0), 0.0024) \cdot {}^{\mathbf{H2}}\mathbf{R}_{\mathbf{patella}}(f_r^p(\alpha_0)) \tag{A.5} $$

$f_x^p(\alpha_0)$ and $f_y^p(\alpha_0)$ are functions that describe the translation of the patella as it slides around the knee joint. $f_r^p(\alpha_0)$ defines the rotation of the patella in relation to the knee

joint angle. All three functions are defined through interpolation points, given as pairs of the knee angle and the corresponding displacement and rotation, respectively.

For $f_x^p(\alpha_0)$ these are:

$$\begin{aligned} P_{f_x^p} = \quad \{ \quad & (-2.09, 0.0173), (-1.39, 0.0324), (-1.04, 0.0381), \\ & (-0.69, 0.0430), (-0.35, 0.0469), (-0.17, 0.0484), \\ & (0.000, 0.0496) \quad \} \end{aligned}$$

And for $f_y^p(\alpha_0)$:

$$\begin{aligned} P_{f_y^p} = \quad \{ \quad & (-2.09, -0.0219), (-1.57, -0.0202), (-1.39, -0.0200), \\ & (-1.04, -0.0204), (-0.69, -0.0211), (-0.35, -0.0219), \\ & (-0.17, -0.0223), (0.005, -0.0227) \quad \} \end{aligned}$$

And finally for $f_r^p(\alpha_0)$:

$$\begin{aligned} P_{f_r^p} = \quad \{ \quad & (-2.09, 0.308), (-2.00, 0.308), (-1.45, 0.306), \\ & (-0.52, 0.270), (0.027, -0.036), (0.170, -0.280) \quad \} \end{aligned}$$

The computation of the actual values of the functions is performed by linear interpolation between the given points.

The transformation from the pelvis to the tibia can be achieved by concatenation of the individual transformation matrices

$$^{\mathbf{pelvis}}\mathbf{M}_{\mathbf{tibia}}(\alpha_0, \alpha_1) = {}^{\mathbf{pelvis}}\mathbf{M}_{\mathbf{femur}}(\alpha_1) \cdot {}^{\mathbf{femur}}\mathbf{M}_{\mathbf{tibia}}(\alpha_0) \tag{A.6}$$

and to the patella with

$$^{\mathbf{pelvis}}\mathbf{M}_{\mathbf{patella}}(\alpha_0, \alpha_1) = {}^{\mathbf{pelvis}}\mathbf{M}_{\mathbf{tibia}}(\alpha_0, \alpha_1) \cdot {}^{\mathbf{tibia}}\mathbf{M}_{\mathbf{patella}}(\alpha_0). \tag{A.7}$$

The transformation matrix that has to be applied to a specific muscle waypoint depends on the segment the waypoint is located in. The waypoints and their segment location are presented in section A.3.

To compute the length of the musculotendinous path, all waypoints have to be transformed into the pelvis frame with the current knee and hip angles as stated in equation 4.10.

A.3 Waypoints of the Musculotendinous Units

The muscle waypoints are computed with a subset of the data published in [DLH+90], which is summarized here for convenience. In tables A.2 to A.7 each musculotendinous unit is defined through three-dimensional waypoints $\hat{P}_i(x,y,z)$ in the individual body segments (pelvis, femur, tibia, patella). The waypoint in the reference frame, $P_i(x,y,z)$, can be obtained by transforming the waypoints with matrices as described in section A.2. The optional range specifies an interval for the knee joint angle. Only if the current joint angle falls within the boundaries of the interval, the waypoint is inserted into the musculotendinous path. Those optional waypoints are wrapping points, which indicate that the tendon wraps around the joint under certain angles. If this field is left blank, the waypoint is always part of the musculotendinous path.

A.4 Force-Length Curves

The interpolation points P_A of the active force-length curve $f_A(\tilde{l}_i^m)$ [DLH+90] are given as pairs of normalized length and normalized force:

$$\begin{aligned} P_A = \quad \{ \quad & (-5.00, 0.000), (0.000, 0.000), (0.401, 0.000), (0.402, 0.000), \\ & (0.404, 0.000), (0.527, 0.227), (0.629, 0.637), (0.719, 0.857), \\ & (0.861, 0.950), (1.045, 0.993), (1.218, 0.770), (1.439, 0.247), \\ & (1.619, 0.000), (1.620, 0.000), (1.621, 0.000), (2.200, 0.000), \\ & (5.000, 0.000) \quad \} \end{aligned}$$

The interpolation points P_P of the passive force-length curve $f_P(\tilde{l}_i^m)$ [DLH+90] are given as pairs of normalized length and normalized force:

$$\begin{aligned} P_P = \quad \{ \quad & (-5.00, 0.000), (0.998, 0.000), (0.999, 0.000), (1.000, 0.000), \\ & (1.100, 0.035), (1.200, 0.120), (1.300, 0.260), (1.400, 0.550), \\ & (1.500, 1.170), (1.600, 2.000), (1.601, 2.000), (1.602, 2.000), \\ & (5.000, 2.000) \quad \} \end{aligned}$$

The computation of the actual values of the function is performed by linear interpolation between the given points.

$\hat{P}_i(x,y,z)$	Segment	Range $[rad]$
(-0.0295,-0.0311,0.0968)	Pelvis	
(0.0334,-0.4030,0.0019)	Femur	$-3.0 \leq \alpha_0 \leq -1.46$
(0.0121,0.0437,-0.0010)	Patella	

Table A.2: Rectus femoris waypoint definition.

$\hat{P}_i(x,y,z)$	Segment	Range $[rad]$
(0.0140,-0.2099,0.0188)	Femur	
(0.0356,-0.2769,0.0009)	Femur	
(0.0370,-0.4048,-0.0125)	Femur	$-3.0 \leq \alpha_0 \leq -1.21$
(0.0274,-0.4255,-0.0131)	Femur	$-3.0 \leq \alpha_0 \leq -1.78$
(0.0063,0.0445,-0.0170)	Patella	

Table A.3: Vastus medialis waypoint definition.

$\hat{P}_i(x,y,z)$	Segment	Range $[rad]$
(0.0048,-0.1854,0.0349)	Femur	
(0.0269,-0.2591,0.0409)	Femur	
(0.0361,-0.4030,0.0205)	Femur	$-3.0 \leq \alpha_0 \leq -1.21$
(0.0253,-0.4243,0.0184)	Femur	$-3.0 \leq \alpha_0 \leq -1.92$
(0.0103,0.0423,0.0141)	Patella	

Table A.4: Vastus lateralis waypoint definition.

$\hat{P}_i(x,y,z)$	Segment	Range $[rad]$
(-0.1192,-0.1015,0.0695)	Pelvis	
(-0.0243,-0.0536,-0.0194)	Tibia	

Table A.5: Semimembranosus waypoint definition.

$\hat{P}_i(x,y,z)$	Segment	Range $[rad]$
(-0.1237,-0.1043,0.0603)	Pelvis	
(-0.0314,-0.0545,-0.0146)	Tibia	
(-0.0113,-0.0746,-0.0245)	Tibia	
(0.0027,-0.0956,-0.0193)	Tibia	

Table A.6: Semitendinosus waypoint definition.

$\hat{P}_i(x,y,z)$	Segment	Range $[rad]$
(-0.1244,-0.1001,0.0666)	Pelvis	
(-0.0081,-0.0729,0.0423)	Tibia	

Table A.7: Biceps femoris (long head) waypoint definition.

B Exoskeleton Geometry

The actuator torque, T_A, the actuator is producing is computed from the force sensor measurement, F_A, with the joint angle, α_0, through

$$T_A = -F_A \frac{P_x^s P_y^s - P_y^s (P_x^s + d_2)}{\sqrt{(P_x^s + d_2)^2 + P_y^{s2}}} \tag{B.1}$$

$$\begin{aligned} \text{with} \quad P_x^s &= d_1 \cos(\alpha_{ts} - \alpha_0) \\ P_y^s &= -d_1 \sin(\alpha_{ts} - \alpha_0) \\ \alpha_{ts} &= \alpha_t + \alpha_s \end{aligned} \tag{B.2}$$

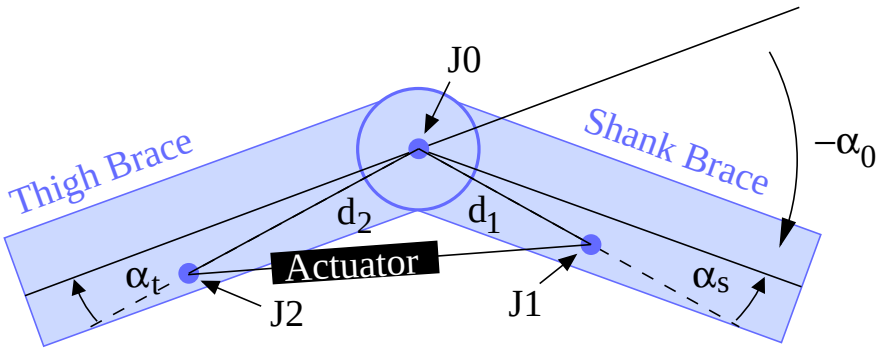

Figure B.1: Geometry of the actuator attachment: J0 is the supported joint, J1 and J2 the joints with which the actuator is attached to the braces covering the limbs. α_0 is the joint angle, and α_s and α_t are displacement angles.

where d_1 is the distance from the supported joint (J0) to the first point where the actuator is attached to the exoskeleton (joint J1), d_2 is the distance from J0 to the second point where the actuator is attached to the exoskeleton (joint J2), and α_s and α_t are displacement angles to avoid singularities when the joint angles is 0, as shown in figure B.1. The required parameters are: $\alpha_{ts} = 0.579$rad, $d_1 = 0.061$m, and $d_2 = 0.362$m.

C Parameters of the Rigid Body Models

Table C.1 describes all parameters that are used in the dynamic model in section 8.1. The location of the center of mass has been moved towards the pelvis to suppress the strong influence of bad trunk angle measurements on the system behavior.

Segment	m_{seg}[kg]	L[m]	W[m]	r
Upper body	60.00	0.60	0.60	0.200
Thigh	8.73	0.50	0.25	0.433
Shank	5.05	0.48	0.20	0.433
Foot	1.26	0.30	0.06	0.429

Table C.1: Data of the body segments: relative segment mass m_{seg}, segment length L, segment width W, and the location of the center of mass in relation to the segment length, r. Figures, except r_u for the upper body, can be found in [Win90a].

Table C.2 shows the points of origin and insertion used for the body models. The points have been chosen by hand. The given relative coordinates have to be multiplied by the length and width of the body segments to obtain the actual coordinates.

Muscle	Origin	Insertion
Hip flexor	$(0.10, -0.10)$	$(0.20, 0.10)$
Hip extensor	$(0.00, 0.05)$	$(0.05, -0.05)$
Knee flexor	$(0.10, -0.05)$	$(0.10, -0.04)$
Knee extensor	$(0.09, 0.05)$	$(-0.03, 0.04)$

Table C.2: Points of origin and insertion of the muscles included in the body model for the knee.

Table C.3 describes all parameters that are used in the model presented in section 8.2. The total body mass is $m_{total} = 83$kg.

Segment	m_{rel}	L[m]	W[m]	r
Upper body	0.6280	0.60	0.60	1.200
Thigh	0.1000	0.50	0.25	0.433
Shank	0.0465	0.48	0.20	0.433

Table C.3: Data of the body segments: relative segment mass m_{rel}, segment length L, segment width W, and the location of the center of mass in relation to the segment length, r. Figures, except r_u for the upper body, can be found in [Win90a].

D Subspace Search Algorithm

This algorithm is used to determine the EMG-related parameters during calibration described in section 5.6.

In every iteration, this algorithm calculates the error function $E(A,S,m)$ at $n_A \times n_S$ points in the 2-dimensional space. It selects the minimum in the subspace and reduces the search interval to the dimensions of the step size around the minimum. The algorithm stops, when the size of the search space is smaller than ε_A and ε_S in the dimensions of A and S respectively.

A_s, A_e: boundaries for the shape interval: $A \in [A_s, A_e]$
S_s, S_e: boundaries for the scale interval: $S \in [S_s, S_e]$
n_A : number of search points in shape interval
n_S : number of search points in scale interval
repeat
  $A_\Delta = (A_e - A_s)/n_A$
  $S_\Delta = (S_e - S_s)/n_S$
  $E_{opt} = \infty$
  for $A = A_s$ to A_e **do**
    for $S = S_s$ to S_e **do**
      Error $= E(A,S,m)$
      if Error $< E_{opt}$ **then**
        $A_{opt} = A$
        $S_{opt} = S$
        $E_{opt} =$ Error
      end if
      $S = S + S_\Delta$
    end for
    $A = A + A_\Delta$
  end for
  $A_s = \max(A_{opt} - A_\Delta, A_s)$
  $A_e = \max(A_{opt} + A_\Delta, A_e)$
  $S_s = \max(S_{opt} - S_\Delta, S_s)$
  $S_e = \max(S_{opt} + S_\Delta, S_e)$
until $A_e - A_s < \varepsilon_A$ and $S_e - S_s < \varepsilon_S$

While not being very optimal in terms of computational cost, the algorithm is quite

robust against running into local minima. As long as the global minimum is not located in valleys more narrow than the interval width divided by the number of search points for every dimension, it will be found.

Bibliography

[AAB05] D.S. Andreasen, S.K. Allen, and D.A. Backus. Exoskeleton with EMG Based Active Assistance for Rehabilitation. *Rehabilitation Robotics, 2005 (ICORR). 9th International Conference on*, pages 333–336, 2005.

[ABH05] S.K. Au, P. Bonato, and H. Herr. An EMG-Position Controlled System for an Active Ankle-Foot Prosthesis: An Initial Experimental Study. *Rehabilitation Robotics, 2005 (ICORR). 9th International Conference on*, pages 375–379, 2005.

[AJL+06] O. Amft, H. Junker, P. Lukowicz, G. Troster, and C. Schuster. Sensing Muscle Activities with Body-Worn Sensors. In *International Workshop on Wearable and Implantable Body Sensor Networks (BSN)*, 2006.

[AK00] A.T.C. Au and R.F. Kirsch. EMG-based prediction of shoulder and elbow kinematics inable-bodied and spinal cord injured individuals. *Rehabilitation Engineering, IEEE Transactions on [see also IEEE Trans. on Neural Systems and Rehabilitation]*, 8(4):471–480, 2000.

[AK05] P.K. Artemiadis and K.J. Kyriakopoulos. Teleoperation of a robot manipulator using EMG signals and a position tracker. *Intelligent Robots and Systems, 2005 (IROS). Proceedings of the 2005 IEEE/RSJ International Conference on*, pages 1003–1008, 2005.

[AK06] P.K. Artemiadis and K.J. Kyriakopoulos. Teleoperation of a Robot Arm in 2D Catching Movements using EMG Signals and a Bio-inspired Motion Law. *Biomedical Robotics and Biomechatronics 2006 (BioRob). The First IEEE/RAS-EMBS International Conference on (about to appear)*, 2006.

[ATHC84] K.N. An, K. Takahashi, T.P. Harrigan, and E.Y. Chao. Determination of muscle orientations and moment arms. *J Biomech Eng*, 106(3):280–2, 1984.

[AW05] A.B. Ajiboye and R.F. Weir. A heuristic fuzzy logic approach to EMG pattern recognition for multifunctional prosthesis control. *Neural Systems and Rehabilitation Engineering, IEEE Transactions on [see also IEEE Trans. on Rehabilitation Engineering]*, 13(3):280–291, 2005.

[BCL+00] I.E. Brown, E. Cheng, N. Lan, R. Davoodi, and G.E. Loeb. A comprehensive model of muscle force generation under dynamic physiological conditions. *Proceedings of the 5th Annual Conference of the International Functional Electrical Stimulation Society*, 2000.

[BD85] J.V. Basmajian and C.J. De Luca. *Muscles Alive: Their Functions Revealed by Electromyography*. Williams & Wilkins, 1985.

[BDK+06] B. Blankertz, G. Dornhege, M. Krauledat, K.R. Müller, V. Kunzmann, F. Losch, and G. Curio. The Berlin Brain-Computer Interface: EEG-based communication without subject training. *IEEE Trans Neural Syst Rehabil Eng*, 14(2):147–52, 2006.

[BLMB04] T.S. Buchanan, D.G. Lloyd, K. Manal, and T.F. Besier. Neuromusculoskeletal Modeling: Estimation of Muscle Forces and Joint Moments and Movements From Measurements of Neural Command. *J. Appl. Biomech*, 20:367–395, 2004.

[BS00] M. Buss and T. Schlegl. A discrete-continuous control approach to dextrous manipulation. *Robotics and Automation, 2000 (ICRA). Proceedings of the IEEE International Conference on*, 1:276–281, 2000.

[CK79] P.R. Cavanagh and P.V. Komi. Electromechanical delay in human skeletal muscle under concentric and eccentric contractions. *European Journal of Applied Physiology*, 42(3):159–163, 1979.

[CMM05] J.U. Chu, I. Moon, and M.S. Mun. A Real-Time EMG Pattern Recognition Based on Linear-Nonlinear Feature Projection for Multifunction Myoelectric Hand. *Rehabilitation Robotics, 2005 (ICORR). 9th International Conference on*, pages 295–298, 2005.

[CRP+05] E. Cavallaro, J. Rosen, J.C. Perry, S. Burns, and B. Hannaford. Hill-Based Model as a Myoprocessor for a Neural Controlled Powered Exoskeleton Arm-Parameters Optimization. *Robotics and Automation, 2005. Proceedings of the 2005 IEEE International Conference on*, pages 4514–4519, 2005.

[CYL+00] F.H.Y. Chan, Y.S. Yang, F.K. Lam, Y.T. Zhang, and P.A. Parker. Fuzzy EMG classification for prosthesis control. *Rehabilitation Engineering, IEEE Transactions on [see also IEEE Trans. on Neural Systems and Rehabilitation]*, 8(3):305–311, 2000.

[DLH+90] S.L. Delp, J.P. Loan, M.G. Hoy, F.E. Zajac, E.L. Topp, and J.M. Rosen. An interactive graphics-based model of the lower extremity to study orthopaedic surgical procedures. *Biomedical Engineering, IEEE Transactions on*, 37(8):757–767, 1990.

[DLM04] M. DiCicco, L. Lucas, and Y. Matsuoka. Comparison of control strategies for an EMG controlled orthotic exoskeleton for the hand. *Robotics and Automation, 2004 (ICRA). Proceedings of the 2004 IEEE International Conference on*, 2:1622–1627, 2004.

[DW00] K. Dietmayer and M. Weser. *Contactless Angle Measurement using KMZ41 and UZZ9001*. Philips Semiconductors, 2000.

[FCH05] D.P. Ferris, J.M. Czerniecki, and B. Hannaford. An Ankle-Foot Orthosis Powered by Artificial Pneumatic Muscles. *J Appl Biomech*, 21(2):189–197, 2005.

[Fer05] D.P. Ferris. Powered Lower Limb Orthoses for Gait Rehabilitation. *Topics in Spinal Cord Injury Rehabilitation*, 11(2):34–49, 2005.

[FH00] B. Freriks and H. Hermens. European Recommendations for Surface ElectroMyoGraphy, Results of the SENIAM Project. *Roessingh Research and Development, The Netherlands*, 2000.

[FH05] C. Fleischer and G. Hommel. Predicting the intended motion with EMG signals for an exoskeleton orthosis controller. In *Proceedings of the IEEE/RSJ Int. Conf. on Intelligent Robots and Systems*, 2005.

[FH06] C. Fleischer and G. Hommel. Torque control of an exoskeletal knee with emg signals. In *Proceedings of the Joint Conf. on Robotics: ISR 2006 and Robotik 2006*, 2006.

[FH07] C. Fleischer and G. Hommel. Calibration of an EMG-based Body Model with six Muscles to control a Leg Exoskeleton. *Proceedings of the IEEE International Conference on Robotics and Automation, 2007, about to appear*, 2007.

[FKRH04a] C. Fleischer, K. Kondak, C. Reinicke, and G. Hommel. Motion calculation based on emg-signal-processing. In *Proceedings of the 7th Int. Conf. on Climbing and Walking Robots (CLAWAR)*, pages 153–161, 2004.

[FKRH04b] C. Fleischer, K. Kondak, C. Reinicke, and G. Hommel. Online calibration of the emg-to-force relationship. In *Proceedings of the IEEE/RSJ Int. Conf. on Intelligent Robots and Systems*, 2004.

[FTKO03] O. Fukuda, T. Tsuji, M. Kaneko, and A. Otsuka. A human-assisting manipulator teleoperated by EMG signals and arm motions. *Robotics and Automation, IEEE Transactions on*, 19(2):210–222, 2003.

[FWB+96] K.A. Farry, I.D. Walker, R.G. Baraniuk, N.J.S. Center, and T.X. Houston. Myoelectric teleoperation of a complex robotic hand. *Robotics and Automation, IEEE Transactions on*, 12(5):775–788, 1996.

[GHJ66] A.M. Gordon, A.F. Huxley, and F.J. Julian. The variation in isometric tension with sarcomere length in vertebrate muscle fibres. *J Physiol*, 184(1):170–92, 1966.

[Hat81] H. Hatze. *Myocybernetic control models of skeletal muscle: Characteristics and applications*. Pretoria: University of South Africa, 1981.

[HC99] H.P. Huang and C.Y. Chen. Development of a myoelectric discrimination system for amulti-degree prosthetic hand. *Robotics and Automation, 1999. Proceedings of the 1999 IEEE International Conference on*, 3, 1999.

[HFM+99] H.J. Hermens, B. Freriks, R. Merletti, D. Stegeman, J. Blok, G. Rau, C. Disselhorst-Klug, and G.M. Hägg. *European recommendations for surface electromyography: results of the SENIAM project*. Roessingh Research and Development, 1999.

[HG02] S.E. Hussein and M.H. Granat. Intention detection using a neuro-fuzzy EMG classifier. *Engineering in Medicine and Biology Magazine, IEEE*, 21(6):123–129, 2002.

[Hil38] A.V. Hill. The Heat of Shortening and the Dynamic Constants of Muscle. *Proceedings of the Royal Society of London. Series B, Biological Sciences*, 126(843):136–195, 1938.

[HKS05] T. Hayashi, H. Kawamoto, and Y. Sankai. Control method of robot suit HAL working as operator's muscle using biological and dynamical information. *Intelligent Robots and Systems, 2005 (IROS). Proceedings of the 2005 IEEE/RSJ International Conference on*, pages 3063–3068, 2005.

[ITKI92] K. Ito, T. Tsuji, A. Kato, and M. Ito. EMG Pattern Classification for a Prosthetic Forearm with Three Degrees of Freedom. *Proc. of IEEE International Workshop on Robot and Human Communication 92 (Tokyo)*, pages 69–74, 1992.

[Jea90] M. Jeannerod. *The Neural and Behavioural Organization of Goal-directed Movements*. Oxford University Press, 1990.

[Kaz05] H. Kazerooni. Exoskeletons for human power augmentation. *Intelligent Robots and Systems, 2005 (IROS). Proceedings of the 2005 IEEE/RSJ International Conference on*, pages 3459–3464, 2005.

[KET+03] K. Kiguchi, R. Esaki, T. Tsuruta, K. Watanabe, and T. Fukuda. An exoskeleton for human elbow and forearm motion assist. *Proc. of IEEE/RSJ Int. Conference on. Intelligent Robots and Systems, 2003*, pages 3600–3605, 2003.

[KH03a] K. Kondak and G. Hommel. Control algorithm for stable walking of biped robots. *Proceedings of the International Conference on Climbing and Walking Robots, Catania, Italy*, 2003.

[KH03b] K. Kondak and G. Hommel. Control and online computation of stable movement for biped robots. *Intelligent Robots and Systems, 2003 (IROS). Proceedings of the 2003 IEEE/RSJ International Conference on*, 1, 2003.

[KHS05] H. Kazerooni, L. Huang, and R. Steger. On the Control of the Berkeley Lower Extremity Exoskeleton (BLEEX). *IEEE International Conference on Robotics and Automation*, pages 4364–4371, 2005.

[KIY+03] K. Kiguchi, K. Iwami, M. Yasuda, K. Watanabe, and T. Fukuda. An exoskeletal robot for human shoulder joint motion assist. *Mechatronics, IEEE/ASME Transactions on*, 8(1):125–135, 2003.

[KKS03] H. Kawamoto, S. Kanbe, and Y. Sankai. Power Assist Method for HAL3 Estimating Operator's Intention Based on Motion Information. *Proceedings of the 2003 IEEE International Workshop on Robot and Human Interactive Communication*, pages 67–72, 2003.

[KL97] T.R. Kane and D.A. Levinson. *Engineering Mechanics OnLine Part 1–Statics*. OnLine Dynamics, Sunnyvale, CA (available from www.autolev.com), 1997.

[KL00] T.R. Kane and D. Levinson. *Dynamics OnLine: Theory and Implementation with Autolev*. Kane Dynamics, Inc., 2000.

[KLLK05] Y.S. Kim, J. Lee, S. Lee, and M. Kim. A force reflected exoskeleton-type masterarm for human-robot interaction. *Systems, Man and Cybernetics, Part A, IEEE Transactions on*, 35(2):198–212, 2005.

[KOT92] K. Kuribayashi, K. Okimura, and T. Taniguchi. A discrimination system using neural network for EMG-controlled prostheses. *Robot and Human Communication, 1992. Proceedings of the IEEE International Workshop on*, 3:63–68, 1992.

[KS01] K. Kasaoka and Y. Sankai. Predictive control estimating operator's intention for stepping-upmotion by exo-skeleton type power assist system HAL. *Intelligent Robots and Systems, 2001 (IROS). Proceedings of the 2001 IEEE/RSJ International Conference on*, 3, 2001.

[KS02a] H. Kawamoto and A. Sankai. Comfortable power assist control method for walking aid by HAL-3. *Systems, Man and Cybernetics, 2002 IEEE International Conference on*, 4:6, 2002.

[KS02b] H. Kawamoto and Y. Sankai. Power Assist System HAL-3 for Gait Disorder Person. *ICCHP*, pages 196–203, 2002.

[KS04] H. Kawamoto and Y. Sankai. Power assist method based on phase sequence driven by interaction between human and robot suit. *13th IEEE International Workshop on Robot and Human Interactive Communication, 2004*, pages 491–496, 2004.

[KS05] H. Kobayashi and H. Suzuki. A muscle suit for the upper body-development of a new shoulder mechanism. *Advanced Robotics and its Social Impacts, 2005. IEEE Workshop on*, pages 149–154, 2005.

[KS06] H. Kazerooni and R. Steger. The Berkeley Lower Extremity Exoskeleton. *Journal of Dynamic Systems, Measurement, and Control*, 128:14–25, 2006.

[KSea95] E.R. Kandel, J.H. Schwartz, and T.M. Jessell et al. *Essentials of neural science and behavior*. Appleton & Lange, 1995.

[KSH06] H. Kazerooni, R. Steger, and L. Huang. Hybrid Control of the Berkeley Lower Extremity Exoskeleton (BLEEX). *International Journal of Robotics Research*, 25(5-6):561–573, 2006.

[KYNK04] S. Kawai, H. Yokoi, K. Naruse, and Y. Kakazu. Study for control of a power assist device. Development of an EMG based controller considering a human model. *Intelligent Robots and Systems, 2004 (IROS). Proceedings of the 2004 IEEE/RSJ International Conference on*, 3, 2004.

[LB96] D.G. Lloyd and T.S. Buchanan. A model of load sharing between muscles and soft tissues at the human knee during static tasks. *J Biomech Eng*, 118(3):367–76, 1996.

[LB03] D.G. Lloyd and T.F. Besier. An EMG-driven musculoskeletal model to estimate muscle forces and knee joint moments in vivo. *Journal of Biomechanics*, 36:765–776, 2003.

[LL04] X. Liu and K.H. Low. Development and preliminary study of the NTU lower extremity exoskeleton. *Cybernetics and Intelligent Systems, 2004 IEEE Conference on*, 2, 2004.

[LLY] X. Liu, K.H. Low, and H.Y. Yu. Development of a lower extremity exoskeleton for human performance enhancement. *Intelligent Robots and*

Systems, 2004 (IROS). Proceedings of the 2004 IEEE/RSJ International Conference on, 4:3889–3894.

[LS02a] S. Lee and Y. Sankai. Power assist control for leg with HAL-3 based on virtual torque and impedance adjustment. *Systems, Man and Cybernetics, 2002 IEEE International Conference on*, 4:6, 2002.

[LS02b] S. Lee and Y. Sankai. Power assist control for walking aid with HAL-3 based on EMG and impedance adjustment around knee joint. *Intelligent Robots and System, 2002. IEEE/RSJ International Conference on*, 2, 2002.

[LS03] S. Lee and Y. Sankai. The natural frequency-based power assist control for lower body with HAL-3. *Systems, Man and Cybernetics, 2003. IEEE International Conference on*, 2, 2003.

[LSW+04] E.C. Leuthardt, G. Schalk, J.R. Wolpaw, J.G. Ojemann, and D.W. Moran. A brain–computer interface using electrocorticographic signals in humans. *Journal of Neural Engineering*, 1(2):63–71, 2004.

[Luc07] C.J. De Luca. Surface Electromyography: Detection and Recording (http://www.delsys.com). 2007.

[MA04] Y. Matsuoka and P. Afshar. Neuromuscular Strategies for Dynamic Finger Movements: A Robotic Approach. *The 26th Annual International Conference of the IEEE Engineering in Medicine and Biology Society*, 2:4649–4652, 2004.

[Mar98] F. Martini. *Fundamentals of Anatomy and Physiology*. Prentice Hall Englewood Cliffs, NJ, 1998.

[MB03] K. Manal and T.S. Buchanan. A one-parameter neural activation to muscle activation model: estimating isometric joint moments from electromyograms. *Journal of Biomechanics*, 36(8):1197–1202, 2003.

[MFG05] M. Mulas, M. Folgheraiter, and G. Gini. An EMG-Controlled Exoskeleton for Hand Rehabilitation. *Rehabilitation Robotics, 2005 (ICORR). 9th International Conference on*, pages 371–374, 2005.

[MGLB02] K. Manal, R.V. Gonzalez, D.G. Lloyd, and T.S. Buchanan. A real-time EMG-driven virtual arm. *Computers in Biology and Medicine*, 32:25–36, 2002.

[Moo03] M.M. Moore. Real-World Applications for Brain–Computer Interface Technology. *IEEE Transactions on Neural Systems and Rehabilitation Engineering*, 11(2):163, 2003.

[MWW83] R.J. Maughan, J.S. Watson, and J. Weir. Strength and cross-sectional area of human skeletal muscle. *The Journal of Physiology*, 338(1):37–49, 1983.

[Nie03] J.B. Nielsen. How we Walk: Central Control of Muscle Activity during Human Walking. *The Neuroscientist*, 9(3):195–204, 2003.

[NKYK03] K. Naruse, S. Kawai, H. Yokoi, and Y. Kakazu. Development of wearable exoskeleton power assist system for lower back support. *Intelligent Robots and Systems, 2003 (IROS). Proceedings of the 2003 IEEE/RSJ International Conference on*, 4, 2003.

[NM65] J.A. Nelder and R. Mead. A simplex method for function minimization. *Computer Journal*, (7):308–313, 1965.

[NNH+98] K. Nagai, I. Nakanishi, H. Hanafusa, S. Kawamura, M. Makikawa, and N. Tejima. Development of an 8 DOF robotic orthosis for assisting human upperlimb motion. *Robotics and Automation, 1998. Proceedings of the 1998 IEEE International Conference on*, 4, 1998.

[NSK05] T. Nakamura, K. Saito, and K. Kosuge. Control of Wearable Walking Support System Based on Human-Model and GRF. *Robotics and Automation, 2005. Proceedings of the 2005 IEEE International Conference on*, pages 4394–4399, 2005.

[NSWK05a] T. Nakamura, K. Saito, Z.D. Wang, and K. Kosuge. Realizing a Posture-Based Wearable Antigravity Muscles Support System for Lower Extremities. *Rehabilitation Robotics, 2005 (ICORR). 9th International Conference on*, pages 273–276, 2005.

[NSWK05b] T. Nakamura, K. Saito, Z.D. Wang, and K. Kosuge. Realizing model-based wearable antigravity muscles support with dynamics terms. *Intelligent Robots and Systems, 2005 (IROS). Proceedings of the 2005 IEEE/RSJ International Conference on*, pages 2694–2699, 2005.

[Onk07] A. Onken. *Development of an EMG-based muscle- and body-model for the determination of the resulting joint moments*. Diplomarbeit, Technische Universität Berlin, Institut für Technische Informatik und Mikroelektronik, 2007.

[PKMC04] J.E. Pratt, B.T. Krupp, C.J. Morse, and S.H. Collins. The RoboKnee: an exoskeleton for enhancing strength and endurance during walking. *Robotics and Automation, 2004 (ICRA). Proceedings of the 2004 IEEE International Conference on*, 3:2430–2435, 2004.

[Pla03] W. Platzer. *Taschenatlas der Anatomie*. Thieme, 2003.

[PNM96] J.R. Potvin, R.W. Norman, and S.M. McGill. Mechanically corrected EMG for the continuous estimation of erector spinae muscle loading during repetitive lifting. *European Journal of Applied Physiology and Occupational Physiology*, 74:119–132, 1996.

[PR06] J.C. Perry and J. Rosen. Design of a 7 Degree-of-Freedom Upper-Limb Powered Exoskeleton. In *Biomedical Robotics and Biomechatronics, 2006. The First IEEE/RAS-EMBS International Conference on*, pages 805–810, 2006.

[RBFA01] J. Rosen, M. Brand, M.B. Fuchs, and M. Arcan. A myosignal-based powered exoskeleton system. In *IEEE Transactions on Systems, Man, and Cybernetics*, volume 31, 2001.

[RFA99] J. Rosen, M.B. Fuchs, and M. Arcan. Performances of hill-type and neural network muscle models - Toward a myosignal based exoskeleton. *Comput. Biomed. Res*, 32(5):415–439, 1999.

[RPM+05] J. Rosen, J.C. Perry, N. Manning, S. Burns, and B. Hannaford. The human arm kinematics and dynamics during daily activities-toward a 7 DOF upper limb powered exoskeleton. *Advanced Robotics, 2005 (ICAR). Proceedings of the 12th International Conference on*, pages 532–539, 2005.

[SB98] T. Schlegl and M. Buss. Hybrid closed-loop control of robotic hand regrasping. *Robotics and Automation, 1998 (ICRA). Proceedings of the 1998 IEEE International Conference on*, 4:3026–3031, 1998.

[SBHR00] D.F. Stegeman, J.H. Blok, H.J. Hermens, and K. Roeleveld. Surface EMG models: properties and applications. *J. Electromyogr. Kinesiol*, 10(5):313–326, 2000.

[Sch03] T. Schlegl. Compensation of discrete contact state errors in multi-fingered manipulation. *Computational Intelligence in Robotics and Automation, 2003. Proceedings of the 2003 IEEE International Symposium on*, 2, 2003.

[SD88] S. Silbernagl and A. Despopoulos. *Taschenatlas der Physiologie*. Thieme, 1988.

[Seg03] J. Seghers. *Mechanical and electrical signs of muscle fatigue and recovery during submaximal continuous and intermittent contractions*. PhD thesis, Katholieke Universiteit Leuven, 2003.

[SGF05] G.S. Sawicki, K.E. Gordon, and D.P. Ferris. Powered Lower Limb Orthoses: Applications in Motor Adaptation and Rehabilitation. *Rehabilitation Robotics, 2005 (ICORR). 9th International Conference on*, pages 206–211, 2005.

[SW91] S.H. Scott and D.A. Winter. A comparison of three muscle pennation assumptions and their effect on isometric and isotonic force. *J Biomech*, 24(2):163–7, 1991.

[TC03] N.G. Tsagarakis and D.G. Caldwell. Development and Control of a Soft-Actuated Exoskeleton for Use in Physiotherapy and Training. *Autonomous Robots*, 15(1):21–33, 2003.

[TVdZ03] M. Thompson, M. Voigt, and M. de Zee. Evaluation of lower extremity musculo-skeletal model using sit-to-stand movement. In *Proceedings of the 19th congress of the International Society of Biomechanics*, 2003.

[Uhl96] K. Uhlmann. *Lehrbuch der Anatomie des Bewegungsapparates*. UTB für Wissenschaft, 1996.

[VBSS90] M. Vukobratovic, B. Borovac, D. Surla, and D. Stokic. *Biped Locomotion: Dynamics, Stability, Control, and Application*. Springer-Verlag, 1990.

[VMIS90] E.J. Vos, M.G. Mullender, and G.J. Ingen Schenau. Electromechanical delay in the vastus lateralis muscle during dynamic isometric contractions. *European Journal of Applied Physiology*, 60(6):467–471, 1990.

[Wal06] M. Walter. *Entwurf und Aufbau einer Steuerungsplattform für ein Exoskelett-System*. Diplomarbeit, Technische Universität Berlin, Institut für Technische Informatik und Mikroelektronik, 2006.

[Whe03] K.R. Wheeler. Device control using gestures sensed from EMG. *Soft Computing in Industrial Applications, 2003 (SMCia). Proceedings of the 2003 IEEE International Workshop on*, pages 21–26, 2003.

[Win90a] D.A. Winter. *Biomechanics and Motor Control of Human Movement*. John Wiley & Sons, Inc., 1990.

[Win90b] J.M. Winters. Hill-based muscle models: a systems engineering perspective. *Multiple Muscle Systems: Biomechanics and Movement Organization*, pages 69–93, 1990.

[WMV00] J.R. Wolpaw, D.J. McFarland, and T.M. Vaughan. Brain–Computer Interface Research at the Wadsworth Center. *IEEE Transactions on Rehabilitation Engineering*, 8(2):223, 2000.

[YINH04] K. Yamamoto, M. Ishii, H. Noborisaka, and K. Hyodo. Stand alone wearable power assisting suit-sensing and control systems. *Robot and Human Interactive Communication, 2004. ROMAN 2004. 13th IEEE International Workshop on*, pages 661–666, 2004.

[Zah90] G.I. Zahalak. Modeling muscle mechanics (and energetics). *Multiple Muscle Systems: Biomechanics and Movement Organization*, pages 1–23, 1990.

[Zaj89] F.E. Zajac. Muscle and tendon: properties, models, scaling, and application to biomechanics and motor control. *Crit Rev Biomed Eng*, 17(4):359–411, 1989.

[ZKC05] A. Zoss, H. Kazerooni, and A. Chu. On the mechanical design of the Berkeley Lower Extremity Exoskeleton (BLEEX). *Intelligent Robots and Systems, 2005 (IROS). Proceedings of the 2005 IEEE/RSJ International Conference on*, pages 3465–3472, 2005.

[ZKWBH95] M. Zardoshti-Kermani, B.C. Wheeler, K. Badie, and RM Hashemi. EMG feature evaluation for movement control of upper extremity prostheses. *Rehabilitation Engineering, IEEE Transactions on [see also IEEE Trans. on Neural Systems and Rehabilitation]*, 3(4):324–333, 1995.

[ZLMF95] S. Zhou, D.L. Lawson, W.E. Morrison, and I. Fairweather. Electromechanical delay in isometric muscle contractions evoked by voluntary, reflex and electrical stimulation. *European Journal of Applied Physiology*, 70(2):138–145, 1995.

[ZW90] F.E. Zajac and J.M. Winters. Modeling Musculoskeletal Movement Systems: Joint and Body Segmental Dynamics, Musculoskeletal Actuation, and Neuromuscular control. *Multiple Muscle systems, JM Winters and SL-Y Woo editors. Springer Verlag, New York*, 1990.